Doctoral Thesis

Thesis Title

Development of Microfluidic Cell Culture Models

of the Blood-Retinal Barriers

Department of Finemechanics

Graduate school of Engineering,

TOHOKU UNIVERSITY

Li-Jiun Chen

ID No.　　B7TD1202

Advising Professor at Tohoku Univ.	Associate Professor Hirokazu Kaji
Research Advisor at Tohoku Univ.	
Dissertation Committee Members Name marked with "○" is the Chief Examiner	○ Prof. Matsuhiko Nishizawa 1 Prof. Takuji Ishikawa 2 Prof. Makoto Ohta 3 Associate Prof. Hirokazu Kaji 4 5 6

TOHOKU UNIVERSITY
Graduate School of Engineering

Development of Microfluidic Cell Culture Models of the Blood-Retinal Barriers

(マイクロ流体デバイスを用いた血液網膜関門モデルの開発)

A dissertation submitted for the degree of
Doctor of Philosophy (Engineering)

Department of Finemechanics

by
Li-Jiun CHEN

January 14, 2020

Development of Microfluidic Cell Culture Models of the Blood-Retinal Barriers

Li-Jiun Chen

Abstract

Due to the fact that approximately 80% of all sensory input is received via the eyes, suffering from chronic retinal diseases that lead to blindness causes a significant decrease in the quality of life. In addition, retinal diseases are common in the elderly; developing pathological analyses and treatments for retinal diseases has become an urgent issue especially in super-aging countries such as Japan. Angiogenesis, the growth of blood vessels from a pre-existing one, plays an important role not only in the growth and regeneration of tissues in humans but also in pathological conditions such as inflammation, degenerative disease and the formation of tumors. There is increasing evidence that pathological angiogenesis is related to and might be an underlying cause of various human diseases, from inflammatory diseases, arthritis, to cancer and metastases. Pathological angiogenesis mechanisms of eye diseases are not fully elucidated; while evaluation of drug candidates against retinal diseases has been done on animal models, serious concerns arise regarding the ethics and costs in addition to the limitations of translating data from animal models to clinical settings.

In vitro cell culture models, an alternative to animal models, enable investigations on specific molecule-of- interest and simply recapitulate complex and chronic conditions. Anatomically, BRB is composed of an inner and an outer barrier: the inner BRB (iBRB) and the outer BRB (oBRB). At the cellular level, debilitating retinal diseases, diabetic retinopathy (DR) and age-related macular degeneration (AMD) involves compromised iBRB and oBRB, respectively. The detailed mechanisms are not fully understood; however, the physiologically tight BRB becomes leaky (breakdown) in DR and AMD. In AMD patients, it is observed that the retinal pigment epithelial (RPE) monolayer cells detach from the Bruch's membrane and the fenestrated choroids invade into the subretinal space (neovascularization). In contrast to AMD, proliferative DR presents alterations preferentially at the retinal level with compromised pericytes and damaged vascular integrity leading to vitreous hemorrhage and eventually tractional retinal detachment. Pathophysiology of neovascularization is complicated due to various factors involved, which include but are not limited to aging, oxygen concentration, energy metabolism, pressure, blood flow, and genetics. To complicate matters further, interactions between mural cells, glial cell (astrocytes) and the microvessels, and between cells and the extracellular matrix (ECM) involve multiple pathways and cytokine networks that remain huge research questions to be answered.

Recently, organ-on-a-chip technology have garnered attention and in vitro physiology has been extensively studied using the on-chip platform due to many of the advantages compared to traditional cell culture. This dissertation evolves around developing on-chip biological models of the blood-retina barrier (BRB), and using the models to elucidate mechanisms of pathological angiogenesis. Microfluidic models of the oBRB and the iBRB were built and characterized. For all of the models, individual cell types were evaluated first to ensure microfluidic cell cultures retain the physiological functions. Thereafter, cell-cell and cell-vessel interactions were evaluated. Due to the complex and vast factors of possible inflammatory conditions taking place in vivo, pathological angiogenesis-related factors investigated were limited to altering glucose concentration (imposing oxidative stress), hypoxia, and elevated Tumor Necrosis Factor (TNF)-alpha concentrations (mimicking inflammation).

There are six main chapters in this dissertation, organized as followed.

Chapter 1. Introduction.
Introducing the motivation and the overall aim and the significance of the developed BRB models in this dissertation. A non-exhaustive literature survey aims to provide all the necessary background to the research, namely, the vascular development at the cellular level (vasculogenesis and angiogenesis), pathological angiogenesis and angiogenic switch, the retinal diseases and limitations in current treatments, various applications of the developed on-chip ocular models and lastly, the models of tissue engineered blood vessels.

Chapter 2. Materials and Methods.
The fundamental techniques necessary in building and evaluating microfluidic cell cultures are described. Other specific methods that are not applicable for all BRB models in this dissertation are kept in the relevant chapter.

Chapter 3. **Cell-cell model of the outer blood-retina barrier.**
A microfluidic oBRB direct-contact cell-cell model is developed. Here, a proposed in vitro angiogenesis process was investigated and tested by examining the co-culture of human retinal pigment epithelial cells (ARPE-19, herein ARPE) and human umbilical vein endothelial cells (HUVEC) inside a microfluidic device. From characterization of the APRE monoculture, the tight junction protein (ZO-1) was found on the cells cultured in the microfluidic device but changes in the medium conditions did not affect the integrity of monolayers as found in the permeability tests. Vascular endothelial growth factor (VEGF) secretion was elevated under low glucose and hypoxia conditions compared to the control. After confirming the angiogenic ability of HUVEC, the cell-cell interactions were analyzed under lowered glucose medium and chemical hypoxia by exposing ARPE cells to cobalt (II) chloride ($CoCl_2$). Heterotypic interactions between ARPE and HUVEC were observed, but proliferation of HUVEC was hindered once the monolayer of ARPE started breaking down. The above characterizations showed that alterations in glucose concentration and/or oxygen level as induced by chemical hypoxia causes elevations in VEGF produced in ARPE which in turn affected directional growth of HUVEC.

Chapter 4. Cell-vessel model of the outer blood-retina barrier.
The evolution from the cell-cell model to the cell-vessel model towards a more realistic oBRB model is discussed. Using microfabrication and tissue engineering techniques, models of microvessels and microvascular network were built and characterized. It was then extended to a two-layer vascular oBRB model, enabling top-down direct-contact cell cultures. Using the device, a co-culture model of the anatomical RPE-Bruch membrane-fenestrated choroids was successfully developed. Adopting the same methodology in Chapter 3, ARPE monolayers and HUVEC microvessels were characterized individually before the RPE-HUVEC co-culture. Inflammatory conditions were imposed onto the models and the responses of vascular network were evaluated. In order to evaluate the barrier function of ARPE, the device was further modified by inserting platinum electrodes for trans-epithelial electrical resistance (TEER) measurement, demonstrating the feasibility of on-chip assessment of the epithelial barrier integrity. The proposed design allows for direct-contact co-culture of cell-cell or cell-vessel, modifiable for real-time evaluation of the state of the epithelial monolayers.

Chapter 5. Angiogenesis sprouting model of the inner blood-retina barrier.
The focus is reoriented from the oBRB to the iBRB. As opposed to the choroids in the oBRB which form based on vasculogenesis, sprouting models of retinal microvessel based on angiogenesis are developed. The barrier integrity of human retinal microvascular endothelial cells (HRMEC) under inflammatory conditions were characterized. In order to understand the mechanisms of angiogenic sprouting under inflammatory conditions, matrix metalloproteinase (MMPs) activity of HRMEC was evaluated. As hepatocyte growth factor (HGF) is one of the factors regulating proliferation of HRMEC, the barrier tightness co-culturing HRMEC and normal human lung fibroblasts (NHLF) under inflammatory conditions was also investigated. Finally, angiogenesis sprouting models of the iBRB formation from different configurations of HRMEC monoculture, HRMEC-human retinal pericytes (HRP) co-culture, and HRMEC-HRP-NHLF tri-culture were investigated to obtain the optimal angiogenesis sprouting model of the iBRB.

Chapter 6. Conclusions and Future Perspective.
Concludes the developed BRB models. Along with the limitations, the future perspective are given.

In summary, models of BRB specific to oBRB and iBRB were developed. The models proposed in this study are albeit at an early stage; with the potential of micro-electro-mechanical systems (MEMS), investigation of systemic effects on the eye by connecting individual fluidic devices in a fluidic network is promising and worthy of investigation.

Table of Contents

List of Table

List of Figures

Abbreviations

Cells,tissue, organss

EC, endothelial cell; **ARPE-19**, Human retinal pigment epithelial cells; **HUVEC,** Human umbilical vein endothelial cells; , **GFP**, green fluorescent protein; **GFP-HUVEC**, GFP-expressing human umbilical vein endothelial cells; **HRMEC**, Human retinal microvascular endothelial cells; **HRP**, Human retinal pericytes; **NHLF**, Normal human lung fibroblasts; **BRB**, blood-retina barrier; **oBRB**, outer blood-retina barrier; **iBRB**, inner blood-retina barrier

Cytokines and growth factors

GF, growth factor; **PDGF**, platelet derived growth factor; **VEGF**, vascular endothelial growth factor; **bFGF**, basic Fibroblast Growth Factor; **TNF**, Tumor Necrosis Factor; **FBS**, fetal bovine serum; **FCS**, fetal calf serum

Extracellular matrix (ECM) and its components

MMPs, matrix metalloproteinase; **PLL**, poly-L-lysine; **FN**, fibronectin

Materials and reagents

PDMS, polydimethylsiloxane; **APMS**, 3-Aminopropyltrimethoxysilane, **FITC**, fluorescein isothiocyanate; **TC**, tissue culture

Measurement system and bioassays

TEER, transepithelial electrical resistance; **FACS**, flow cytometry; **ELISA**, Enzyme-linked immunosorbent assay; **IF**, immunofluorescence

Non-categorized

2D, two-dimensional; **3D**, three-dimensional; **μFD**, microfluidic device; **TE**, Tissue engineering/tissue engineered; **TEBV**, tissue engineered blood vessel; **BV**, blood vessel

1   Introduction

This chapter outlines the fundamentals of this dissertation, mainly, the necessary background and the motivation behind the development of microfluidic models of the blood-retina barrier (BRB) and their significance. The non-exhaustive literature survey compiles the necessary background to the research, namely, the vascular development at the cellular level (vasculogenesis and angiogenesis), pathological angiogenesis and angiogenic switch, the retinal diseases and limitations in current treatments, the ocular-on-chips built using different techniques, mainly, microfabrication and vascularization techniques employed in tissue engineering and various applications and lastly, the models of tissue engineered blood vessels. Design considerations are mentioned in relevant sections. The research questions, goals and the scope of each model are described, and the chapter is ended with a detailed outline of each chapter of the dissertation.

1.1   Vasculature development: angiogenesis and vasculogenesis

A sound understanding of normal vascularization is important in order to recapitulate the anatomical, physiological and functional aspects of blood supply in the successful construction of a biomimetic vascularized tissue. The walls of large blood vessels have three distinct layers: intima (innermost layer), a thromboresistant confluent monolayer of endothelial cells (ECs) attached to a basement membrane (40-120 nm); media (middle layer), a dense population of concentrically organized smooth muscle cells (SMCs) with bands or fibers of elastic tissues; and, adventia (outermost layer), a collagenous extracellular matrix (ECM) containing mainly fibroblasts and perivascular nerves (1). Native vasculature is formed in vivo by vasculogenesis and angiogenesis (1). The formation of specialized blood vessel types through arteriogenesis, venogenesis or lymphangiogenesis (2) is not the main focus of this review.

Vasculogenesis takes place mainly during embryogenesis in developing organs. In this process, new blood vessels are formed from endothelial progenitor cells (EPCs) that are derived from mesodermal stem cells (MSCs). The EPCs migrate to different regions to form discrete blood islands, eventually fuse together to form a vascular plexus and ECs (1). The ECs migrate and organize into nascent endothelial tubes to form capillaries (1). The capillaries are composed of a single monolayer of ECs, basement membrane and pericytes, while the recruitment of pericytes, smooth muscle cells (SMCs) and fibroblast layers around the endothelial tubes remodel the tubes into more mature and larger blood vessels (arterioles, arteries, venules, veins) (1,3). In response to hypoxia or other vascular injuries, EPCs migrate to injured sites, and incorporate into the injured vessel, giving rise to mature ECs that contribute to formation of new vessel or reparation of existing vessels (4).

Angiogenesis is the formation of new blood vessels from pre-existing vessels and/or from EPCs. The formation of blood vessels through angiogenesis is important in embryo development, ovulation, wound healing, and in pathological conditions such as arthritis and metastasis (5). Depending on the physiological processes involved, angiogenesis is classified as (i) de novo angiogenesis occurring in embryonic development and in female

reproduction; (ii) therapeutic angiogenesis in tissue repair; and (iii) pathological angiogenesis in certain disorders such as inflammatory diseases and blindness (5). Two types of angiogenesis occur in utero and in virtually all tissues and organs of adults (2): (i) sprouting angiogenesis, where sprouts composed of ECs grow toward an angiogenic stimulus such as vascular endothelial growth factor-A (VEGF-A), and (ii) intussusceptive or splitting angiogenesis, where a single vessel splits into two (6). Angiogenic processes result from a sequence of events influenced by cell-cell and cell-ECM interactions (6). The first step in the process is the breakage of the basement membrane; this induces endothelial tip cells to sprout from existing vessels and provide a framework for new vessels. Supporting cells such as pericytes mature, stabilize and determine the structure of the new vasculature (3). Angiogenic processes initially lead to the development of capillaries; depending on the types of vessel, angiogenesis may be followed by arteriogenesis, in which the vascular structures mature and grow in diameter to produce thicker vascular walls (7). As the vessel walls mature, ECs and supporting cells (SMCs and pericytes) become tightly integrated with the surrounding matrix (8).

A number of factors involved in angiogenesis have been identified; the main protagonists are vascular endothelial growth factor (VEGF), basic fibroblast growth factor (bFGF), the transforming growth factor beta (TGFβ) family and hypoxia (hypoxia-inducible transcription factor, HIF) (9). Other factors that have angiogenic properties include angiopoietins, (Ang-1), hepatocyte growth factor (HGF), platelet-derived growth factor (PDGF-BB), insulin-like growth factor family (IGF-1, IGF-2), and neurotrophins (NGF) (9). Anti-angiogenic factors including thrombospondin (TSP), and dopamine agonists exert inhibitory action on angiogneic signaling pathways. TGFβ and inflammatory factor tumor necrosis factor (TNFα) are growth modulators that are found to have stimulatory or inhibitory action (10). The roles of growth factors has been thoroughly reviewed recently (22, 23).

1.2   Instances where angiogenesis is undesirable

Pathological angiogenesis shares many processes with physiological angiogenesis (13). However, the pathological angiogenic cascade is persistent and unresolved upon the establishment of vascular perfusion and becomes driven by the pathological condition (13) (see Table 1 for summary of organ-specific, angiogenesis-dependent and inflammation-induced diseases). Uncoordinated responses of vascular endothelial and mural cells to the heterogeneous angiogenic cues provided by tissues and organs result in impaired organ development or disease states (13). In acute inflammatory responses, the endothelium shows impaired endothelial vasomotor function and also expresses inflammatory markers such as vascular cell adhesion molecule-1 (VCAM-1), intracellular adhesion molecule-1 (ICAM-1), and E-selectin (14). Pathological angiogenesis can be observed at three levels: (i) cellular level, (ii) tissue level, or (iii) whole-organ level. Migration of endothelial tip cells is the first step in angiogenesis and Cell cultures have often been employed to test the effects of different angiogenic stimuli and inhibitors on cell growth, proliferation, and cell-cell interactions. More recently, however, attempts have been made to model processes involved in the formation and maturation of blood vessels in order to more realistically mimic the underlying processes of angiogenesis. As the spatiotemporal relationships between angiogenic factors are also important and can be represented

better by scaling up the models, in situ implants and animal models are being used.

1.2.1 Roles of angiogenesis in inflammation and degenerative diseases

Inflammation and angiogenesis are distinct and separable processes (2). However, dual functionality of angiogenic factors (i.e., possess both pro-inflammatory and pro-angiogenic effects) suggests that these are two closely related processes (2). Furthermore, there is growing evidence that angiogenesis tends to prolong and intensify the inflammatory response (2). The inflammatory process is highly coordinated by pro- and anti-inflammatory molecules that regulate cell chemotaxis, migration and proliferation to control tissue damage during pathogenic or traumatic injury (15). Endothelium is found to play a major role in inflammation as it involves the migration and extravasation of immune cells through the microvasculature (15). In the chronic phase of inflammation, neovascularization by angiogenesis and vasculogenesis restore the oxygen and nutrient supply to the injured tissue (13). Release of angiogenic factors is stimulated by inflammatory mediators produced by immune cells which target fibroblasts and ECs (15). Inflammatory cells also directly release angiogneic factors at inflammatory loci, exerting mitogenic and migratory effects in endothelium (15).

Inflammation generally ends up in a healing process. The switch from an inflammatory response toward the healing process is regulated by local anti-inflammatory signals (15). Whenever pro-inflammatory molecules exceed anti-inflammatory molecules, inflammation becomes exacerbated resulting in the increased production of proteases, proteoglycans, lipid mediators and prostaglandins (15). Chronic inflammatory conditions have been found to associate to a wide variety of diseases including psoriasis, rheumatoird arthritis, ostheoarthritis, metabolic syndrome-associated disorders (e.g. obesity and diabetes), ocular disorders, Crohn's disease and cancer (15).

1.2.2 Angiogenesis and formation of tumors

The formation of tumors (tumorigenesis) involves the development of new blood vessels. Therefore, understanding the growth of tumors will add to our knowledge on the regulation of pathological angiogenesis. Regardless of the type of tumor, the blood vessels are irregularly-shaped, dilated and are not organized into definitive vessel structures such as arteries, arterioles, or capillaries. The rapid vascularization necessary to serve fast-growing cancers coupled with poor lymphatic drainage create a leaky (16,17) and hemorrhagic tumor vascular network, which is in stark contrast to the controlled vessel density in normal tissues (18). There is also evidence that native immune cells recruited into tumors stimulate the endothelium and are responsible for an indirect tumor vascularization (19,20). One of the prominent features of tumor blood vessels is that they fail to become quiescent and are capable of constant growth (18). The microvasculature, regulated by stromal cells, is closely coupled to the tumor phenotype, development, progression and tumor products (18,21). Unlike normal vasculature where pericyte associations reduce EC proliferation, there is a reduction in vessel association with pericytes in tumors, which might explain the tortuous vascular structure, abnormal vessel diameter and sensitivity to VEGF-A inhibition (3,18). The formation of tumor vasculature has been reviewed (18) while endogenous angiogenesis stimulators and inhibitors are summarized by Brannon-Peppas and Blanchette (17) .

1.2.3 Tumor growth is dependent on functional blood vessels

Ide et al. (22) first postulated the hypothesis that angiogenesis is necessary to support tumors from results obtained in an experiment in which an epithelioma was implanted into rabbit ears and found to induce formation of new capillaries. Folkman et al. found that inoculation of tumor cells into isolated perfused organs resulted in tumors of 1-2 mm^3 with no neovascularization; thus, the absence of neovascularization was correlated with a restriction in tumor growth (23) . This conclusion was confirmed in an experiment in which cultured tumor cells were placed in the cornea of a rabbit eye which is avascular. It was found that if capillaries were physically prevented from reaching the implant or the implant was inhibited from undergoing angiogenesis, the tumor nodule showed highly restricted growth (24) . Analysis of vascular permeability of different glioma xenografts showed that functional microvessels are dependent on the distances to vessel perfusions, hypoxic area and permeability (25) . In another study, the perfusion failure of individual microvessels within the glioma center was found to be partly compensated by an increase in diameters (26) . These examples illustrate the fact that tumor growth requires development of blood vessels. Despite the fact that tumor vessels recruit endothelial precursor cells, the rate of endothelial precursor cell incorporation is generally low and depends on the nature of the tumor, suggesting that most tumor neovascularization occurs via angiogenesis as opposed to vasculogenesis (18) .

Although many animal models have provided evidence for the dependence of tumor growth on neovascularization, vessel density is not a definitive indicator of angiogenesis dependence and aggressiveness of a tumor (18,27,28) . For example, astrocytomas, known as 'non-angiogenic tumors', rely on vascular-rich brain parenchyma to grow along blood vessels without initiating angiogenesis (18) . The term 'vasculogenic mimicry' has been used to describe the de novo generation of microvascular channels by genetically deregulated, aggressive tumor cells without participation of ECs and independent of angiogenesis (29) . In vivo tumor models have shown that tumor growth depends on the its environment, i.e., subcutaneous or the tissue of origin (orthotopically) (30) . In normal tissues, the degree of vascularization and oxygen/ nutrient demand are tightly coupled; however, they are loosely coupled or may be uncoupled in tumors, resulting in the dissociation of VEGF from regulation by oxygen concentration (27) . In addition, angiogenesis differs among tumor types, stages and microenvironment, implying that the oxygen and nutrient requirements are variable (18). The permeability of tumor blood vessels is also variable amongst different tumor regions and tumor types (25). Using advanced imaging techniques, the metabolic microenvironment such as the pH and transport through the microvascular wall as well as interstitial space in tumors can be quantified and analyzed (31) .

1.2.4 The angiogenic switch

It has been proposed that the balance between pro- and anti-angiogenic factors can determine the formation or absence of vascularization (18). This so-called angiogenic switch, depends on a local imbalance between positive and negative regulators of angiogenesis, and leads to the formation of tumors when the level of activators is higher than that of inhibitors. Tumor vascularization and metastatic growth result in cases where proangiogenic activities prevail (32) . Pro- and anti-angiogenic molecules can emanate from cancer cells, ECs,

stromal cells, blood and the ECM, and the relative contributions vary with tumor type and tumor site (28,33) . This results in the activation of the angiogenic switch at different stages of tumor progression as is observed in a variety of human tumors and mouse models of multistage cancers (18) . Several studies on disseminated tumor cells have found that they may undergo proliferative arrest if they infiltrate an organ that lacks the appropriate adhesive and signaling interactions, suggesting that dormancy is induced by maladaptation (34) . Indeed, microenvironmental signals that cause low-mitogenic activity and induce high-stress signaling to trigger quiescence may play a role in the dormancy mechanisms (35) . It has been reported that infiltration of reactive fibroblasts (myofibroblasts) into tumors provides a switch for exit from dormancy of implanted ovarian carcinoma spheroids (36) . Although signals that trigger the angiogenic switch have been identified (metabolic stress, mechanical stress, immune/inflammatory response and genetic mutations) (33), the molecular controls of the abnormalities and how the interplay between environmental and genetic mechanisms influences tumor angiogenesis are not fully understood (17,18,33) .

1.3   Retina structure, diseases and ocular drugs

Humans eyes (Fig. 1.3-1), similar to the rest of the body, our eyes are susceptible to physical injury, chemical insult, inflammation, diseases, and tumors. However, it is challenging, if not impossible, to access the inner structure of an eye to study and manage the ocular diseases. Inarguably, the retina is one of the most important structures of the eye. Although small in size (approximately 0.5 mm tissue), it plays an important role in human vision.

1.3.1 The barriers of the retina

The blood-retinal barrier (BRB) maintains a constant milieu and limits nonspecific transport between the circulating blood and the retina. It can be further classified as outer blood-retinal barrier (oBRB), formed by the monolayer of RPE and inner blood-retinal barrier (iBRB), formed by the retinal capillaries (Fig. 1.3-1, insets). Retinal capillaries contains complex tight junctions of retinal capillary endothelial cells (ECs) resting on the basal lamina that is covered by processes of Müller cells and astrocytes. Pericytes, encased in the basal lamina, exist in close contact albeit as a non-continuous layer with the ECs hence do not contribute to the diffusional barrier (9). Astrocytes, Müller cells, and pericytes are considered to model the vascular growth and integrity of iBRB by transmitting regulatory signals to retinal ECs indicating changes in the microenvironment of the retinal neuronal circuitry (9). The inner two thirds of the human retina is nourished by retinal capillaries and the remainder is covered by choriocapillaris via the oBRB (7). The retinal vasculature gets its input from the central retinal artery (CRA), which bifurcates at the optic disc into several branches that provide the blood supply of the entire inner retina (10). Similarly, the central retinal vein leaves the eye through the optic disc and drains blood into the cavernous sinus. The BRB is responsible for the efflux of neurotransmitter metabolites from the retina and the supply of nutrients to the retina to maintain visual functions (7). The rate of turnover of photoreceptors (renewal of photopigments and phagocytosis of the photoreceptor disks by RPE) is also essential to vision, which is dependent on the integrity of the RPE monolayer (8). Dysfunction in vascular cells can cause the breakdown of BRB, resulting in retinal diseases as listed in the next section.
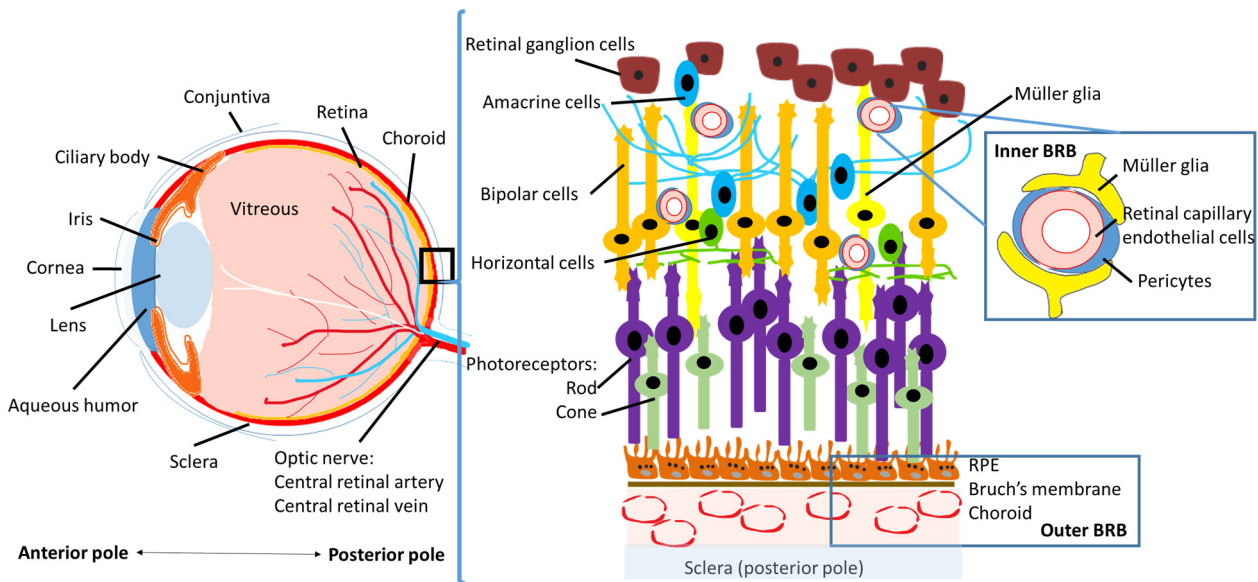
Fig.   1.3-1 Human eye anatomy.

Illustration depicts the anatomical structure of BRB of which the microfluidic models are built. The retina depicted in the black box is magnified on the right, showing distinctive layers of the retinal tissue. Inset images show the components of the blood-retinal barrier (BRB). Image is not to scale.

1.3.2   Retinal diseases

Retinal diseases often result in severe vision loss and pose a serious socioeconomic burden. As a whole, the BRB is dependent on the retinal ECs, the perivascular supporting cells, and the RPE cells as they are the targets and producers of eicosanoids, growth factors, and cytokines (9). Breakdown of the BRB may be mediated by locally released cytokines and induces an inflammatory reparative response that stimulates further release of cytokines, and growth factors. For comprehensive descriptions on retinal diseases, readers are referred to (11), in which retinal diseases and disorders due to hereditary, infections, traumas, and tumors are discussed in detail. Some of the common diseases caused by retinal degeneration and compromised BRB are summarized below.

1.3.2.1 Neovascularization

During normal retinal vascular development, vascular ECs proliferate and migrate through the extracellular matrix (ECM) in response to cytokines, resulting in the formation of new blood vessels in an ordered fashion (12). The term neovascularization refers to the phenomenon when the unregulated processes result in dysfunctional blood vessels, leading to hemorrhage, or retinal detachment. A related term, angiogenesis, is devoted to the phenomenon of formation of blood vessels from the pre-existing blood vessels. Ocular angiogenesis is a major cause of visual impairment and the microvascular complications are associated with numerous ocular diseases, including, but not limited to, retinopathy of prematurity, ischemic retinal vein occlusions, rubeotic glaucoma, age-related macular degeneration, and diabetic retinopathy.

1.3.2.2 Age-related Macular Degeneration

Age-related macular degeneration (AMD) is prevalent in the elderly. It is classified into dry-type and wet-type, each accounts for 85% and 15% of all AMD patients, respectively (13). The atrophic dry-type occurs due to the compromised RPE cells, leading to buildup of deposits called drusen at the RPE layer, beneath the macula. This leads to progressive RPE atrophy (geographical atrophy). In exudative wet-type AMD, the formation of blood vessels arises from the choroidal microvascular bed that invades the sub-retinal space. The newly formed, abnormal blood vessels tend to break, and leak fluid, damaging the macula and resulting in a rapid and severe loss of central vision.

1.3.2.3 Diabetic retinopathy

Diabetic retinopathy (DR) is the most frequent microvascular complication of diabetes mellitus, and the most common cause of blindness in the working-age population (14), which can be classified into two stages: non proliferative (non-PDR) and proliferative (PDR) (13). Factors such as hyperglycemia, inflammation, nerve growth factor autophagy and epigenetics have been identified to be involved in the pathogenesis of diabetic retinopathy (14). In contrast to AMD which affects the sub-retinal space, DR presents alterations preferentially at the retinal level (13). Typical symptoms in non-PDR are micro-aneurysms, retinal hemorrhages, and exudates caused by loss of pericytes and deranged vascular integrity (14). Increased intraocular VEGF levels due to capillary occlusion of retinal vessels contribute to PDR, where proliferation may grow at the optic disk or elsewhere in the retina into the vitreous. This leads to vitreous hemorrhage and eventually tractional retinal detachment.

1.3.2.4 Macular edema

Macular edema is a non-specific sign of ocular disease and occurs in a wide variety of ocular situations such as uveitis, trauma, intraocular surgery, vascular retinopathies, hereditary dystrophies, diabetes, and AMD (9). It is the final common pathway of many intraocular and systemic insults, consisting of a localized expansion of the retinal intracellular and/or extracellular space in the macular area (15). The amount of fluid normally present in the retina is balanced by the osmotic and hydrostatic pressure between the retina and the surrounding vasculature, which are compartmentalized by the BRB according to Starling's law (16). An altered retinal environment can result in macular edema, with accumulations of fluid in the retinal layers around the fovea. In retinal vein occlusion, macular edema results from the breakdown of the vascular endothelium associated with increased intravascular hydrostatic pressure (16).

Diabetic macular edema is caused by the disrupted iBRB due to hyperglycemia, increased levels of growth factors, inflammation and cytokines (14). In diabetes, the iBRB is leaky and fluid and proteins leak from the retinal vessels in the inner retina and spread to the retinal surface and toward the RPE (16). This further causes impairment of pericytes, leading to exudation of fluid, proteins and lipids via paracellular and transcellular transport mechanisms (14).

1.3.3 Treatments for retinal diseases

1.3.3.1 Ophthalmic drugs targeting neovascularization

Significant progress has been made in identifying factors that promote and inhibit angiogenesis. Preclinical studies on cell adhesion molecules (integrins), matrix metalloproteinases (MMPs) and numerous proteolytic cleavage fragments of matrix molecules have shown to be associated to angiogenesis (12). Many well-known angiogenesis activators have been identified, including vascular endothelial growth factors (VEGF), fibroblast growth factors (FGF), placental growth factor (PIGF), epidermal growth factor (EGF), angiogenin, and tumor necrosis factor-α (TNF-α). Angiogenesis inhibitors include, but not limited to, thrombospondin-1, angiostatin, endostain, or PEX (12). Several compounds approved for treating neovascularization of the eye are on the market, including Pegatanib (Macugen, Eyetech Pharmaceuticals/Pfizer), Bevacizumab (Avastin, Genentech, Inc./Roche) and Ranibizumab (Lucentis, Genentech/Novartis) (12). In additional to targeting angiogenic molecules, clinical treatments such as laser coagulation and photodynamic therapy (PDT) have also been employed in targeting choroidal vascular permeability and edema (17, 18).

1.3.3.2 Ocular drug administration

The drug delivery systems utilize topical (local), systemic, intraocular routes of administration to the posterior segment of the eye (19). Topical application of ophthalmic medications in the form of solutions, suspensions, ointments, gels or emulsions is the easiest of all the methods of administration. However, most of the applied dose is washed out or absorbed systematically, ultimately eliminated by metabolic processes (20). Moreover, the ocular barriers effectively protect the eye from foreign materials which also hinder efficient absorption of pharmaceuticals (7). When a drug is administered systematically, hepatic first-pass metabolism often reduced the bioavailability of the drug implying that a relatively high drug concentration is needed in the plasma to reach a therapeutic effective dose in the eye (9, 22, 23). Sustained release of oral drugs exposes the whole body to the drug, often giving rise to undesired side effects (23).

Intraocular delivery via intravitreal injection is an effective way at getting drugs to the posterior segment. The injection is commonly done by injecting a drug solution (mainly anti-VEGF agents: ranibizumab, bevacizumab, or aflibercept) into the vitreous cavity with a 27- or 30- gauge needle (24). Intraocular administration can be further classified into subconjunctival, intravitreal, transcleral, and iontophoretic routes, which are invasive but more efficient than topical instillation (19).

Device-based approaches to retinal diseases, such as intraocular and periocular implants have also garnered attention due to their potential in reducing the frequency of administrations of drugs. Non-biodegradable or biodegradable drug delivery devices (DDS) are transplanted directly into the vitreous body or surface of an eyeball. Although complications might arise due to instillation and removal procedures of the DDS, the device can release the drug over a prolonged period of time, reducing the frequency of the invasive surgical procedure (24). Microscale devices in the form of microneedles (MNs) (25-27), drug-infusion micropumps (28, 29), microchip (30, 31), and microreservoir devices (32, 33), as well as drug delivery vehicles using supramolecules (34, 35) have all been investigated as different means of delivering ocular drugs. A recent review have

comprehensively summarized various types of DDS (24).

1.4 Ocular models

Animal models including naturally transparent tails of amphibian larvae, or specialized viewing chambers implanted into rabbit ears, mouse skin, and hamster cheek pouches have been used to circumvent the opacity of living tissues, allowing observing the details of angiogenic sprouting in real time (36). Subsequently, these studies lead to discovery of diffusible, tumor-derived molecules that promote vascular growth and validation of the central paradigm of tumor-induced vascular chemotaxis (36). Well-developed models such as rabbit corneal pockets (37-39), chick chorioallantoic membranes (40-43) and laser-induced choroidal neovascularization (CNV) model of mouse/rat eye (44, 45) are widely employed in studying choroidal angiogenesis, providing fundamental yet simple models advancing our understanding on angiogenesis processes in the eye. Aforementioned standardized assays and animal models allow qualitative study of angiogenesis processes but have low-throughput and are unable for exploring new cellular mechanisms (46). Another challenge to analyzing angiogenesis in vitro is to reconstruct tissue sections in 3D; even if they are successfully reconstructed, 3D images often do not communicate the dynamic nature of vascular growth. Moreover, the region near the tips of angiogenic sprouts—a critical area of control of vascular invasion and morphogenesis—is rarely found in tissue sections (36).

Lab-on-a-chip is gaining much attention in recent years due to the associated advantages of miniaturized systems: minimal sampling volumes and relatively low costs. Organ-on-a-chip, a subset of lab-on-a-chip, is often associated with replicating tissue- or organ-level functions in integrated microfluidic devices to answer fundamental research questions such as cell physiology or to explore disease pathophysiology. Several microfabrication techniques exist, which are used for different research applications, ranging from fabrication of biosensors and disease models, to vascularization of engineering tissues for medical studies (37–39). Narrowing down on the medical applications, many in vitro models have been built utilizing Bio- MEMS or static transwell system to study different human organs. MEMS and microfluidic on-chip models have been covered and readers are referred to the reviews (38–43).

Microfabrication and nanofabrication enable fabricating sophisticated structures down to micro- and nanoscales with optional integrated electrical and/or mechanical elements. Microfabrication has also been actively employed in studying angiogenesis and vascularization processes. The fast fabrication processes allow mass production of in vitro models for experimental uses and avoid costs associated in breeding and maintaining animals. Micro- and nano-sized structures can be precisely fabricated in vitro; along with natural or synthetic soft material, in vivo microenvironments can be realistically replicated. In addition, the platforms are customizable, enabling testing specific stimuli of interest.

Based on the retinal diseases outlined in previous section, this section first outlines different methodologies in fabrication of microvessels; the rest of the section discusses approaches to retinal diseases from various aspects using on-chip disease models. The physiological factors and design considerations of engineered on-chip

models are discussed where appropriate. The technical details of fabrications of the in vitro microvessels and the characteristics of these microvessels are summarized elsewhere (47, 48), while protocols for perfusable microvessels are available (49, 50) hence they are not covered in details here.

1.4.1 Fabrication of biomimetic microvascular models

Broadly, biomimetic microvascular models are fabricated in 3 different ways: self-organization of ECs (Fig. 1.4-1 A), cell transfer based on electrochemical processes (Fig. 1.4-1 B), and direct seeding of ECs into a microvessel (Fig. 1.4-1 C), all of which enable rapid fabrication of perfusable microvascular networks.
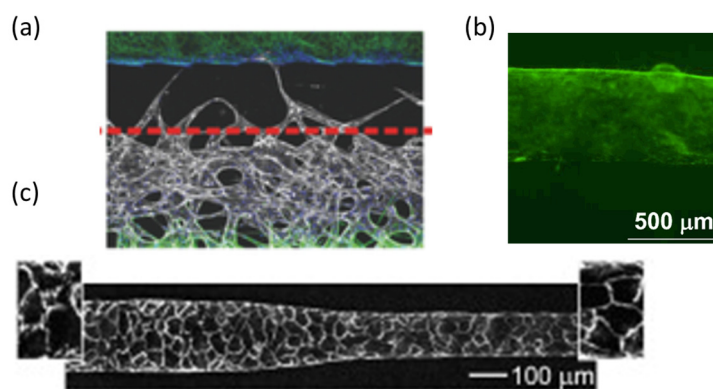
Fig. 1.4-1 Morphology of microvessels resulting from different methods of fabrication.
(a) vascular network formed by embedding ECs in the fibrin hydrogel matrix (51); (b) endothelial layer (GFP-HUVECs) transferred onto the internal surface of a microchannel in the collagen gel along with electrochemical desorption of the oligopeptide (52); (c) the fluorescence image of a microvessel formed from a mold with a tapered geometry using the subtractive fabrication method (53). All figures were reproduced with permission.

1.4.1.1 Self-organization of endothelial cells

For 2D angiogenesis studies, ECs are cultured in a flat dish until they are confluent, forming a monolayer that resembles endothelial lining of blood vessels. Although this method yields a useful model of proliferative responses to endothelial injury in blood vessels, monolayer cultures of ECs on rigid substrata do not typically organize into capillary-like tubes (36). Another common approach to vascularization and angiogenesis studies is the self-organization of ECs within 3D biological gels. In simulating processes of angiogenesis, in vivo angiogenesis assays that measure vascular ingrowth into polymeric sponges or plugs of gelled basement membrane proteins implanted subcutaneously are more ideal (36), as they enable studying of morphological structures of blood vessels. Microfluidic devices in which hydrogels are confined in the desired microchannels demarcated using micro-pillars provide cells with a more in vivo-like microenvironment, and have been used to model blood-retinal barrier (51). The microfluidic platform has also been used to generate interconnected 3D capillary beds using collagen type I gel embedded with alginate microbeads (~152.5 µm) (54). Human microvascular endothelial cells (hMVECs) seeded in channels were encouraged to sprout with either an exogenous supply of growth factors, or by the encapsulation of angiogenic cell lines that secret growth factor (54). Although the resultant vasculature is on the millimeter scale, the versatile technique allows different cell

types to be encapsulated in alginate beads and to be assembled into any size and shape in controlling bead ratios and cell densities, producing native microvasculature-like structure and function.

1.4.1.2 Subtractive method using sacrificial elements inside microfluidic scaffolds

The subtractive method involves fixing a needle or wire (at the desired diameters, typically in the micron range) in a gel precursor which is then removed after polymerization of the gel. The end result is the formation of a hollow microchannel where ECs can be seeded for angiogenesis research. The techniques can be extended into fabricating multiple endothelial tubes encapsulated inside a single scaffold, enhancing the complexity of a model. Other potential applicabilities of the model include controlling the composition of the interstitial fluid, and to generate gradients of cytokines for in vitro studies of angiogenesis (55).

Using a similar strategy, so-called "sacrificial molds", a template is used to pattern microvasculature or tissue constructs. The template is encapsulated within ECM and is dissolved once the hydrogel has been cross-linked. Golden and Tien (56) used micropatterned gelatin mold encapsulated inside collagen gels to fabricate perfusable, interconnected microfluidic networks. In addition to natural hydrogels, synthetic hydrogels including poly(ethylene glycol) diacrylate (PEGDA), poly(glycerol-sebacate) (PGS), poly-caprolactone (PCL) have been used as the ECM matrix scaffold in fabricating engineered microvessels. The cross-section of the resultant microfluidic channel fabricated from sacrificial molds is often rectangular, which is convenient to form than rounded ones but is thought to be one of the factors leading to non-uniform shear stress across the cross-section (55). It is necessary to consider optimization of the network geometry in order to obtain in vivo-like cell densities and to ensure appropriate transport capacities without excessive vascular resistance or volume (55).

1.4.1.3 Electrochemical cell transfer

Transferring ECs using an electrochemical reaction have also been used to fabricate perfusable, vascular-like structures. Using self-assembled monolayers (SAMs) of alkanethiol or oligopeptides, SAM desorption from the surface resulted in cell detachment, and can be deposited on a receiving substrate. In the study conducted by Osaki et. al., confluent cell sheets were transferred via desorption of oligopeptides from the surface (52). Subsequently, the cell sheets were transferred to collagen gel along with electrochemical desorption of the molecular layer, resulting in endothelial cell-lined vessels. The sprouting of vasculature under fluidic shear stress and the angiogenic stimuli were investigated. Nadr et. al. integrated zwitterionic oligopeptide SAM-based cell deposition with photopatterning of the gelatin methacrylate (GelMA) hydrogel to generate perfusable, microvascular structures (57). HUVECs seeded on gold substrates modified with oligopeptide based-SAM were transferred to the hydrogel after photocrosslinking of GelMA prepolymer with or without electrical potential. Photocrosslinking of hydrogel resulted in efficient (>97%) monolayer transfer while electrochemical-prompted transfer preserve cell morphology (57).

1.4.2 Evaluation of the blood-retinal barrier function

The breakdown of the barrier function of the BRB occurs in a number of retinal diseases as described in section

2.3. Barrier function refers to the ability of a vessel wall to restrict passage of molecules and ions across the endothelium and its glycocalyx (58), and is one of the most important properties of a microvessel model. It has been evaluated by transepithelial electrical resistance (TEER) and/or permeability to molecular tracers of different sizes under normal and pathological conditions. A more restrictive barrier will have a tighter junction, hence higher TEER values and lower permeability to molecular tracers. Wisniewska-Kruk et. al. built a BRB model with bovine retinal endothelial cells (BRECs), bovine retinal pericytes (BRPCs), and rat glial cells (astrocytes) to investigate pathology of Diabetic Mellitus Edema (DME) (59). In vitro BRB model was assembled by culturing BRECs with BRPCs and/or astrocytes on the collagen-coated transwell insert and the barrier properties are assessed by measuring TEER values. VEGF-dependent changes occurring in DME were assessed by examining specific in vivo BRB properties, including expression of endothelial junction proteins (occluding, claudin-5, VE-cadherin and ZO-1), and the specific pumps (glucose transporter-1, and efflux transporter P-glycoprotein). By using electrode-embedded microchips, Wang et. al. built a tri-culture in vitro blood-brain barrier model (BBB) that replicated the anatomical organization of BBB (60). Mouse brain microvascular ECs, pericytes, with/without astrocytes were seeded in layered microchannels forming three-dimensional bi- and triculture models of the BBB. The microfluidic device was made of upper and lower PDMS microchannels separated by a porous membrane (Fig. 1.4-2 a) with Ag/AgCl electrodes embedded in the respective channels (Fig. 1.4-2) to take real-time transepithelial electrical resistance (TEER) measurement across cultured ECs.
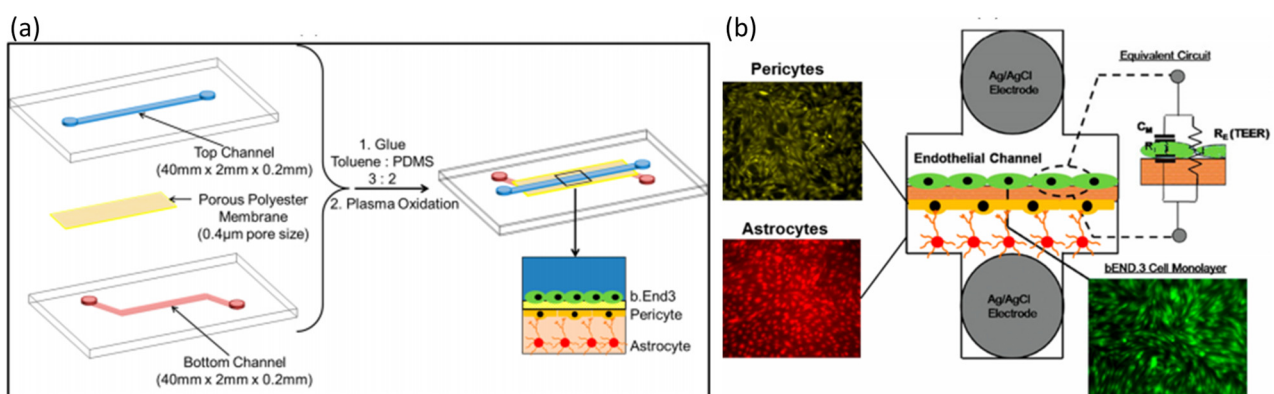
Fig. 1.4-2 Electrodes-embedded microfluidic device for evaluating the barrier function of the monolayer of cells.

(a) exploded view of the device; (b) Ag/AgCl electrodes were embedded in the upper and lower channels of the microfluidic device for the direct measurement of transepithelial electrical resistance (TEER). Figures were reproduced from (60) with permission.

An alternative approach to evaluate the barrier property is by quantifying the permeability of fluorescence molecules via fluorescence microscopy. Chrobak et. al. fabricated a perfusable, functional in vitro microvessels of human umbilical vein endothelial cells (HUVECs) and human dermal microvascular endothelial cells (HDMECs) using the subtractive method (61). In the study, Alexa-Fluor-488-labeled bovine serum albumin (BSA) or Alexa-Fluor-488-labeled 3 kDa dextran were perfused in the microvessels. Intensity of fluorescent

molecules diffused to the surrounding matrix at different time points was quantified to evaluate the permeability and the barrier function when different biologics were perfused in the microvessels (histamine, thrombin, and TNF-α).

1.4.3 Effect of shear stress

Physiological blood flow parameters such as shear stress have a critical role in vessel maturation and stabilization. Changes of the retinal vascular caliber have been found to associate with vascular damage from aging, arteriosclerosis, inflammation and endothelial dysfunction (62). Not limited to retinopathy, changes of the retinal vasculature have been found to associate with stroke (63) and patients of Alzheimer's disease (64). Studies of the vascular response to shear stress have broad clinical relevance in vascular homeostasis and pathophysiology, as found in the case where atherogenic phenotype of ECs is induced under low or unsteady shear levels (58). Fluidic shear stress is found to regulate angiogenic sprouting, and studies have found significant changes in the orientation of ECs and vascular architecture when grown under dynamic flows (65). The vessels degrade under absence of any special treatment, often sloughing off as a sheet or denuding as individual cells resulting in a substantially decreased perfusion rate (55). Galie et. al. investigated the threshold of fluidic shear stress that regulated angiogenic sprouting, specifically focusing on the effects of transmural and luminal flows on the endothelium (66). Microvessels (~400 μm in diameter) were fabricated using the subtractive method and encased in a bilayer PDMS adhered to a glass coverslip. A linear syringe pump was used to generate flow in the microvessels. The group demonstrated that a threshold of shear stress above 10 dyn/cm^2 would induce sprouting regardless of whether the shear is exerted by transmural or luminal fluid flow. They further found that both types of flow induced expression of matrix metalloproteinase 1, and the up-regulation was required for the flow-induced sprouting. For interconnected vascular networks, consistency of shear throughout the network is important in obtaining tight barrier function and that the global shear stress should be above 15- 20 dyn/cm^2 to eliminate focal leaks (53).

Mechanical signals such as hydrostatic pressure, stretch, and shear stress are shown to exert pleiotropic effects on vascular function (53). Acute increases in shear stress weakens the barrier function of endothelial monolayers whilst chronic exposure (over 24 h) to elevated shear appears to enhance barrier function in vitro (53). Price et. al. investigated effect of chronic exposure to various mechanical factors on engineered microvessels (53). Specifically, the shear stress, luminal pressure and transmural pressure (as measured by radial strain) were imposed on the vessels of three configurations: single cylindrical vessels, tapered vessels and vessels aligned parallel to an empty channels. Vascular stability was evaluated based on permeability to molecular tracers and adherens junction marker VE-cadherin. The authors found that shear stress was the dominant regulator of the barrier function, while transmural pressure was the main factor in vascular stability (53). Barrier-promoting effects of shear stress are thought to be due to activation of the small GTPase Rac, which leads to active reorganization of actin filaments.

1.4.4 Thrombosis studies

Thrombosis is the process whereby a blood clot, or thrombus, forms in a blood vessel, obstructing the flow

through the circulatory system. Under normal circumstances, the endothelium provides a nonadhesive and antithrombotic interface for the transport of blood through the vessel, whereas during inflammation, the endothelium promotes the formation of the thrombi via local expression and secretion of adhesive proteins (67). Zheng et. al. investigated angiogenic remodeling and thrombosis using a microfluidic vascular network (µVN) under normal and pathological conditions (67). The µVNs in a quiescent state and a stimulated state induced by exposure to phorbol-12-myristate-13-acetate (PMA) were examined, during which whole human blood (citrate-stabilized with labeled platelets) was perfused. Results showed that in stimulated vessels, large aggregates of platelets formed immediately on the endothelial surface, grew to fill a substantial fraction of the lumen and were shed into the flowing blood. Platelets continued to accumulate over time on the vessel wall, and leukocytes were observed to attach and migrate through the endothelium into the collagen matrix.

Many angiogenesis inhibitors have been linked to an increased risk for thrombosis although the mechanisms remain ill defined (68). For instance, complications in patients during treatment with bevacizumab (Avastin) combined with chemotherapy include, but not limited to, hypertension, bowel perforation, and particularly toxicities in relation to thromboembolic complications (68). The µVN platform opens the possibility to further investigate blood-endothelium interactions and stability of the blood vessels under hydrodynamic stresses and transport processes. Furthermore, it has the potential to advance our understanding on inflammatory responses and tumor-associated neoangiogenesis in drug testing and drug-delivery strategies that target microvascular function.

1.4.5 Neovascularization studies
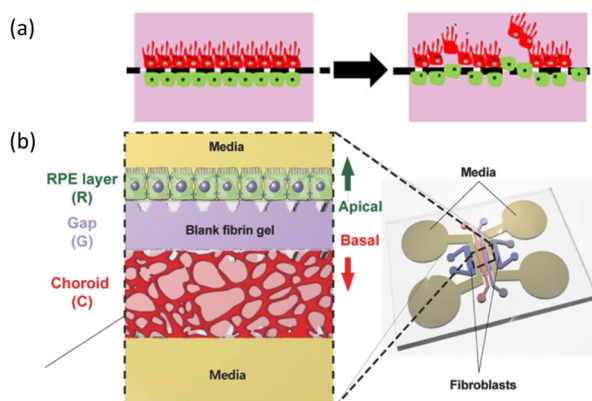
Fig. 1.4-3 Two of the common approaches to studying neovascularization examining (a) cell migration (69) **and (b) morphological changes of the vasculature** (51) **over time. Figures were reproduced with permission.**

As the first step of angiogenesis involves breakage of the basement membrane and migration of endothelial tip cells (70), cell migration is extensively studied using a variety of platforms. Cell-cell interactions have been investigated using planar, membrane-less microfluidic devices in a tumor/endothelium co-culture model with two detachable, complementary substrates made of polystyrene (PS) and polydimethylsiloxane (PDMS) (71). In a slightly different fashion, a microfluidic device with microchannels separated by a porous membrane was

used to study oBRB and pathological angiogenesis (69). The cellular interactions between co-culture of HUVEC and ARPE-19 under altered microenvironments were studied and the results showed heterotypic interactions between the cells inside the microfluidic device (Fig. 1.4-3 a). In another study modeling wet AMD on-a-chip (Fig. 1.4-3 b) (51), ECs were allowed to self-organized into 3D vascular networks within the fibrin hydrogel matrix, adjoining the RPE monolayer. The device was designed such that ECs, RPE and fibroblasts could be cultured in separate microchannels. The microchannels were separated by an array of microposts that enabled surface tension-guided patterning of the fibrin matrix in the channels (51). Choroidal neovascularization was stimulated; inhibitory effect of an antiangiogenic compound, bevacizumab, was used to alleviate the pathological angiogenesis using the model. In a different study, Nguyen et. al. focused on the in vitro vasculature under angiogenic conditions inside the microfluidic device (72). Using the subtractive method, parallel cylindrical channels encased in a collagen matrix within a microfabricated PDMS gasket were fabricated and connected to fluid reservoirs. Angiogenic factors were perfused in an empty channel, exposing the endothelial-lining channel to a gradient of angiogenic factors. Invasion and sprouting under effects of various proangiogenic factors were analyzed. The potential utility of these models span from elucidating the molecular mechanisms to modeling pathological neovascularization under different angiogenesis stimuli and/or shear stress.

1.4.6 Signaling studies

The versatile microfabrication technique allows studying single-cell response to certain external stimuli. Moreover, fabricating platforms capable of point access reagent delivery to probe the transport of signaling events is possible. Dodson et. al. fabricated a microfluidic tissue culture platform with multiple reagent access points for probing tissue slices (Fig.1.4-4, (73)). Negative pressure (~7 kPa) was applied onto the whole mice retina to pull it into tight contact with the thin film PDMS layer, which confined the tissue to the access point only. The histological stain toluidine blue was used to test the delivery of reagents to specific points of the intact tissue. The retina-on-a-chip also has the potential to be used for studying complex interactions between various kinds of cells and localization of signaling molecules or drugs.
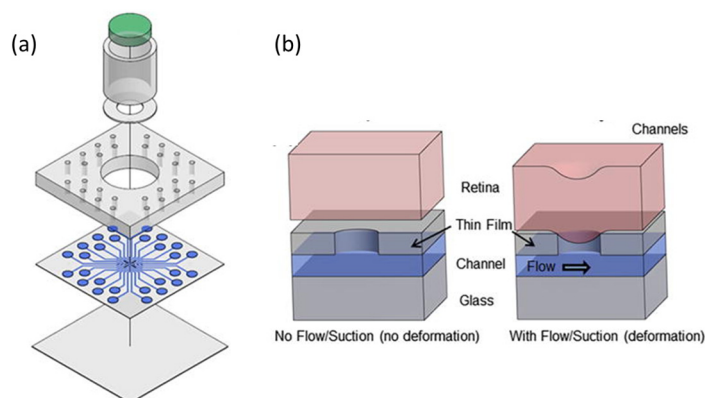
Fig.   1.4-4 Microfluidic platform for point access reagent delivery.
(a) exploded view with media cylinder (consisting the retina well, agar gel (green, at the top), glass cylinder), a thin film PDMS layer with access through-holes, the molded microchannel from PDMS, and a glass coverslip; (b) schematics of deflection of retina into through-holes in PDMS thin film layer. Without flow or suction, the retina

does not deform and seal the through-hole and channel; the retina deforms when negative pressure is applied to the outlet, sealing the access channel and allowing for fluid flow. All channels are 300 μm wide and all through-holes are 1 μm in diameter. Figures were reproduced from **(73)** with permission.

1.5   Model of in vitro microvessels

The models described below are designed to investigate particular types of vasculature development. Angiogenesis is modelled by inducing sprouting from existing monolayers of ECs (similar to that in vivo) by seeding cell monolayers onto the surface of a gel or by entrapping EC-coated microcarrier beads within a gel (44) . Vasculogenic models use ECs dispersed throughout a scaffold, and observe their spreading and association into microvessels (44) . Depending on the design and fabrication techniques, microvessel models vary in complexity and physiological relevance.
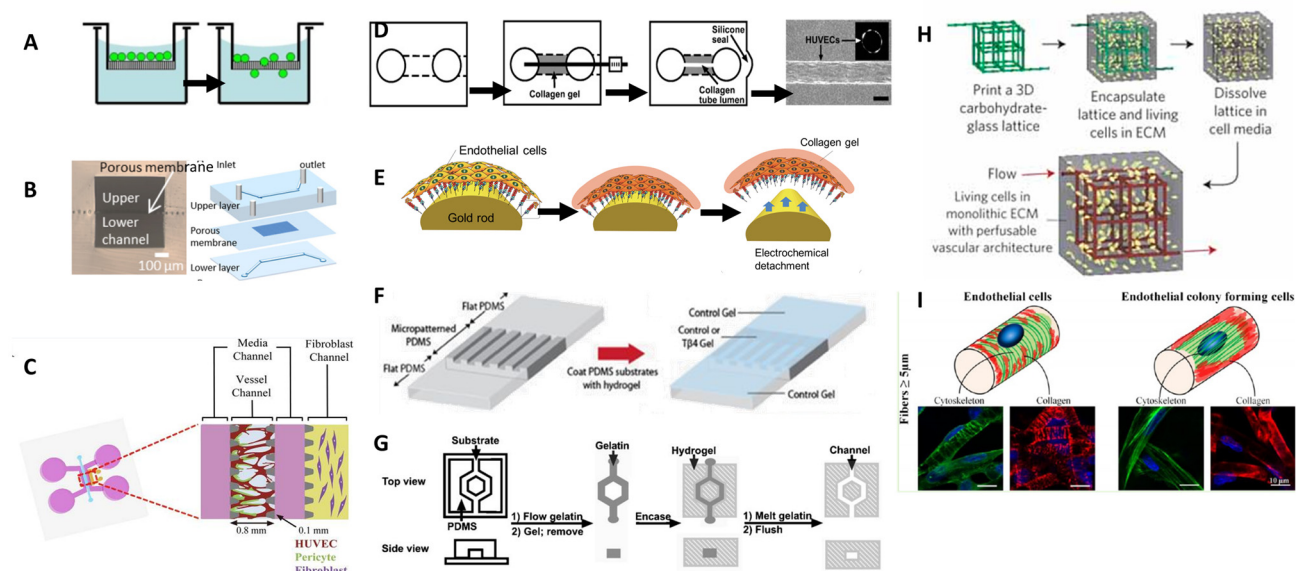
Fig.   1.5-1 Different approaches to study angiogenesis and to fabricate microvessels.

(A) Schematic of Boyden Chamber Assay for chemotaxis studies; cells are depicted as green circles (41). (B) Microfluidic device used for investigating co-culture (HUVEC/ARPE-19) under angiogenic stimuli. Microscopic cross-section (left) with a porous membrane separating the microchannels; exploded view of the microfluidic device (right) (45). (C) Microfluidic device for vasculogenesis and angiogenesis study: microchannels separated by micropillars can house hydrogels in the desired channel; ECs sprouting and vessel formations through spacing between micropillars could be observed (46). (D) Subtractive method whereby a needle is removed once the collagen gel has polymerized, leaving an empty microchannel. ECs are seeded into the microchannel, forming microvessels (47). (E) HUVECs are electrochemically transferred from cylindrical needles (template) to the collagen gel, forming in vitro microvessels in a rapid manner (48). (F) Micromolding is used to make patterned surface for guiding cellular alignment and growth to fabricate microvessels (49). (G) Microfluidic gels fabricated from embedding collagen gels over the sacrificial element (gelatin), patterned using the substrate fabricated from soft lithography. Gelatin is washed away after collagen has gelled (50). (H) Sacrificial molding from a 3D printed template in constructing patterned vascular architectures; carbohydrate glass lattice (agarose, alginate, PEG,

fibrin and matrigel) is encapsulated in ECM and dissolved in cell media (51). (I) Effect of microenvironment (fiber diameters) and cell types (endothelial colony forming cells vs. HUVECs) in fabricating in situ vascular TE (52). All figures were adapted and reprinted with permission.

1.5.1 Microfluidics-based models.

Advances in micro- and nano-fabrication technologies have enabled exploitation of microfluidic devices. For example, photolithography can be used to design and fabricate a structure customized to a particular experimental objective. Once the master mold is constructed, rapid prototyping of microfluidic devices via soft-lithography is possible. The technology is versatile and allows production of a variety of microfluidic devices for various applications. Descriptions of the fabrication processes involved in photolithography and soft-lithography have been presented elsewhere (53–60) .

The Boyden assay, originally designed for the analysis of leukocyte chemotaxis, is based on a chamber of two medium-filled compartments separated by a microporous membrane (Fig. 1.5-1 A, (41)). In many ways microfluidic devices complement the Boyden assays for investigating EC proliferation and migration. With a similar configuration to the Boyden assay, the microchannels within a microfluidic device are compartmentalized using a porous membrane (Fig. 1.5-1 B, (45)), allowing studies designed for co-cultures or tri-culture of cells. Cell-cell interactions have also been investigated using planar, membrane-less microfluidic devices such as in a tumor/endothelium co-culture model (HeLa/HUVEC) with two detachable, complementary substrates made of polystyrene (PS) and polydimethylsiloxane (PDMS) (61). Cell-cell migration and invasion have been analyzed by monitoring the direction and speed of movements of cells (61). To demonstrate the versatility of these systems, a microfluidic device was assembled with a detachable substrate and a PDMS channel patterned by soft lithography and a glass plate to investigate the effect of directed medium flow in HeLa/HUVEC co-cultures (62). In contrast to static culture assays, microfluidic systems provide a controllable microenvironment where mechanical properties can be modulated.

As the ECM consists of collagen, fibronectin, and other cell types, a Microfluidic devices in which hydrogels can be incorporated into the micro-chamber have been developed to provide cells with a more in vivo-like microenvironment. Hydrogels are confined in the desired microchannels and demarcated using micro-pillars, as shown in Fig. 1.5-1 C (46). As ECM provides anchorage points for cells and serves as a reservoir of growth factors, the cultured cells have different morphologies compared to those cultured without hydrogel. Natural ECM such as collagen, fibrin, or a mixture of hydrogels at a different ratio has been loaded into devices to support the growth of cells. Optimization of techniques for cell manipulation in culture will allow cells to express their inherent biological characteristics inside the microdevices.

The next step up from a single model platform is use of so-called 'organs-on-chips', which permit studying tissue- and organ-level physiology. In an organ-on-chips model, the microarchitecture and/or organ-specific microenvironment is designed to intrinsically mimic the function of the organ (63). For example, a biomimetic lung-on-a-chip microdevice has been developed that mimics inhalation by mechanical stretching of a flexible

PDMS membrane (64). In order to test whether the microsystem showed pulmonary inflammation as in a whole living lung, immune cells were included in the fluid flowing through a channel and neutrophil recruitment was observed; this experiment proved that the microdevice could display organ-level responses (64). Ghaemmaghami et al. recently reviewed the key microengineering technologies for biomimetic tissues on a chip (intestine, liver, lung, muscle, etc.) that can be used for diagnostics and drug screening applications (65). Organ-specific on-chip models are summarized in Table 1.

1.5.2 In vitro assembly of vessels with cells and degradable synthetic or biological scaffolds.

A range of natural and synthetic hydrogels have been used as the ECM matrix scaffold in fabricating TEBVs, including collagen, fibrin, matrigel, poly(ethylene glycol) diacrylate (PEGDA), poly(glycerol-sebacate) (PGS), poly-caprolactone (PCL), and silk fibroin protein. Some experiments have made use of variant microfluidic device models that exploit a subtractive method in their construction. First, a needle or wire (at the desired diameters, typically in the micron range) is inserted in a gel precursor; the needle/wire is then removed after polymerization to fabricate microchannels (Fig. 1.5-1 D, (47)). The end result is the formation of a hollow microchannel where ECs can be seeded for angiogenesis research. Using a similar strategy, so-called "sacrificial molds" can be used as a template for patterning microvasculature (photolithographic patterned molds, Fig. 1.5-1 G, (50)) or 4D tissue constructs (Fig. 1.5-1 H, (51)). These templates are encapsulated within ECM and dissolved once the hydrogel has been cross-linked. Patterning vasculature using a 3D printer (Fig. 1.5-1 H (51), 4A) is another rapid and inexpensive way for generating desirable structures (e.g. convoluted tumor vessels). In vitro microvessels have also been fabricated by inducing directed capillary sprouting using micropatterned substrates (Fig. 1.5-1 F, (49)) or by electrochemically transferring confluent cell sheets grown on needles (Fig. 1.5-1 E, (48)). The technical details of fabrications of in vitro microvessels and the characteristics of these microvessels are summarized elsewhere (1,66). Large vessels (greater than 5 mm in diameter) may be replaced by alloplasts such as polytetrafluoroethylene (PTFE), a material causing problems with patency particularly in low-flow conditions for vessels smaller than 5 mm (67).

1.5.3 Scaffold-free self-assembly from cell sheets.

Microvascular assembly and lumen formation can be studied by self-assembly of ECs seeded onto or embedded into gels. In the gels, the ECs form complex topologies patterned by nature with lumen sizes of the same order of magnitude as native capillaries (44,47). Open lumens formed via self-organization of ECs, however, have not been shown to be capable of producing functionally interconnected microvessels (47). L' Heureux et al. introduced cell sheet tissue engineering in which non-aligned sheets of SMCs are cultured and rolled into tubes to create the medial layer of a blood vessel; sheets of non-aligned fibroblasts are then rolled outside the SMCs to create the outer layer of the blood vessel (tunica adventitia) (14,67). Finally, ECs are seeded inside the tubular structure and grown to confluence. The constructs undergo maturation in a pulsatile bioreactor and the fibroblasts and SMCs align around the circumference and generate their own ECM, thereby generating an in vivo engineered BV that prevents aneurysm and rupture (14). The maturation step allows SMCs to differentiate from a synthetic to a contractile phenotype, which is necessary for the vessel to develop the appropriate contractility (14). The sheet-based approach can also be exploited for fabricating 3D

vascularized tissue by directly delivering the cell sheet to the injured tissues or by stacking 2D vascularized tissues into thick 3D structures.

1.5.4 Remodeling of nascent vasculature and design considerations of TEBVs.

Newly formed in vivo vasculature is constantly subjected to physiological and pathological remodeling; it is therefore important to incorporate physiological considerations into TEBVs as much as is feasible. Nascent vessels formed through angiogenesis need to undergo maturation or vessel regression will occur (68). The morphology of vessels is controlled by mural cells that are modulated by both EC signaling responses and contractile vasoconstriction, which collectively regulate hemodynamic parameters (69). Heterotypic cell-cell contacts between ECs and mural cells affect the activities of paracrine factors such as VEGF which regulate EC responses (69). By providing heterotypic cell-cell contacts and ECM deposition and soluble factors, mural cells play an important role in keeping capillary diameters uniform; the cells also play a role in homeostasis, which further implies an enhanced blood flow to the tissues (69).

The orientation of the ECM orientation and the components of the blood vessels govern mechanical properties such as the elasticity of the vessels, and specific characteristics such as anisotropic responses to stress/strain conditions, non-linear stiffening, and the strength to strain rate (1). It has been shown that 3D scaffold topography and the presence of TGH- 1 increase elastin gene expression and synthesis of contractile markers by human coronary artery SMCs but do not affect elastin synthesis in 2D cultures (14). Due to phenotypic plasticity of SMCs, the absence of an intact endothelium induces conversion of SMCs to a more synthetic phenotype resulting in cell proliferation, MMP mediated enzymatic degradation of ECM and vessel wall remodeling via newly secreted ECM (14). Additionally, SMC proliferation and migration are inhibited by elastic fibers, which comprise 30-50% of the dry weight of native vascular tissues (14). Substrate composition and topography influence elastin production by SMCs or fibroblasts, which is otherwise prevented in TEBVs by reduced translation of tropoelastin mRNA in cells (other than neonatal cells) and by inefficient tropoelastin recruitment and crosslinking into the elastic matrix (14).

During remodeling of the vasculature, lumen diameter and wall thickness change in response to local needs (67). The ECs respond to intraluminal factors such as perfusion rate and fluid flow shear stress, and extraluminal metabolic factors such as oxygenation, to produce the mature vascular network (67). Hemodynamic factors are critical for survival of vascular networks and for structural adaptations of vessel walls (2). Fluid shear stress stimulates ECs to produce nitric oxide and prostacyclin, which are antithrombotic and promote vasodilation by SMCs (14). Maturation of the nascent vessels is controlled in part by a spatio-temporal pattern and concentration of signaling cues presented to ECs. Shear stress modifies the contact between neighboring ECs and the ECM, which in turn upregulates growth factors such as PDGF. The increase in growth factors activates downstream pathways by attracting perivascular cells and promoting their attachment to the endothelium (67). The oxygen levels within tissues also regulate vasculature remodeling. Hypoxic tissues secrete growth factors and chemokines that stimulate the formation of a functional vessel (angiogenesis). When perfusion of the tissue increases and the supply of oxygen meets demand, quiescence

can be re-established resulting in a stable vascular network. Dysfunctional vascular remodeling due to an imbalance between vasodilators (nitric oxide) and vasoconstrictors (endothelin-1) results in irreversible loss of vessels and thickening of the vascular muscular coat, as found in chronic obstructive lung disease (33). Taken together, a mature blood vessel is dependent on multiple interconnected factors; from the presence of necessary components such as mural cells to the presentation of receptors in the microenvironment will all affect the downstream signaling cascades hence the nature of the vasculature.

1.6   Motivation behind development of the retina-on-a-chip

As discussed in the retinal diseases (Chapter 1.3), **many of the retinal diseases involved compromised blood-retina barrier (BRB, Fig.1.3-1), including the debilitating mascular edema, diabetic retinopathy (DR), and age-related macular degeneration (AMD)**. Clinical evaluations of the retina employing fundoscopic examination, angiography, vitreous fluorometry and optical coherence tomography have aided ophthalmologists in diagnosing the retinal vascular diseases (retinopathy). However, these examinations, as well as cross-sectional studies allow only observations of the resulting diseased vasculature and are limited to finding causes to the disease. **In order to further understand the disease pathophysiology, and to perform preclinical tests on the effect of ocular drugs, models of the retina offers a better approach**.

Microfabrication is an emerging technology for patterning and fabricating devices at micro and nano-scale. Such techniques allow for precise control over surface microarchitecture, topography and feature size (2). Organ-on-a-chip models are developed based on the MEMS technology, enabling cell cultures or ex vivo tissues to be grown on pre-designed in vitro microchip over a period of time. On-chip analysis is made possible by miniaturizing chemical and biological reactions, facilitating genomic screening, pharmaceutical development and diagnostic medicine. The advantages of microscale devices are that they are portable, and implantable, which are also a desirable property for drug delivery devices (DDS). The technical details of microelectromechanical systems (MEMS) manufacturing technologies (3, 4) and soft lithography on cell culturing have been reviewed elsewhere (5, 6) and are not focused here. This chapter highlights the applications of the microfluidic models in studying retinal vascular diseases and the potential applications of the disease models in evaluating ocular drugs. The background on anatomy and retinal vascular diseases are outlined, followed by biomimetic microenvironment platforms and engineered retinal vessels. The design considerations of the models are also mentioned throughout the relevant sections.

One of the most advanced and rapidly developed applications of MEMS is organ-on-a-chip, a 3-D microfluidic cell culture chip that sustains one or more types of cells or tissues. Literally, microfluidic refers to manipulating fluids at microscale. This approach enables maintaining growth and proliferation of cells continuously in vitro. Human lung, gut, kidney, liver, brain and more tissues have been cultured in microfluidic chips. Out of all the organs being reproduced, however, **less attention is focused on eyes**. Vision, one of the senses that humans rely heavily on without realizing it, is **affected even with a slight alteration in eye pressure or glucose level**, let alone external injuries. Due to the complexity and being a fragile organ, investigations on eye diseases have

been difficult and getting inconsistent results is not unusual. Therefore, **the aim here is to develop microfluidic models of the BRB in the hope to use them as disease models for studying retinal vascular diseases**.

1.7 Scope of the research

1.7.1 Level of the biological model

The BRB models developed here are limited to cellular level analysis, investigating responses of cells and microvessels under angiogenesis-related factor as well as interactions between cell-cell (oBRB, Chapter4), cell-vessel (oBRB, Chapter 5) and sprouting vessel-ECM and sprouting vessel-mural cells (iBRB, Chapter 6) under pathological microenvironments.

1.7.2 Methods on mimicking pathological angiogenesis

Many factors contributed to pathological angiogenesis and most of them work in cohort in spatiotemporal relationships. Due to the complexity involved in the biological pathways, pathological angiogenesis-related factors investigated are limited to altering glucose concentration (imposing oxidative stress), hypoxia, and elevated Tumor Necrosis Factor (TNF)-alpha concentration (mimicking inflammation).

1.7.3 Evaluation methods

Morphological changes of cells and microvessels are evaluated in conjunction with the functional responses. Microvascular morphology, cell-cell interactions, and cell-vessel interactions are processed and analyzed with image processing. Functional responses are analyzed by (1) barrier functionality and (2) secretion of cytokines under stimulation.

The cells contributing to the barrier functionality (human retinal pigment epithelial cells, ARPE-19 and human retinal microvascular endothelial cells, HRMEC) are evaluated in the transwell culture and in the microfluidic devices. In evaluating the barrier function of the proposed models, trans-epithelial electrical resistance (TEER) and/or perfusion of fluorescently labelled molecules across the barriers are used. Quantification of cytokines is based on Enzyme-linked immunosorbent assay (ELISA) and flow cytometry (FACS).

1.8 Significance of the developed BRB models

1.8.1 Specificity of the developed biological models

As aforementioned, ocular models especially retina-on-chip models have not been well-developed, and many studies employed human *dermal* microvascular endothelial cells or *bovine* endothelial cells in formation of microvasculature. In this study, cell types specific to the *human retina* are used to minimize variations in results that might arise using cells from other origins or species. As the inherent properties of endothelial cells (ECs) differ between origins and species, the BRB models developed here adopt ARPE and HRMEC for investigation of inflammation, while HUVEC is used in studying vascularization and used as the model of choroids. As

opposed to many of the published co-culture models that used conditioned medium in evaluating the effect of relationship between different cell types, direct-contact of co- and tri-culture cells and/or vessels in one device are developed here, mimicking the anatomy of the oBRB and iBRB. This takes into account the spatiotemporal relationships of multiple factors and cytokines involved, as well as the short half-life of growth factors such as VEGF and bFGF that might lose their activities due to the time lapse in collecting and imposing the conditioned medium, biasing subsequent observation and findings.

1.8.2 Design of the proposed microfluidic device

The design of the one-layer multichannel device is not novel, but based on based on Jeon research group (46) and Kamm research group (70). However, analysis of microvasculature models is mostly qualitative to date; here quantification of vasculature, as well as, qualitative analysis in conjunction with functional response of cells and microvessels are used to evaluate the models. This provides new angle of analysis of microvasculature and cell-vessel interactions under pathological microenvironments.

Adding to the pre-existing design, the one-layer device is modified into a two-layer multichannel microfluidic device here and to my knowledge it is also the first in vitro microfluidic model design that offer two advantages: (1) The device proposed in this study can be used as a multi-culturing cells and/or vessels model for various applications, with the potential of connecting individual fluidic devices in a fluidic network, mimicking human physiology as demonstrated in the work of Edington et. al. (71); (2) the device is modifiable with insertion of electrodes for TEER measurement. The top-down multichannel microfluidic device has proven to be versatile and applicable for studying different organs of origins and the device is discussed in Chapter 5.

1.8.3 Clinical significance of the research findings

The significance of the research findings on clinical settings and hopefully, contribution to translational research from each model is described herein.

oBRB cell-cell model

Direct co-culture of the ARPE-HUVEC cell-cell heterotypic interactions under pathological microenvironments are identified, contributing to the disease model of the oBRB and in vitro angiogenesis process.

oBRB cell-vessel model

The direct-contact co-culture of ARPE- HUVEC model is developed, but has not been thoroughly tested as a disease model in this work. The multi-culturing model is promising, however, in providing insights on cell-vessel interactions for studying disease pathophysiology in the future.

Angiogenesis sprouting model of the iBRB

There are only limited published in vitro iBRB models; while many models have been developed using ECs

non-specific to the retina, most of them made use of the non-direct culturing system. Although the proposed iBRB model here is at the preliminary stage, HRMEC under inflammatory conditions, and the roles of human retinal pericytes (HRP) and hepatocyte growth factor (HGF) in angiogenesis sprouting are investigated, adding to understanding of different factors involved in controlling angiogenic sprouting.

Overall, there is a huge potential of the developed models to be used as in vitro disease models and as drug testing platforms. As angiogenic switch remains unclear and angiogenesis plays a huge role in tumor microenvironment, the models have a huge potential in investigation systemic effects on the retina.

1.9   Outline of the thesis

The remaining main chapters in this dissertation are organized as followed: The fundamental techniques necessary in building and evaluating microfluidic cell cultures are described in **Chapter 2** Materials and Methods. Other specific methods used but are not applicable for all BRB models are kept in the relevant chapter. In **Chapter 3**, a microfluidic oBRB direct-contact cell-cell model is developed and used as a model of pathological angiogenesis, investigating the cell-cell interactions of ARPE and HUVEC. **Chapter 4** evolves around development of microvascular models using microfabrication and tissue engineering techniques before finalizing the top-down tri-culture of oBRB cell-vessel model. It was then modified to evaluate the barrier function of ARPE by inserting platinum electrodes for trans-epithelial electrical resistance (TEER) measurement, demonstrating the feasibility of on-chip assessment of the epithelial barrier integrity. The focus is reoriented in **Chapter 5,** from the oBRB to the iBRB, discussing the sprouting models of retinal microvessel based on angiogenesis. Angiogenesis sprouting model of HRMEC was developed; the role of mural cell using HRP and one of the growth factors sustaining angiogenesis, the hepatocyte growth factor (HGF), secreted by normal human lung fibroblasts (NHLF) was investigated. The optimal angiogenesis sprouting model of the iBRB was proposed. **Chapter 6** concludes the three developed BRB models. Along with the limitations, the future perspective are given.

References

1. Hasan A, Paul A, Vrana NE, Zhao X, Memic A, Hwang Y-S, et al. Microfluidic techniques for development of 3D vascularized tissue. Biomaterials. 2014 Aug;35(26):7308–25.

2. Adair TH, Montani J-P. Angiogenesis [Internet]. San Rafael (CA): Morgan & Claypool Life Sciences; 2010 [cited 2017 May 15]. (Integrated Systems Physiology: from Molecule to Function to Disease). Available from: http://www.ncbi.nlm.nih.gov/books/NBK53242/

3. Raza A, Franklin MJ, Dudek AZ. Pericytes and vessel maturation during tumor angiogenesis and metastasis. Am J Hematol. 2010 Aug 1;85(8):593–8.

4. Saketkoo LA, Distler O. Is There Evidence for Vasculitis in Systemic Sclerosis? Curr Rheumatol Rep. 2012 Dec 1;14(6):516–25.

5. Kanwar JR, Mahidhara G, Kanwar RK. Antiangiogenic therapy using nanotechnological-based delivery system. Drug Discovery Today. 2011 Mar;16(5–6):188–202.

6. Carmeliet P, Jain RK. Molecular mechanisms and clinical applications of angiogenesis. Nature. 2011 May 19;473(7347):298–307.

7. Rouwkema J, Khademhosseini A. Vascularization and Angiogenesis in Tissue Engineering: Beyond Creating Static Networks. Trends in Biotechnology. 2016 Sep 1;34(9):733–45.

8. Yancopoulos GD, Davis S, Gale NW, Rudge JS, Wiegand SJ, Holash J. Vascular-specific growth factors and blood vessel formation. Nature. 2000 Sep 14;407(6801):242–8.

9. Madeddu P. Therapeutic angiogenesis and vasculogenesis for tissue regeneration. Exp Physiol. 2005 May;90(3):315–26.

10. Góth MI, Hubina E, Raptis S, Nagy GM, Tóth BE. Physiological and pathological angiogenesis in the endocrine system. Microsc Res Tech. 2003 Jan 1;60(1):98–106.

11. Lee K, Silva EA, Mooney DJ. Growth factor delivery-based tissue engineering: general approaches and a review of recent developments. J R Soc Interface. 2011 Feb 6;8(55):153–70.

12. Khan F, Tanaka M, Rafi Ahmad S. Fabrication of polymeric biomaterials: a strategy for tissue engineering and medical devices. Journal of Materials Chemistry B. 2015;3(42):8224–49.

13. Chung AS, Ferrara N. Developmental and Pathological Angiogenesis. Annual Review of Cell and Developmental Biology. 2011;27(1):563–84.

14. Fernandez CE, Achneck HE, Reichert WM, Truskey GA. Biological and engineering design considerations for vascular tissue engineered blood vessels (TEBVs). Curr Opin Chem Eng. 2014 Feb

1;3:83–90.

15. Costa C, Incio J, Soares R. Angiogenesis and chronic inflammation: cause or consequence? Angiogenesis. 2007 Sep 1;10(3):149–66.

16. Gerlowski LE, Jain RK. Microvascular permeability of normal and neoplastic tissues. Microvascular Research. 1986 May;31(3):288–305.

17. Brannon-Peppas L, Blanchette JO. Nanoparticle and targeted systems for cancer therapy. Advanced Drug Delivery Reviews. 2012 Dec;64, Supplement:206–12.

18. Bergers G, Benjamin LE. Tumorigenesis and the angiogenic switch. Nat Rev Cancer. 2003 Jun;3(6):401–10.

19. Albini A, Tosetti F, Benelli R, Noonan DM. Tumor Inflammatory Angiogenesis and Its Chemoprevention. Cancer Res. 2005 Dec 1;65(23):10637–41.

20. Stockmann C, Schadendorf D, Klose R, Helfrich I. The Impact of the Immune System on Tumor: Angiogenesis and Vascular Remodeling. Front Oncol [Internet]. 2014 Apr 8;4. Available from: http://www.ncbi.nlm.nih.gov/pmc/articles/PMC3986554/

21. Quail DF, Joyce JA. Microenvironmental regulation of tumor progression and metastasis. Nat Med. 2013 Nov;19(11):1423–37.

22. Stephenson JA, Goddard JC, Al-Taan O, Dennison AR, Morgan B. Tumour Angiogenesis: A Growth Area-From John Hunter to Judah Folkman and Beyond. Journal of Cancer Research [Internet]. 2013 Jul 28 [cited 2017 May 16]. Available from: https://www.hindawi.com/archive/2013/895019/abs/

23. Folkman J, Long DM, Becker FF. Growth and metastasis of tumor in organ culture. Cancer. 1963 Apr;16:453–67.

24. Hanahan D, Folkman J. Patterns and Emerging Mechanisms of the Angiogenic Switch during Tumorigenesis. Cell. 1996 Aug 9;86(3):353–64.

25. Verhoye M, van der Sanden BPJ, Rijken PFJW, Peters HPW, Van der Kogel AJ, Pée G, et al. Assessment of the neovascular permeability in glioma xenografts by dynamic T1 MRI with Gadomer-17. Magn Reson Med. 2002 Feb 1;47(2):305–13.

26. Vajkoczy P, Schilling L, Ullrich A, Schmiedek P, Menger MD. Characterization of Angiogenesis and Microcirculation of High–Grade Glioma: An Intravital Multifluorescence Microscopic Approach in the Athymic Nude Mouse. Journal of Cerebral Blood Flow & Metabolism. 1998 May 1;18(5):510–20.

27. Folkman J. Angiogenesis-dependent diseases. Seminars in Oncology. 2001 Dec 1;28(6):536–42.

28. Döme B, Hendrix MJC, Paku S, Tóvári J, Tímár J. Alternative vascularization mechanisms in cancer: Pathology and therapeutic implications. Am J Pathol. 2007 Jan;170(1):1–15.

29. Shirakawa K, Kobayashi H, Heike Y, Kawamoto S, Brechbiel MW, Kasumi F, et al. Hemodynamics in Vasculogenic Mimicry and Angiogenesis of Inflammatory Breast Cancer Xenograft. Cancer Res. 2002 Jan 15;62(2):560–6.

30. Staton CA, Stribbling SM, Tazzyman S, Hughes R, Brown NJ, Lewis CE. Current methods for assaying angiogenesis in vitro and in vivo. International Journal of Experimental Pathology. 2004 Oct 1;85(5):233–48.

31. Jain RK. Delivery of molecular medicine to solid tumors: lessons from in vivo imaging of gene expression and function. Journal of Controlled Release. 2001 Jul 6;74(1–3):7–25.

32. Folkman J. Role of angiogenesis in tumor growth and metastasis. Seminars in Oncology. 2002 Dec 16;29(6, Supplement 16):15–8.

33. Carmeliet P, Jain RK. Angiogenesis in cancer and other diseases. Nature. 2000 Sep 14;407(6801):249–57.

34. Giancotti FG. Mechanisms Governing Metastatic Dormancy and Reactivation. Cell. 2013 Nov 7;155(4):750–64.

35. Aguirre-Ghiso JA, Bragado P, Sosa MS. Targeting dormant cancer. Nat Med. 2013 Mar;19(3):276–7.

36. Granot D, Addadi Y, Kalchenko V, Harmelin A, Kunz-Schughart LA, Neeman M. *In vivo* Imaging of the Systemic Recruitment of Fibroblasts to the Angiogenic Rim of Ovarian Carcinoma Tumors. Cancer Res. 2007 Oct 1;67(19):9180–9.

37. Chen L-J, Kaji H. Modeling angiogenesis with micro- and nanotechnology. Lab Chip. 2017 Dec 5;17(24):4186–219.

38. Weibel DB, DiLuzio WR, Whitesides GM. Microfabrication meets microbiology. Nature Reviews Microbiology. 2007 Mar 1;5(3):209–18.

39. Joel Voldman, Martha Grey, Martin Schmidt. Microfabrication in Biology and Medicine. Annual Review of Biomedical Engineering. 1999;1(1):401–25.

40. Perestrelo AR, Águas ACP, Rainer A, Forte G. Microfluidic Organ/Body-on-a-Chip Devices at the Convergence of Biology and Microengineering. Sensors. 2015 Dec;15(12):31142–70.

41. Hulkower KI, Herber RL. Cell migration and invasion assays as tools for drug discovery. Pharmaceutics. 2011 Mar 11;3(1):107–24.

42.   Sackmann EK, Fulton AL, Beebe DJ. The present and future role of microfluidics in biomedical research. Nature. 2014 Mar;507(7491):181–9.

43.   Herland A, Meer AD van der, FitzGerald EA, Park T-E, Sleeboom JJF, Ingber DE. Distinct Contributions of Astrocytes and Pericytes to Neuroinflammation Identified in a 3D Human Blood-Brain Barrier on a Chip. PLOS ONE. 2016 Mar 1;11(3):e0150360.

44.   Morin KT, Tranquillo RT. In vitro models of angiogenesis and vasculogenesis in fibrin gel. Exp Cell Res. 2013 Oct 1;319(16):2409–17.

45.   Chen L-J, Ito S, Kai H, Nagamine K, Nagai N, Nishizawa M, et al. Microfluidic co-cultures of retinal pigment epithelial cells and vascular endothelial cells to investigate choroidal angiogenesis. Scientific Reports. 2017 Jun 14;7(1):3538.

46.   Kim J, Chung M, Kim S, Jo DH, Kim JH, Jeon NL. Engineering of a Biomimetic Pericyte-Covered 3D Microvascular Network. PLoS ONE. 2015;10(7):e0133880.

47.   Chrobak KM, Potter DR, Tien J. Formation of perfused, functional microvascular tubes in vitro. Microvasc Res. 2006 May;71(3):185–96.

48.   Osaki T, Kakegawa T, Kageyama T, Enomoto J, Nittami T, Fukuda J. Acceleration of Vascular Sprouting from Fabricated Perfusable Vascular-Like Structures. PLOS ONE. 2015 Apr 10;10(4):e0123735.

49.   Chiu LLY, Montgomery M, Liang Y, Liu H, Radisic M. Perfusable branching microvessel bed for vascularization of engineered tissues. PNAS. 2012 Dec 11;109(50):E3414–23.

50.   Golden AP, Tien J. Fabrication of microfluidic hydrogels using molded gelatin as a sacrificial element. Lab Chip. 2007 Jun;7(6):720–5.

51.   Miller JS, Stevens KR, Yang MT, Baker BM, Nguyen D-HT, Cohen DM, et al. Rapid casting of patterned vascular networks for perfusable engineered three-dimensional tissues. Nature Materials. 2012 Jul 1;11(9):768–74.

52.   Fioretta ES, Simonet M, Smits AIPM, Baaijens FPT, Bouten CVC. Differential Response of Endothelial and Endothelial Colony Forming Cells on Electrospun Scaffolds with Distinct Microfiber Diameters. Biomacromolecules. 2014 Mar 10;15(3):821–9.

53.   Madou MJ. Manufacturing Techniques for Microfabrication and Nanotechnology. CRC Press; 2011. 672 p.

54.   Campo A del, Greiner C. SU-8: a photoresist for high-aspect-ratio and 3D submicron lithography. J Micromech Microeng. 2007;17(6):R81.

55. Alderman BEJ, Mann CM, Steenson DP, Chamberlain JM. Microfabrication of channels using an embedded mask in negative resist. J Micromech Microeng. 2001;11(6):703.

56. Bratton D, Yang D, Dai J, Ober CK. Recent progress in high resolution lithography. Polym Adv Technol. 2006 Feb 1;17(2):94–103.

57. Lin C-H, Lee G-B, Chang B-W, Chang G-L. A new fabrication process for ultra-thick microfluidic microstructures utilizing SU-8 photoresist. J Micromech Microeng. 2002;12(5):590.

58. Kane RS, Takayama S, Ostuni E, Ingber DE, Whitesides GM. Patterning proteins and cells using soft lithography. Biomaterials. 1999 Dec 1;20(23):2363–76.

59. Qin D, Xia Y, Whitesides GM. Soft lithography for micro- and nanoscale patterning. Nat Protocols. 2010 Mar;5(3):491–502.

60. Park TH, Shuler ML. Integration of Cell Culture and Microfabrication Technology. Biotechnol Progress. 2003 Jan 1;19(2):243–53.

61. Kaji H, Yokoi T, Kawashima T, Nishizawa M. Controlled cocultures of HeLa cells and human umbilical vein endothelial cells on detachable substrates. Lab Chip. 2009 Feb 7;9(3):427–32.

62. Kaji H, Yokoi T, Kawashima T, Nishizawa M. Directing the flow of medium in controlled cocultures of HeLa cells and human umbilical vein endothelial cells with a microfluidic device. Lab Chip. 2010 Aug 25;10(18):2374–9.

63. Huh D, Hamilton GA, Ingber DE. From 3D cell culture to organs-on-chips. Trends in Cell Biology. 2011 Dec;21(12):745–54.

64. Huh D, Matthews BD, Mammoto A, Montoya-Zavala M, Hsin HY, Ingber DE. Reconstituting Organ-Level Lung Functions on a Chip. Science. 2010 Jun 25;328(5986):1662–8.

65. Ghaemmaghami AM, Hancock MJ, Harrington H, Kaji H, Khademhosseini A. Biomimetic tissues on a chip for drug discovery. Drug Discov Today. 2012 Feb;17(3–4):173–81.

66. Bogorad MI, DeStefano J, Karlsson J, Wong AD, Gerecht S, Searson PC. Review: in vitro microvessel models. Lab Chip. 2015 Oct 27;15(22):4242–55.

67. Oliver Cassell CS, Stefan Hofer OP, Morrison WA, Knight KR. Vascularisation of tissue-engineered grafts: the regulation of angiogenesis in reconstructive surgery and in disease states. British Journal of Plastic Surgery. 2002 Dec 1;55(8):603–10.

68. Freed LE, Guilak F, Guo XE, Gray ML, Tranquillo R, Holmes JW, et al. Advanced Tools for Tissue Engineering: Scaffolds, Bioreactors, and Signaling. Tissue Engineering. 2006 Dec 1;12(12):3285–305.

69. Hegen A, Blois A, Tiron CE, Hellesøy M, Micklem DR, Nör JE, et al. Efficient in vivo vascularization of tissue-engineering scaffolds. J Tissue Eng Regen Med. 2011 Apr 1;5(4):e52–62.

70. Chen MB, Whisler JA, Fröse J, Yu C, Shin Y, Kamm RD. On-chip human microvasculature assay for visualization and quantification of tumor cell extravasation dynamics. Nat Protoc. 2017 May;12(5):865–80.

71. Edington CD, Chen WLK, Geishecker E, Kassis T, Soenksen LR, Bhushan BM, et al. Interconnected Microphysiological Systems for Quantitative Biology and Pharmacology Studies. Sci Rep. 2018 Mar 14;8(1):1–18.

2   Materials and Methods

This chapter has established the necessary background behind this research. Specifically, relevant studies on applying microfabrication techniques on eye diseases were discussed. Subsequent chapters will focus on building angiogenesis models in an attempt to achieve the research aim outlined in the previous sub-section. The methods and protocols in photolithography, soft lithography, cell culturing, data capturing and data analysis are listed in this chapter. Parameters and cell types used for building each of the developed model are also summarized.

2.1   Fabrication of the microfluidic device
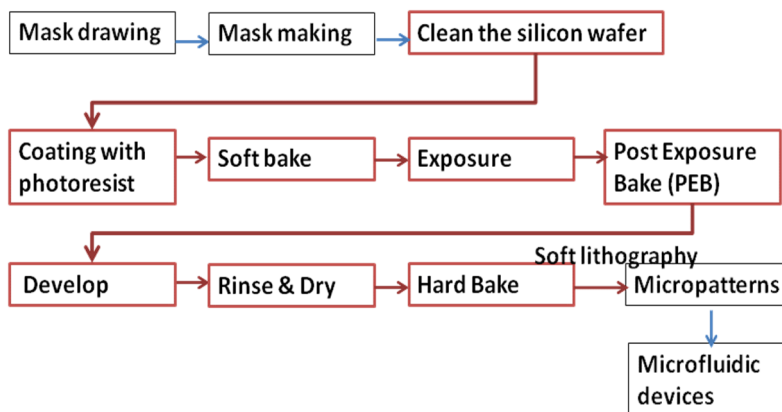
Fig.   2.1.1-1 Process flow of photolithography.

2.1.1 Photolithography

A photomask is an opaque plate (usually made of quartz) with holes or transparencies that allow light to pass through in a defined pattern. The desired pattern was designed in compatible software (AutoCAD, SOLIDWORKS, LayoutEditor etc). The files have to be saved in dxf extension in order to be read by the laser writer. Note also avoid lengthy file names for which the conversion software of the laser writer has difficulty opening the file.

2.1.1.1 Photomask fabrication

Once the design of a mask is drawn, masks can be made in the clean room, one of the facilities under the MNC center (Micro/Nano-Machining Research and Education Center) at the university. Briefly, the dxf file was converted into lic files that are used by the laser writer. Users are prompted to set values for various parameters. One of the important concepts is the choices of "layer". *Every layer that should become part of the conversion has to be selected*; "CUT", "OR", "XOR" functions are to be chosen between any two layers in the design (Fig. 2.1.1-1). The complete conversion process was provided in the user manual inside the facility.
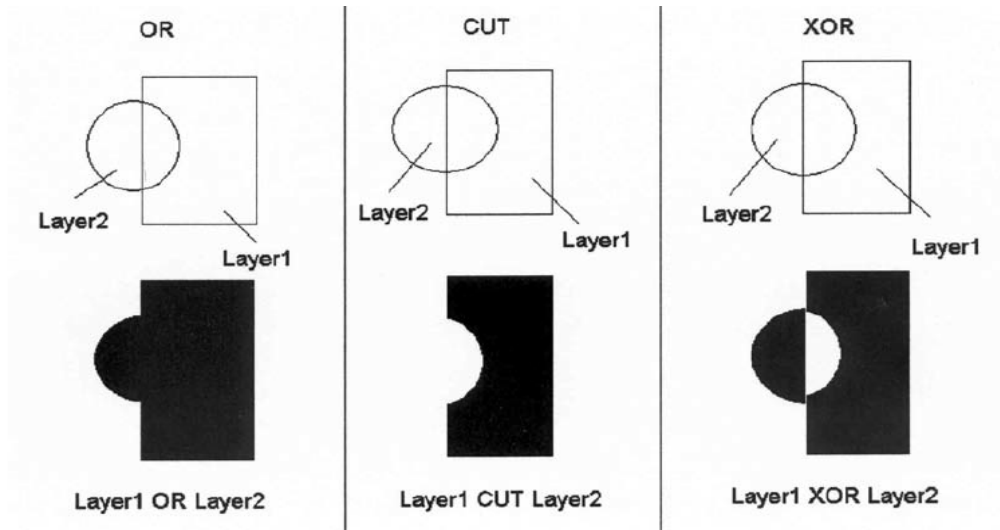
Fig. 2.1.1-1 Layer options for mask drawing software.

Photomask

The design patterns drawn from the software Layout editor.

Fig 2.1.1-2 shows the raw files of mask patterns for the microchannel and the micropillars that were used in this study.
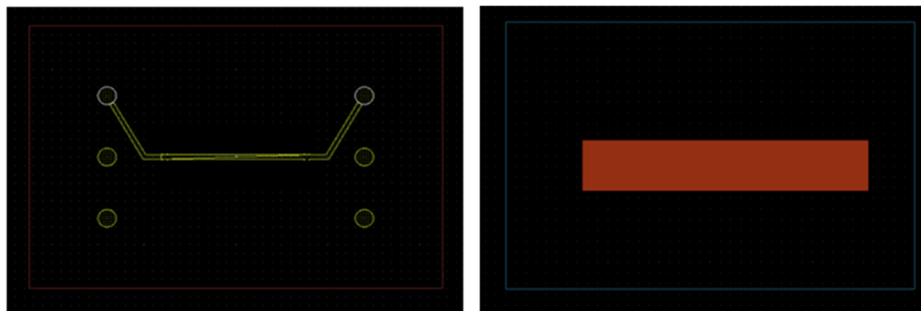
Fig. 2.1.1-2 Examples of the DXF files.

2.1.1.2 Making master molds

After the mask(s) was made, photolithography was performed to produce micropatterned silicon wafers – the master molds of microchannels and micropillars. Photolithography is the process of transferring geometric shapes on a mask to the surface of a silicon wafer – the concept of lift-off technique, where selective parts of photoresist (defined by a photomask) stays or removed depending on the types of photoresists used (SU-8 photoresist, AZ photoresist, etc.). The main steps had been illustrated in red boxes in the flow chart (Fig 2.1.1-1).

Protocol: photolithography (see Table 2.1.1-1)

1. In a fume hood, prepare the Piranha solution on ice by mixing H_2S0_4 and H_2O_2 (v/v: 3:1) inside PYREX glass (or glassware that has low-thermal expansion property). Add H_2O_2 into H_2SO_4 slowly by a dropper. Piranha solution should be prepared just enough so that silicon wafers can be immersed completely inside

the solution. Note that H_2O_2 is 30 % (w/w) in H2O.

2. Slowly, place the silicon wafers into Piranha solution. Leave the samples inside a fume hood overnight for the reactions to be finished.

3. Discard the Piranha solution accordingly, and wash the wafers with distilled water 3 times inside a sonicator. Dry and store silicon wafers in clean dishes until further use.

4. Place the silicon wafer on a 200 C hotplate for 5 min, make sure that vapours are completely evaporated. Remove the wafer, and wait until its temperature dropped back to room temperature.

5. Coat the wafer with SU-8 photoresist with empirically defined spinning parameters (see Table 2-1). Be careful of the air bubbles as it will generate discontinuity in the resulting structure.

6. Soft bake*: return the wafers back to the hotplate.

7. Exposure*: align the mask on the wafer – make sure there is no air bubbles trapped inside the photoresist. Place the wafer under UV light according to the set time.

8. Post exposure bake (PEB)*: immediately after the exposure, remove the wafer from the mask and return it to the hotplate. Patterns should be visible within 5 min after baking. Do not overbake the wafer; cool it down to room temperature before proceeding to the next step.

9. Developing: Inside a fume hood, agitate the wafers inside SU-8 developer. Leave it inside the solution until the photoresist has been completely washed away. The thicker the photoresist is, the longer the time it requires for the photoresists to come off. Should the SU-8 developer solution turns opaque, discard the used developer solution and wash the wafers in new one.

10. Dip the wafer into Ethanol-IP twice to wash the silicon wafer (twice, in 2 separate beakers). If the wafer does not come out clean after the wash step, change the opaque SU-8 solution to fresh ones and repeat step 9 again.

11. Hard bake: bake the silicon wafer at 150C for 30 min. Handle the wafers carefully and prevent scratching micropatterns off. Do not shorten the hard back time. Cool the wafer down to room temperature.

Master molds

The master mold patterned from photolithography step (Fig. 2.1.1-3). They are used for as master molds for fabricating microchannels and the porous membrane.
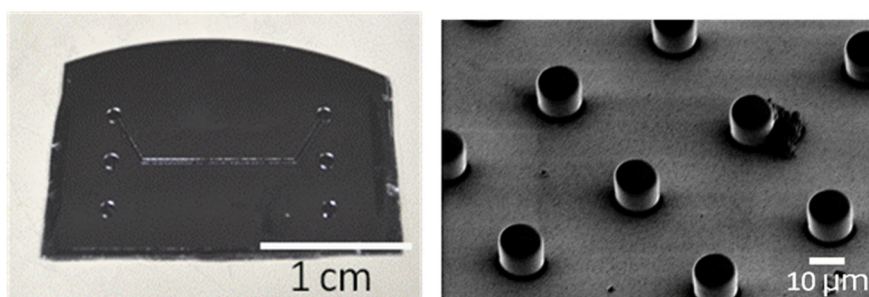
Fig. 2.1.1-3 Images of the silicon master molds. Left: silicon wafer with the patterned microchannel; right: micropillars inclined 30 degrees under a SEM microscope.

Table 2.1.1-1 Parameters for photolithography..

Refer to the photolithography protocol. Abbreviations: RT, room temperature; RPM, revolution per .minute.

	oBRB cell-cell model, microchannel (chapter 3)	oBRB cell-cell model, micropillars (chapter 3)	oBRB cell-vessel model, bottom layer (chapter 4)	oBRB cell-vessel model, top layer (chapter 4)	iBRB model (chapter 5)
Height (micron)	100	10/40*	200	200	200
Coating	SU-8 3050 500 RPM 10s, 1200 RPM 30s	SU-8 3050 500 RPM 10s , • 10 μm pillar : 3000 RPM, 60s (100 RPM/s) • 40 μm pillars: 5000 RPM 100s (100 RPM/s)	SU-8 2100 500 RPM 10s, 1500 RPM 30s	SU-8 2100 500 RPM 10s, 1500 RPM 30s	SU-8 2100 500 RPM 10s, 1500 RPM 30s
Soft bake	65°C 5min, 95° C 45min.	65°C 5 min, 95°C 30 min	65° C 5min, 95° C 45min.	65° C 5min, 95° C 45min.	65° C 5min, 95 ° C 45min.
Exposure time (s) at 250 mJ/cm²	21	20	27	27	27
PEB time (sec)	65°C 5 min, 95°C 10 min	65 °C 1 min, 95°C 5 min	65°C 5 min, 95°C 10 min	65 ° C 5 min, 95 ° C 10 min	65°C 5 min, 95°C 10 min

Note 1: there are various types of SU-8 photoresists available; choices depend on the height of the structure to be made. For more details on available products, see Epoxy series resists offered by MicroChem (1).

Note 2: spinning parameters and baking times vary pending on the height of the structures to be made. For example, taller microchannels have a slower RPM and longer baking time for the same type of photoresist used.

Note 3: the height of a structure that can be made is limited and can be approximated by the *aspect ratio* (diameter to height of a structure).

2.1.2 Soft lithography

The master molds, or the final products of photolithography (section 2.1.3) can be used repetitively by applying lift-off technique. Polymer 1H,1H,2H,,2H-Perfluorooctyltrichlorosilane, Oakwood Chemical, Polyimetylsiloxiane (PDMS, SILPOT184) was poured over the master mold. The cross-linked polymer is elastic yet hard enough to be able to stand by itself. The device was made of micropatterend PDMS in this study.

PDMS was poured onto the master mold of the microchannel and cured, resulting in microchannel engraved on PDMS slabs shown in Fig. 2.1.1-4.
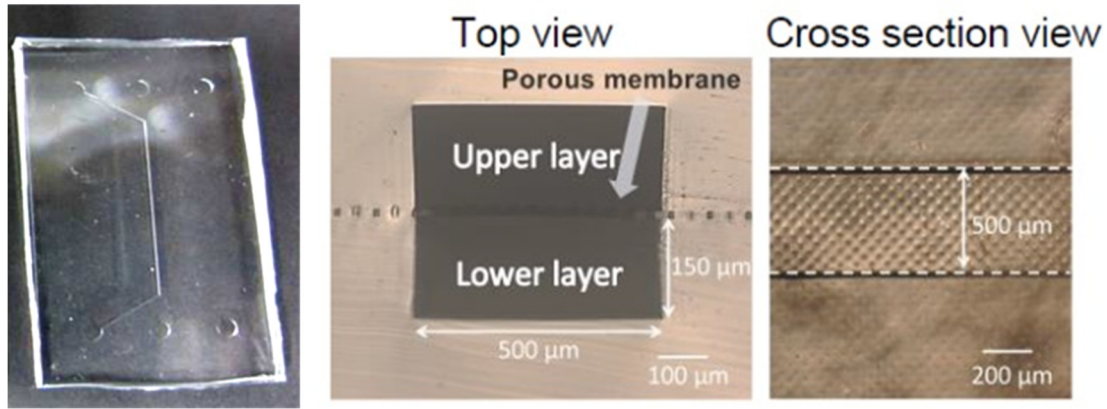
Fig. 2.1.2-1 PDMS molds from soft lithography.

The PDMS slab resulting from soft lithography, and its microscopic top and cross-section views.

2.1.2.1 PDMS
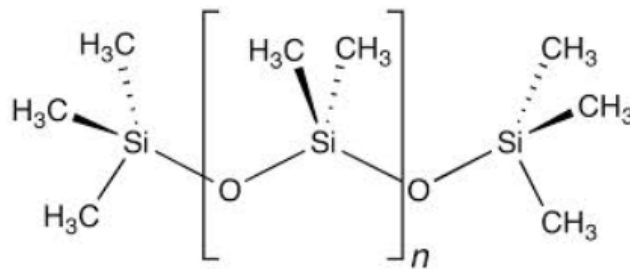
Fig. 2.1.2-2 Structure of PDMS. Reprint from (44).

Polydimethylsiloxane (Fig. 2.1.2-1, PDMS, $(C_2H_6OSi)_n$) is a polymer containing carbon and silicon and is widely used for fabricating microfluidic chips. For the fabrication of microfluidic devices, PDMS (liquid) mixed with a cross-linking agent is poured into a microstructured mold and heated to cross-link the polymer to obtain an elastomeric replica of the mold. Depending on the monomer chain, the non-cross-linked PDMS has a low n (almost liquid) or semi-solid (high n). The PDMS is usually hydrophobic in nature, i.e., it has a lower wettability to polar solvents such as water. It becomes hydrophilic after surface treatment but retains its hydrophobicity after a few hours. PDMS oxidation using plasma produces silanol terminations (SiOH) on its surface, which makes PDMS hydrophilic for a certain time interval (on the scale of minutes). This process also makes the surface resistant to the adsorption of hydrophobic and negatively-charged molecules (2). Due to the creation of the Si-O-Si bonds, oxidation is thus used to covalently bond PDMS slabs together or to an oxidized glass surface (2). Due to the rapid manufacturing, low cost, permeability to gases, thermally stable, biocompatible (with some restrictions) and optically transparent that enables both cell-culture and observation. It is also structurally stable to water (does not allow micro-structure deformation) hence it is widely used in microfluidic applications. However, the gas permeability makes it also permeable for water vapour (3), which could potentially change the osmolarity of the cell culture medium.

PDMS can be made by mixing the pre-polymer to the cross-linking agent at a ratio of 10:1. It is ready to use after removing air bubbles.

2.1.2.2 Processing methods: preparing micropatterned PDMS

The procedure is summarized schematically in Fig. 2.1.2-2.

1. Gently blow the dust (if any) on the wafer and clean the wafer for 45 s inside a plasma cleaner. Coat the wafer with 1H,1H, 2H, 2H-Perfluorooctyltrichlorosilane under vacuum overnight.
2. Position the wafer in a petri dish and fill it with PDMS polymer. Leave the apparatus in a desiccator to remove air bubbles. Cross-linked the PDMS at 70 C for 3 h.
3. Cut the PDMS slab and remove it from the silicon wafer carefully to not break the photoresist.
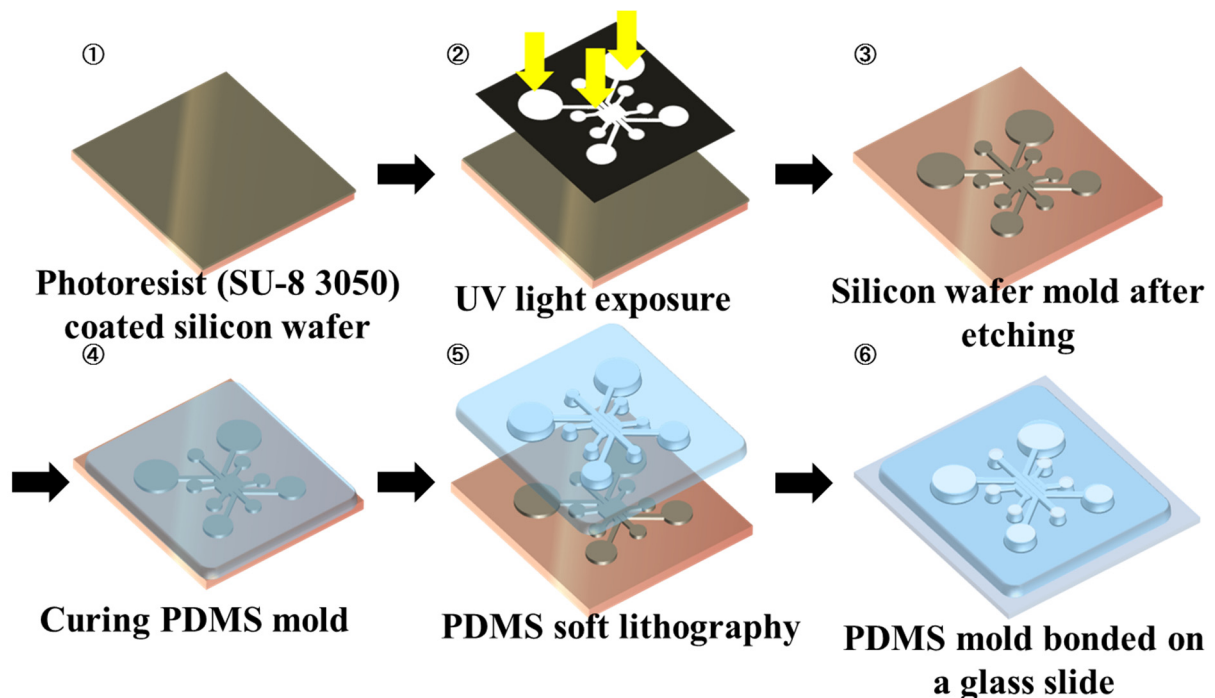
Fig. 2.1.2-3 Processing method: preparing micropatterned PDMS.

2.1.2.3 Plasma treatment for bonding

PDMS molds following soft lithography are punched with holes for in/outlets and taped to remove dust. It is then bonded to a 24 mm x 24 mm glass slide (one-layer device) or another slabs of PDMS sandwiching a piece of porous membrane of different materials (two-layer device).

To render the PDMS surface hydrophilic, PDMS slabs and the glass slides are treated with oxygen plasma to etch hydrocarbons and leave silanol (SiOH) groups on the surface. The oxidized PDMS or glass surface are placed in contact with each other to form bridging Si-O-Si bond at the interface, creating an irreversible bond.

Following parameter values were based on the Harrick Plasma cleaner, and optimization is required with different plasma generators.

- Treatment time for PDMS-glass takes 15-20 seconds, while treatment time for PDMS-PDMS takes 30-50 seconds. Time is based on using oxygen as the process gas. Prolonged treatment (plasma exposure) causes cracking in PDMS and migration of low molecular mass molecules from bulk to surface, decreasing the number of hydrophilic SiOH groups and resulting in weak or incomplete bonding (4).
- Use oxygen or room air as the process gas. If room air was used, decrease the above treatment time.
- RF power: medium or high

2.1.3 Defects

As straightforward as it seems, photolithography defects could happen. For example, problems such as detachment of SU-8 photoresist (Fig 2.1.3-1), air bubbles generated in SU-8 photoresist, or fallen micropillars etc. all render the master molds unusable. The height of the micropillars made should be determined beforehand by inspecting the aspect ratio as mentioned in fabrication section.
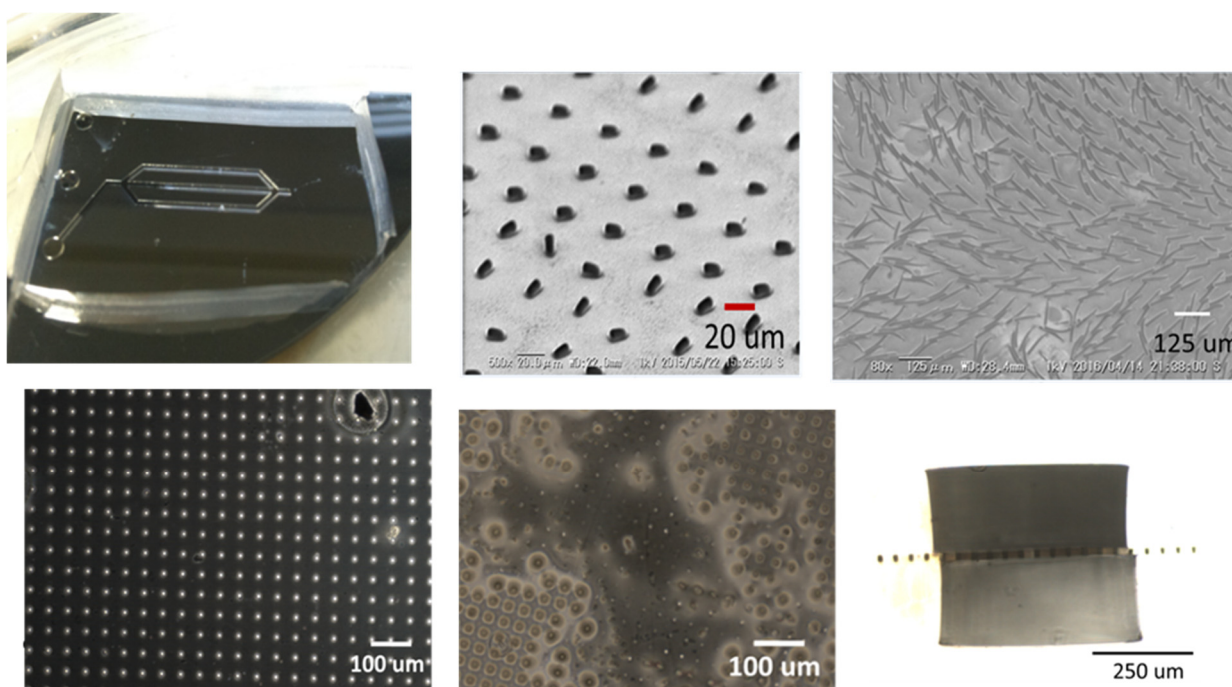
Fig. 2.1.3-1 Defects and human errors in device fabrication.
Top row: detachment of SU-8 photoresist (part of the channel remained), middle: fallen micropillars which could be due to improper handling; right: the micropillars made at 50 μm could not sustain itself aspect ratio. Bottom row: microscopic view of PDMS membrane with a hole (left), fallen micropillars resulting in non-porous PDMS membrane (membrane), misalignment of microchannels (human error). Human errors could also lead to different cell culturing area.

Previously, photoresist adhesion strengthening liquid (OAP) was coated on Silicon wafers before applying SU-8 photoresists; OAP, as the name suggested, was used to strengthen the bonding between SU-8 photoresist and the silicon wafer. However, the resulting micropatterns detached from the silicon wafer. There are many possible reasons to the detachment of the photoresist, including temperature, humidity, and cleanliness of the wafer. After excluding OAP, the microatterns turned out fine hence the detachment problem lied in OAP – possibly the expiration date of the solution. In addition, the silicon substrate has to be absolutely clean in microfabrication processes, as dust or particles can potentially affect the coating parameters. If necessary, the silicon wafer can be cleaned in Piranha solution. From experiments, it was found that photolithography was successful without uses of piranha solution (provided uncut, clean Silicon wafer was used).

The viscosity of PDMS, and the height of the micropillars, determined the success rate of a porous membrane. Without addition of hexane, lumps, rather than holes, resulted on the membrane, indicating high viscosity of PDMS prevents protrusions of micropillars, despite making them taller from 10 to 40 um. As hexane was evaporated after heating stage, the membrane was not toxic for cell culturing.

2.2   Cell culture techniques

Cell culture is inarguably an important part in the cell-based biological/medical applications in MEMS. The experimental results will be invalid if the cells could not adapt to the microenvironments; the experiments will be unsuccessful if the cells could not stay alive inside the micro-devices. Therefore, to establish the cell culture in artificial environments is a crucial problem to be addressed. The appropriate culture conditions would to mimic the physiological conditions *in vivo et situ* with respect to temperature, pH, osmolarity and oxygen supply (5). Most of the cells are maintained in an incubator set at 37°C in a humidified atmosphere containing 5% CO_2, although the temperature varies for different cell types.

This subsection summarized different cells used in developing models; the protocols and techniques outlined below are written based on adherent cells, which is the type of cells used in this study.

2.2.1 Cell types and culturing conditions

The different types of cells used in the models, along with the culturing condition and media used, are all summarized in this section.

2.2.1.1 Cell culture media

Cell culture media has a variety of supplements, namely the essential amino acids, glucose, etc to facilitate and sustain the growth of cells. The media are formulated for different types of cells, with slight variations in compositions such as amino acids, vitamins or inorganic compounds (e.g. KCl, NaCl). While epithelial cells can grow relatively well under the standard culture media, neuronal cells or primary cells require additional supplements for the optimal growth. The classic media include Minimum Essential Medium (MEM), Dulbecco's Modified Eagle's Medium (DMEM), RPMI (Roswell Park Memorial Institute) Media, and Ham's

Nutrient Mixtures (Ham's F-10). Growth factors are usually supplemented to the basal growth medium to stimulate replication and regulate apoptosis of cells cultured in vitro. Serum provides a wide variety of macromolecular proteins, nutrients, carrier proteins, hormones and attachment factors for cell growth, metabolism and proliferation. The most commonly used type of serum is fetal bovine serum (FBS, serum of fetal calf origin). Antibiotics (antibiotics and antimycotics, Penicillin-Streptomycin, etc.) are also supplemented to the media to lower the chances of contamination. Certain media are supplied with phenol red, a pH indicator dye, that is also used to judge the conditions of cell cultures (yellow, red, bring pink correspond to pH 6.6, 8.0 above 8.1). Furthermore, it is useful in evaluating the condition of an incubator in the event when CO2 supply is run out.

DMEM, a bicarbonate buffered system, is governed by following reactions:

$$H_2O + CO_2 \ <-> \ H_2CO_3 \ <-> \ H^+ + HCO_3^-$$
$$H_2O + CO_2 + NaHCO_3 \ <-> \ H^+ + Na^+ + 2HCO_3^-$$
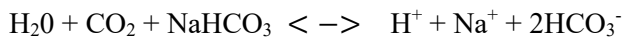
Indicating that reactions are driven to the left when CO2 is lost and that media turn bright pink (alkaline).

2.2.1.2 Culturing conditions for cell proliferation

Below summarized the cell culture media and the culturing conditions (seeding density and extra surface coating for culturing) for the respective cell types. Culturing media are changed every 48 h and cells are passaged when they are 80-90% confluent. Unless mentioned specifically, cells reach 80% confluent two days after seeding under optimal cell conditions and normal culturing environments with the seeding density below.

ARPE-19

Culturing

- DMEM (Dulbecco's Modified Eagle's Medium, High glucose, Wako)
  (D-glucose 4.5g/L, Phenol Red 15 mg/L, Sodium Pyruvate 110 mg/L), supplemented with 10% FBS and 1% antibiotic-antimycotic (100X, Gibco)
- Seeding density: 20000 cells/ cm^2 culturing surface (confluent in 2-3 days)
- Coating: tissue culture treated flasks or fibronectin 10 ug/ml or 0.1% gelatin for non TC-treated surface

Long-term ARPE-19 cultures (weeks – months culture for differentiation)

- DMEM (Dulbecco's Modified Eagle's Medium, High glucose, Wako)
  (D-glucose 4.5 g/L, Phenol Red 15 mg/L, Sodium Pyruvate 110 mg/L), supplemented with 1% FBS and 1% antibiotic-antimycotic (100X, Gibco).

Conditioning ARPE for experiments (the basal medium)

This is used as the conditioning medium and the medium for the control group in the experiment.

- DMEM low glucose ((D-glucose 1 g/L, Phenol Red 15 mg/L, Sodium Pyruvate 110 mg/L)
- B27 (Gibco 17504044)
- 1% antibiotic-antimycotic (100X, Gibco).

Media for experiments
- High glucose: the basal medium (conditioning medium) supplemented with additional D+ glucose to the final desired concentration. Filter the medium through 0.45 um Millipore before use.
- Hypoxia: the basal medium (conditioning medium) supplemented with 150 µM of cobalt(II) chloride ($CoCl_2$, Wako). Typically, 100x $CoCl_2$ is made in PBS(-), and the solution is diluted to 1x in the basal medium for experiments. Filter the medium through 0.45 um Millipore before use.
- Tumor Necrosis Factor α (TNFα, Wako): TNFα is a pro–inflammatory cytokine, contributes to inflammation-associated angiogenesis and mediates choroidal angiogenesis by upregulating VEGF expression in RPE.
- Lucentis ®: It is the trade name of Ranibizumab, a humanized monoclonal antibody fab fragment, originally derived from a mouse monoclonal antibody. It binds to circulating VEGF, inhibiting the binding of VEGF to its cell surface receptors. The inhibition leads to a reduction in neoangiogenesis, making it one of the treatments to cancers and eye diseases as in diabetic retinopathy and diabetic macular edema.

HUVEC & GFP-HUVEC
- EBM-2 Bulletkit (Endothelial Cell Basal Medium, Lonza), accompanied supplements 0.5 ml hEGF, 0.2 ml heparin, 0.2 ml hydrocortisone, 10 ml FBS, 0.5 ml GA-1000, 2 ml hFGF- β, 0.5 ml Ascorbic acid, 0.5 ml VEGF, 0.5 ml R3-IGF-1.
- Seeding density: 4000 cells/ cm^2 (confluent in 2-3 days) or 8000 cells/ cm^2 (recommendation seeding density from the data sheet)
- Coating: 0.1% gelatin or Collagen type IV at 2 ug/ml

Conditioning HUVEC for experiments (the basal medium)
This is used as the conditioning medium and the medium for the control group in the experiment.
- EGM (Lonza), supplemented removing VEGF, and bFGF. Note: medium contains 2% FBS.

Media for experiments
- Condition medium as the basal medium, and supplement D+glucose (high glucose), $CoCl_2$ (hypoxia), or TNFα (10 ng/ml).

HRMEC & GFP-HRMEC
- Endothelial cell culture medium (Angioproteomie)
- Seeding density: 4000 cells/ cm^2
- Coating: 0.1% gelatin or Collagen type IV at 2 ug/ml

Conditioning HUVEC for experiments (the basal medium)

This is used as the conditioning medium and the medium for the control group in the experiment.

- Serum-free complete medium (Cell system, CSSF4Z0500R).

Media for experiments

- Serum-free complete medium (Cell system, CSSF4Z0500R) supplement D+glucose (high glucose), CoCl$_2$ (hypoxia), or TNFα (10 ng/ml).

HRP

- Pericyte culture medium (Angioproteomie)
- Seeding density: passaging at 1:2 split ratio (confluent in 5-7 days)
- Coating: 0.1% gelatin or Collagen type IV at 2 ug/ml

NHLF

- DMEM (Dulbecco's Modified Eagle's Medium, High glucose, Wako)
  (D-glucose 4.5g/L, Phenol Red 15 mg/L, Sodium Pyruvate 110 mg/L), supplemented with 10% FBS and 1% antibiotic-antimycotic (100X, Gibco)
- Seeding density: 10000 cells/ cm^2 culturing surface
- Coating: tissue culture treated flasks or 0.1% gelatin for non TC-treated surface

2.2.1.3 Surface coating for cell culture

Here list the substances used to culture the five different types of cells in this research. General protocols are given and the specific concentration of each substance needs to be optimized for different cell types of interest. Do note that variations in concentration can arise from the same product of different lot numbers.

Fibronectin

Rinse the surface with D-PBS(-), and cover the culturing surface with fibronectin at 10 -20 ug/ml. Incubate the culture dish at 37 degree for at least 2 h (overnight, preferably). Aspirate the solution and wash the surface with D-PBS(-) before culturing cells.

Optional: for better adhesion of fibronectin onto the surface, treat the surface with corona discharge and coat PLL for 1 h at 37 degree before fibronectin coating.

Gelatin (Wako)

Dissolve the required amount of gelatin (Wako) in distilled water to make 0.1% gelatin concentration. Autoclave the solution and let cool before use. For coating, cover the entire culturing surface and incubate the culture dish at 37 degree for at least 1 h. Aspirate the gelatin solution, let dry and keep the culture dish at a sterilized location (e.g., clean bench) until use.

Collagen type I or Collagen type IV (Corning)

Rinse the surface with D-PBS(-). Use the collagen monomer as it is at a concentration of 2 ug/ml in PBS(-). Incubate the culture dish at 37 degree for at least 2 h. Aspirate the solution and wash with D-PBS(-) before use.

2.2.2 Measuring cell growth and cell sub-culturing (passaging)

Growth of a particular cell type can be judged from the morphology, population colonies/cell numbers, and typical length of time for cells to growth etc. The total cell number over time is a good measure of a biological response because it is broadly defined and influenced by many different factors, including mitogens, changes in nutrient level, transport, membrane integrity, attachment factors and more (6). The total cell number vs time plotted on a so-called growth curve is used in order to analyze the growth characteristics quantitatively. A growth curve makes clear the total cell number with respective to time hence differentiates the effects of factors which might also affect cell number, say, by lengthening the lag phase. It generally will show the lag phase (the time it takes for the cell to recover from subculture, attach and spread); the log phase (cell numbers begins to increase exponentially); a plateau phase (culture becomes confluent and the growth rate slows or stops), see Fig 2.2.2-1. It is clear from a glance at what days the culture is supposed to be sub-cultured (passaging).
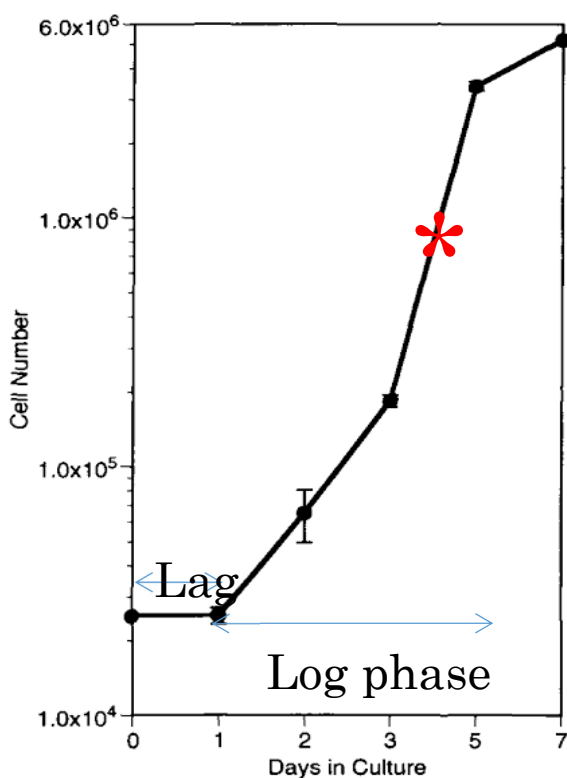
Fig. 2.2.2-1 Typical cell growth curve.

Red star indicates the best timing for sub-culturing (correspond to ~ day4). Lag phase: before the cells start to grown, the log phase of growth, and the beginning of the plateau phase when contact-inhibited cells will cease growing. Plateau phase is not labelled. Adapted from (6).

Cell passaging is necessary in sustaining the life of growing cells. A cell culture flask only provides the cell a fix and limited amount of space; the contact-inhibited cells will cease proliferation once the provided space is fully occupied. A general practice is thus to re-culture a fraction of the population into a new flask to provide cells with more space and nutrients (culture medium). Methods in passaging vary with the types of cells, which can be broadly classified into adherent and floating cells. As this study dealt with adherent cells, the method applies to adherent cells are given below.

The protocol below was written based on ARPE-19 cultured in a T75 flask.
1. Once the cell has reached 80% confluence (inspected under a microscope), cells in a flask were washed with DPBS (-) to remove the component of serum.
2. Cover the cells in flask with 1 ml Trypsin –EDTA and incubated it for no more than 5 min.
3. Hit the flask to facilitate cell detachment and make sure that the majority of cells have detached (appeared round). If most of the cells are still attached on the flask, incubate for an additional 30 s and repeat step 3 but make sure that the whole process does not exceed 7 min.
4. Using 10 ml warmed DME High glucose (10% FBS) to collect and re-suspend the cells in trypsin into a centrifuge tube for centrifugation at 1500 RPM for 5 min.
5. Remove the supernatant and add in 1 ml fresh, pre-warmed DME medium. Pipette the pellet to break it apart.
6. A split ratio of 1:4 or 1:5 is recommended for ARPE-19. Aliquot the cells into a new T75 flask with 10 ml pre-warmed DME medium.

Note 1: Centrifugation time and speed can be adjusted within certain ranges such that cells are not freely floating after centrifugation.
Note 2: Modify the trypsin-incubation time and culture medium volume for passaging other cell types.
Note 3: For typical cell passaging, the following two types of trypsin were used.
- Trypsin (0.25% EDTA), Gibco (aliquot and stored at -30 degree; heat to 37 degree before use)
- TrypLE (Gibco) (store at room temperature and use directly)
Typical incubation time for TrypLE is 2-3 minutes longer than Trypsin and required to be optimized for the specific cell type.

2.2.3 Cell counting and hemocytometer
A hemocytometer gives the most direct measurement of cell number and therefore cell growth. Knowing how many cells are introduced into the experimental system is also important. Strictly speaking, viability of cells is inspected on top of cell counting as cells might die from handling processes such as trypsinization. Hence, the use of a dye (e.g., trypan blue) plus hemocytometer counts give a robust indication on total viable number of cells.

Cell number per mm^3 volume is given by:

$$\text{cell number counted}\Big/ \text{number of grids counted} \times \text{volume of a grid(mm}^3)$$

To convert into cell number per ml from mm^3, the above equation is multiplied by 1000. Different types of hemocytometer has different height and sizes of grids hence different grid volumes. Refer to Fig. 2.2.3-1 for Thoma hemocytometer. The general rule is that cells are IN (counted) if they fall on two pre-determined sides of a grid; e.g., top and left are IN, right and bottom are OUT (not counted).
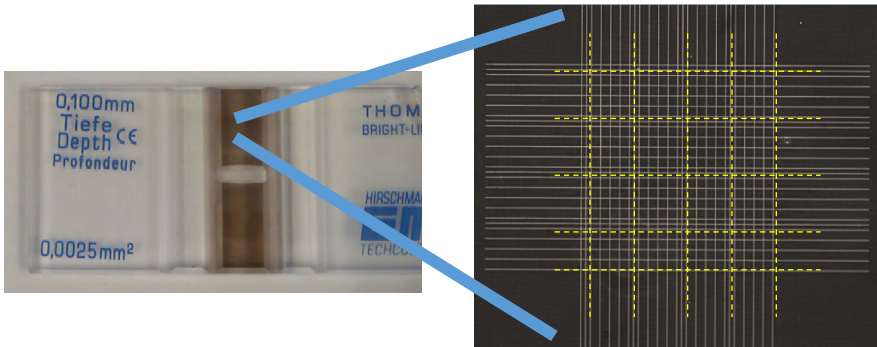
Fig. 2.2.3-1 Hemocytometer (Thoma) and magnification of the central grids where cells can be counted and numbers calculated.

2.2.4 Thawing and cryopreservation

One of crucial components in the culturing is to preserve cells for future uses. Cells bought from providers usually come in a vial (5 x 10^5 cells/ml). It is typically sub-cultured for uses and storage for later uses.

- Cell Banker

2.2.4.1 Step in cryopreservation:

The processes are the same as cell passaging (section 2.2.2), except in step 5, add in 1 ml CellBanker instead of DME medium. Pipette everything (cells and CellBanker solution) into a cryopreservation vial. CellBanker does not need to be warmed and do not pipette the cell cluster. Label the necessary information, date, cell type, total cell number, passage number, person in charge (name) on the vial and immediately put it inside a controlled rate freezing apparatus into a -80 °C freezer. Work quick as CellBanker are toxic to cells. Move the cells the next day into liquid nitrogen chamber for long term storage. Record the information in the notebook.
* leave the controlled rate freezing apparatus in a 4 °C fridge for at least 24 h prior use.

2.2.4.2 Step in thawing frozen cells:

1. Thaw the cryovial in a hot water bath until it has completely dissolved. Do not leave it in the water bath for over 2 min.
2. Using 10 ml warmed DME High glucose (10% FBS) to collect and re-suspend the cells in CellBanker into a centrifuge tube for centrifugation at 1500 RPM for 5 min. Do not pipette the pellet.

3. Remove the supernatant and add in 1 ml fresh, pre-warmed DME medium. Pipette the cluster to break it apart.
4. Aliquot the solution into a new T75 flask with 10 ml pre-warmed DME medium. Change the cell medium the next day and continue the culture.

2.2.5 Contamination

Mammalian cell cultures can encounter two categories of contamination: (1) chemical, including impurities in the medium, serum and H2O supply; (2) biological, including bacteria or fungi. Mycoplasma (a genus of bacteria) is specifically detrimental to cells as it is unaffected by many common antibiotics. There are also risks of cross contamination with other cells hence proper handling and an aseptic environment is important. Refer to Fig. 2.2.5-1.
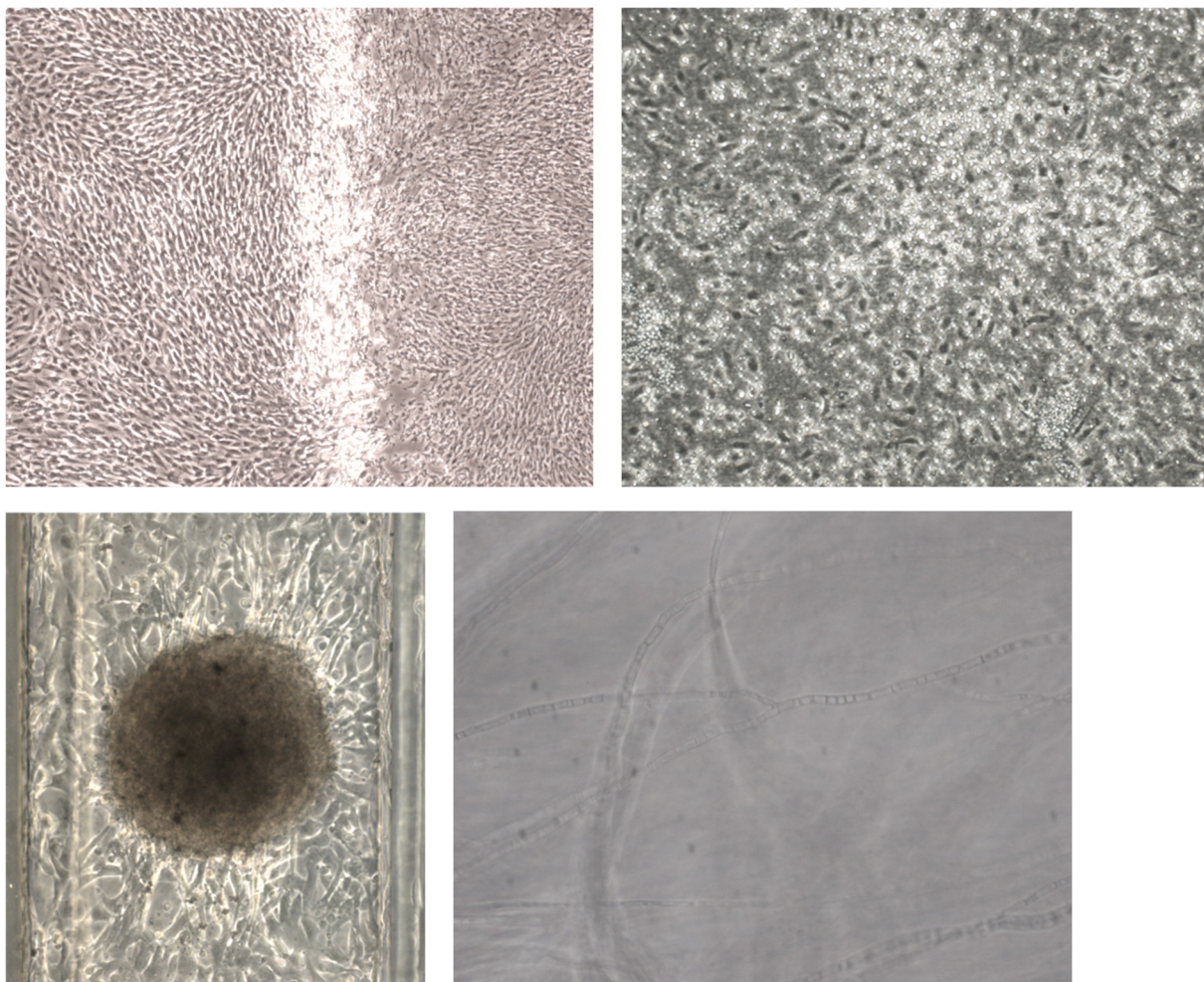
Fig.   2.2.5-1 Contamination that happened to the cell culture.

Top row left/right: bacteria and yeast, both viewed at the magnification 40X). Bottom row: mold inside a microfluidic device viewed at 100X and the edge of the colony magnified at 200X.

2.3 Cell tracking and staining for observation

This section is devoted to data capturing and analysis techniques frequently used throughout the whole research, which, are not limited to this study but are applicable to other similar applications. Protocols necessary for microscopic observations of samples, image processing, and statistical analysis were described; in addition, techniques used in characterization of ARPE were also illustrated.

### 2.3.1 Cell tracking

Staining of samples can be classified broadly into in vivo staining (staining of a biological matter while it is still alive) and in vitro staining (non-living biological matters). Different cell stains and dyes exist such as well-known Haematoxylin and Eosin Staining. Cell staining in microscopy is useful in highlighting the structural elements of the sample/specimen to be observed. A particular aspect of this research was to observe the cell movement and interaction. Cell locations were *tracked* and recorded hence specialized probes that are nontoxic to *living* cells are of paramount importance. The fluorescent probes used throughout the study was the CellTracker™ Fluorescent Probes (Molecular probes) which is abbreviated as CellTracker probes herein. It is capable of monitoring cell movement, proliferation, migration and invasion. As the experiments spanned less than 48 h, short-term cell tracking probes were chosen (Molecular Probes®, CellTracker Green CMFDA (Cat. No. C7025) and CellTracker Red CMTPX (Cat. No. C34552)). See Fig. 2.3.1-1.

2.3.1.1 Principles of CellTracker

CellTracker probes have been designed to freely pass through cell membranes; howoever, once inside the cells are transformed into cell-impermeant reaction products. The CellTracker contain a chloromethyl or bromomethyl group that reacts with thiol groups, utilizing a glutathione S-trasnferase-mediated reaction. In most cells gluthathione levels are high (up to 10 mM) and glutathione transferase is ubiquitous (7).

After conversion to impermenant versions, the CellTracker probes are well retained in living cells through several generations – they are transferred to daughter cells but are not transferred to adjacent cells in a population. Cells loaded with the CellTracker probes display fluorescen for at least 72 h and brightly fluorescent at physiological pH (7).

Experimental protocols: CellTraker probes
CellTracker Green CMFDA and CellTracker Red CMTPX were used to stain HVUEC and ARPE respectively.

2.3.1.2 Preparations

- Warm adequate volume of *serum-free* cell culture medium/media for the cells to be stained. Take at least enough volume to cover the cell culture flasks/dishes homogeneously. At the same time, warm the medium/media that cells are used to be cultured in (ie., containing serum).
- Decide on the fluorescent probes concentration desired and calculate the volume of CellTracker probes needed using the formula C1V1 = C2V2, where,

C1, C2, V1, V2 refers to the master concentration of CellTracker probes (10 mM), final (desired) CellTracker

probes to be used in the experiments, reconstituted CellTracker probes volume (ul), volume of cell culture medium (ml) as prepared in the previous step.

2.3.1.3 Reconstitute CellTracker probes (stock solution)

1. Add 11 µl of anhydrous dimethylsulfoxide (DMSO) into a new vial of cell tracker (50 µg). This will give a master concentration of 10 mM reconstituted CellTracker probes.
2. With the lid close, agitate the bottle to make sure the powder and DMSO are homogenously mixed.
3. Pipette the required amount of cell tracker, and re-freeze the leftover in a -30°C fridge for future uses.

2.3.1.4 Protocol for loading CellTracker probes

1. Take the required amount of reconstituted CellTraker probes and mix into pre-warmed serum free cell culture medium.
2. Aspirate the cell culture medium. Rinse the cell culture flasks/dishes thoroughly with Phosphate-buffered saline PBS(-) to remove the serum. It is recommended to rinse the cultural surface twice.
3. Cover the cultural surface with the medium prepared in step 1. Incubate the cells in an incubator for 25 - 35 min. 30 min is enough to stain ARPE and HUVEC cells.
4. Remove the medium containing CellTracker probes and rinse the cultural flasks/dishes with PBS. Load the pre-warmed serum-containing medium as prepared previously.
5. Incubate the cells in an incubator for at least 30 min before experiments.

Cells loaded with the probes can be observed under fluorescent microscope set to appropriate filters.
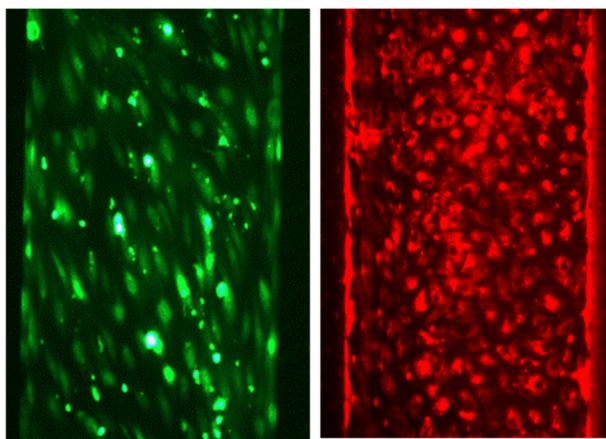
Fig. 2.3.1-1 HUVEC (left) and ARPE (right) stained with CellTracker probe green and red viewed at 100X.

2.3.2 Immunofluorescence staining

Immunofluorescence (IF) staining relies on the principle of binding of antibody to the antigen. To enhance the fluorescence signal, most of IF involves the binding of secondary antibodies to the primary antibodies, which are directly bound to the target antigen(s). The secondary antibody used has to be raised in a different species than the primary antibody of interest.

Steps staining ARPE-19 cells for the tight junction protein ZO-1. Before each step below, wash the sample with 2% FBS in PBS(-).

1. ARPE-19 cells in the microchannel were fixed with 4% paraformaldehyde (Wako) in room temperature, 10 min.
2. Permeabilized by 0.2% Triton X-100 (v/v in PBS(-)) under room temperature, 10 min.
3. Blocked by 7% (w/v) bovine serum albumin (30 min) in room temperature*.
4. The sample was incubated with the primary antibody anti-ZO-1 (1:100 dilution; mAb rabbit 40–2300, Invitrogen, CA) overnight at 4 °C.
5. The sample was then stained with Alexa-Fluor 546-conjugated donkey anti-rabbit antibody (1:1000 dilution; A10040, Invitrogen, CA) and 4′,6-diamidino-2-phenylindole dihydrochloride (DAPI, Invitrogen, CA) 1 h, room tmerperature.

Note*: Alternatively, 2% FBS in PBS can be used in blocking non-specific binding of proteins.

2.4 Bioassays

2.4.1 Enzyme-linked immunosorbent assay (ELISA)

ELISA is a plate-based assay technique used for detecting and quantifying substances such as peptides, proteins, antibodies and hormones. All ELISAs rely on the specific interaction between an epitope found on an antigen and a matching antibody binding site. The antibodies used in an ELISA can be either monoclonal or polyclonal (derived from unique antibody producing cells or a pool of antibodies purified from animal sera that are capable of binding to multiple epitopes, respectively) (8). Polyclonals are more typically used for the secondary detection layer in indirect ELISAs while monoclonal antibodies are more typically used for capture or primary detection of the antigen (8). After the antigen-antibody reactions, a colour reagent is added into the sample and colour develops in proportion to the amount of antigen/analyte (in this case, VEGF) in the original sample. The colour is stopped and the intensity is measured, and interpolated from a standard curve .

There are four kinds of ELISA assay tests available which chosen based on the antibodies available and the complexity of the samples (Fig. 2.4.1-1):

- *Direct ELISAs* involve attachment of the antigen to the polystyrene plate followed by an enzyme-labeled antibody.
- *Indirect ELISA*s also involve attachment of the antigen to the polystyrene plate except the primary antibody is not labeled. An enzyme-conjugated secondary antibody is added and attached to the primary antibody. This format is used most often to detect specific antibodies in sera.
- *Sandwich ELISAs* involve attachment of a capture antibody to the polystyrene plate. Samples containing known or unknown antigen are then added in a matrix or buffer that will minimize attachment to the solid phase. An enzyme-labeled antibody is then added for detection.

- *Competitive ELISA*s involve the simultaneous addition of competing antibodies or proteins. The decrease in signal of samples where the second antibody or protein is added gives a highly specific result.
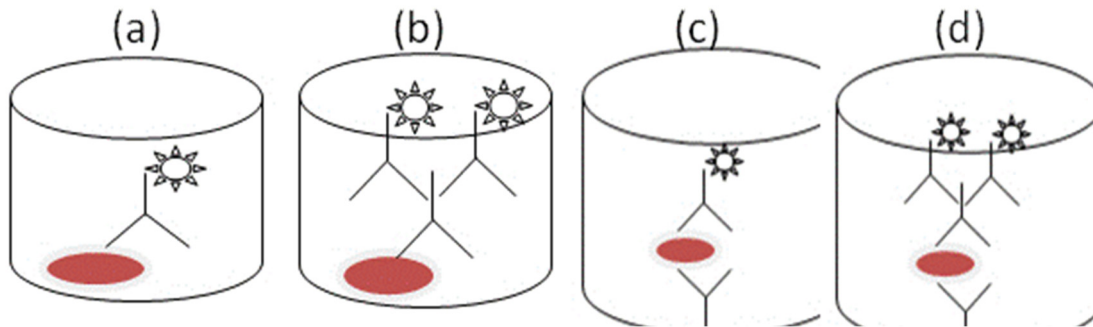
Fig. 2.4.1-1 Illustrations of different formats of ELISAs.

(a) Direct ELISA; (b) indirect ELISA; (c,d) direct and indirect sandwich ELISA schematics. Reprinted from (8).

Human VEGF ELISA kit (catalog # DVE00, R&D systems) was used in measuring VEGF-A165 secreted by ARPE throughout the study. The assay employs the quantitative sandwich enzyme immunoassay technique.

Protocol

The detailed ELISA protocol for VEGF-A165 measurement (adapted from R&D systems) is listed out in this section. This protocol differs from the one from the manufacturer in that only the required amounts of reagents were reconstituted. The ELISA kit contains all the required regents.

Note 1: if the *approximate* VEGF-A165 concentration range is known (before the actual measurement), dilute the samples in folds (2X, 3X, 4X, etc.) in Diluent RD5K in the preparation stage. This will lower the possibility of having concentrated samples (outside the standard curve). If the sample contains 10 % FBS, dilute the samples 50 folds in advance.

Note 2: prepare the appropriate amount of reagents, (diluted) samples and controls for duplicate assay. It is recommended to assay samples in duplicate.

2.4.1.1 Protocol: ELISA assay

Preparation:
- Record the standards and samples assayed on a plate layout sheet (provided).
- Bring all reagents to room temperature before use.
- Calculate the volume of Wash buffer needed and dilute the amount needed 25 folds.
- e.g., volume of wash buffer needed: 96 ELISA wells to be sampled x 400 ul/well x 3 times wash x 2 repetition = 230.4 ml. Take 240 ml (safety margin)/25 = 9.6 ml of wash buffer, diluted in 240 – 9.6 = 230.4 ml distilled water.
- Thaw the samples (if there are frozen); record the total sample volumes if total amount of VEGF is desired.
- Make the VEGF standard curve: add 1ml of RD5K into the VEGF standard (resulting in master conc. 2000 pg/ml). Let it sit 15 min. Perform a serial dilution with RD5K: pipette 500 ul from the master solution

and add 500 ul of RD5K into Eppendorf tubes resulting in final VEGF concentrations 2000, 1000, 500, 250, 125, 62.5, 31.2, 15.6, 0 pg/ml (0 pg/ml indicates RD5K only). Mix each tube thoroughly before the transfer.

- Remove excess microplate strips from the plate frame, return them to the foil pouch containing the desiccant pack and reseal.

Assay procedure

1. Add 50 ul of Assay diluent RD1W to each well.
2. Add 200 ul of standard, control, (diluted) samples to the respective wells as drawn on the layout. Cover with adhesive strips (provided) and leave it in room temperature for 2 h.
3. Aspirate each well and wash (400 ul/well), repeating the process twice for a total of 3 washes. Wash by filling each well with Wash Buffer (400 ul) using a squirt bottle, manifold dispenser, or autowasher. Complete removal of liquid at each step is essential to good performance. After the last wash, remove any remaining Wash Buffer by aspirating or decanting. Invert the plate and blot it against clean paper towels.
4. Add 200 ul of VEGF conjugate to each well. Cover with a new adhesive strip Incubate for 2 h at room temperature. Prepare the required volume of Substrate Solution during the waiting time up by mixing Color Reagents A and B together in equal volumes (Substrate Solution has to be used within 15 min). Protect Color Regent from light.
5. Repeat the aspiration/wash as in step 3.
6. Add 200 ul of Substrate Solution to each well. Protect from light. Leave it in room temperature for 20 min.
7. Add 50 ul of Stop Solution to each well. Shake gently to ensure through mixing. Colour changes should be observed.
8. Determine the optical density of each well within 30 min, using a microplate reader set to 450 nm. If wavelength correction is available, set to 540 nm or 570 nm. If wavelength correction is not available, subtract readings at 540 nm or 570 nm from the readings at 450 nm. This subtraction will correct for optical imperfections in the plate. Readings made directly at 450 nm without correction may be higher and less accurate.

Readings within 0 -2000 pg/ml (standards) can be interpolated from the standard curve.

2.4.2 Flow cytometry

As an alternative to ELISA to quantify cytokines present in the sample, LEGENDplex (BioLegend) kit was used to simultaneously quantify up to 13 cytokines present in the sample. Angiogenesis panel was used (LEGENDplex 740697). Kit preparation, assay preparation and procedure were followed as described in the provided protocol. Flow cytometer BD FACSAria was used to read the samples with the specific parameters below (voltages require adjustment pending on the flow cytometer and the kit, but use the following values to start off when using LEGENDplex kit):

- FSC: 247 - 302

- SSC: 242 - 269
- FITC: 403 – 445
- APC: 313 – 397
- YG-PE: 412 – 478
- When reading samples use the flow rate 3.8

Conditioned media of samples were collected and stored in a -30 freezer if assay was not run immediately after. Assay was performed using 1ml FACS microtubes or a 96-well microplate. When the assay was performed on a 96-well plate, the samples were transferred to 1ml FACS microtubes before reading. Note that 1ml FACS microtubes are not supported by BD FACSCanto series of flow cytometers.

2.5   Statistical analysis

Statistical testing is one of the important sectors in the research that is often neglected. Inaccurate statistical analyses could lead to false interpretations hence invalid conclusions. On the other hand, statistical significant results suggest but do not imply biological significance. Herein this section is devoted to introducing and explaining the statistical techniques relevant in this study. The factor that is most commonly used to gauge the significance is the p-value, which returns a probabilistic significance of a hypothesis testing. In addition, independence and numbers of samples are important in biological samples to ensure robust statistical tests.

Quantitative results from this study include the HUVEC migration tests, FITC-dextran permeability analysis, and VEGF secretion analysis for microfluidic devices and transwell inserts. In co-culture studies, significance tests on ARPE detachment between different conditions were also analyzed.

The data were presented in boxplots for clarity of visualization and were expressed as mean ±standard error (SE). Each experiment conducted in this study included three replicates, and three independent experiments were performed. Log transform was applied to skewed data which was then back-transformed for analysis. A level of p less than 0.05 was considered to be statistically significant.

2.5.1   Statistical software

The platform used throughout this research was R version 3.2.5 (R Foundation for Statistical Computing), a free software environment for statistical computing and graphics. It is capable of data manipulation, classical statistical tests, calculation and is equipped of highly extensible graphical techniques. One of the advantages of R is the capability to produce well-designed publication-quality plots including mathematical symbols and formulae where needed (9). The software can be downloaded from the website by choosing the appropriate CRAN mirror. The necessary packages required for different statistical models can then be downloaded once the software is installed. In addition to R, there are many other statistical software available to run tests such as SPSS Statistics.

2.5.2   Critical assumptions and Statistical tests

Depending on the nature (qualitative or quantitative), number and organization of samples, appropriate

methods on data analysis are used. For quantitative analysis, common tests include the two-sample t-test, ANOVA (analysis of variance), ANCOVA (analysis of covariance) and multiple regressions. Statistics belongs to another field of study; this sub-section describes only the statistical tests and models used in this research. In order to use the models, certain assumptions should not be violated, namely, the independence, normality, variance and linearity of the residuals from samples. Alternatively, data are transformed and fit to the model if the assumptions are violated. All the quantitative results from this research were collected from at least 3 samples per experiment and 3 independent experiments were performed. Normality, variance and linearity were checked using the built-in R functions before fitting the data to the statistical models.

2.5.3 T-test

A t-test is any statistical hypothesis test in which under the null hypothesis, the test statistic follows a t-distribution (Student's t-distribution), a continuous probability distribution. In contrast to a normal distribution which describes a full population, t-distribution describes samples drawn from a full population. It is used to assess the statistical significance between two sample means.

2.5.4 Analysis of variance (ANOVA)

T-tests are relatively simple and intuitive. However, it is not equipped for analysis if we have more than 2 samples that we want to examine at the same time. In this regard, ANOVA, a collection of statistical models, is used to analyze the differences among group means. ANOVA can only tell us if there is any significant difference from at least two groups; it does not tell us the specific groups where significance arises from hence further tests are necessary (post hoc test). One-way ANOVA is used to determine whether there are any statistically significant differences between the means of three or more independent groups while two-way ANOVA compares the mean differences between groups that have two independent variables on one continuous dependent variable. Post-hoc Tukey HSD was used when necessary in this study.

References

1. MicroChem. SU-8 3000 Permanent Epoxy Negative Photoresist [Internet]. http://www.microchem.com/Corp-About.htm#. [cited 2017 Jan 25]. Available from: http://www.microchem.com/Corp-About.htm#

2. PDMS: A review [Internet]. Elveflow. [cited 2017 Jan 25]. Available from: http://www.elveflow.com/microfluidic-tutorials/microfluidic-reviews-and-tutorials/the-poly-di-methyl-siloxane-pdms-and-microfluidics/

3. Thuenauer R, Rodriguez-Boulan E, Römer W. Microfluidic approaches for epithelial cell layer culture and characterisation. Analyst. 2014 Jul 7;139(13):3206–18.

4. sabyo-si. Harrick Plasma : Applications : Microfluidic Devices [Internet]. https://www.sanyo-si.com/. [cited 2020 Jan 14]. Available from: https://www.sanyo-si.com/wp-content/uploads/ac5eeb0504e268a02377114c323c4bce.pdf

5. Brunner D, Frank J, Appl H, Schöffl H, Pfaller W, Gstraunthaler G. Serum-free cell culture: the serum-free media interactive online database. ALTEX. 2010;27(1):53–62.

6. Mather JP, Roberts PE. Introduction to Cell and Tissue Culture: Theory and Technique. Springer Science & Business Media; 2007. 247 p.

7. CellTracker Red CMTPX Dye - Thermo Fisher Scientific [Internet]. [cited 2017 Jan 25]. Available from: https://www.thermofisher.com/order/catalog/product/C34552

8. Bio-Rad. Types of ELISA [Internet]. Bio-Rad. [cited 2017 Jan 10]. Available from: https://www.bio-rad-antibodies.com/elisa-types-direct-indirect-sandwich-competition-elisa-formats.html

9. R: What is R? [Internet]. [cited 2017 Jan 10]. Available from: https://www.r-project.org/about.html

3   Cell-cell model of the outer blood-retina barrier

As aforementioned in the introductory remark, unwanted angiogenesis and choroid neovascularization are causes to many debilitating diseases of eyes, from blurry vision to total blindness. A perfect solution on angiogenesis does not exist. However, seeing the deficiency in the present methods, angiogenesis and vasculogenesis remain unsolved completely – the underlying mechanisms that cause the blood vessels to invade remain unclear. Further, seeing the advantages offered by MEMS system, this study took the advantage of microfabrication to investigate micro-cellular environment and signs of angiogenesis. As choroidal neovascularization is promoted and exacerbated when there are changes in the extracellular microenvironment *in vivo*, glucose concentration and hypoxia were investigated in an attempt to mimic the effect of changing microenvironments. This chapter also explains the microfluidic-based and hydrogel-based models in fabrication of microvessels.

3.1   Materials and Methods

Transferable methods on microfabrication and photolithography are described in Chapter 2, Materials and Methods. The following section only give details on fabrication of device components that are not covered in the previous chapter. Similarly, cell culture conditions are also explained in Chapter 2.

3.1.1   The two-layer single microchannels device as the oBRB model

3.1.1.1 Device specifications

Molds for micropillars were made in the same way as described in Chapter 2.1. A few more steps are required to make PDMS porous membranes.

Micropillars and PDMS membrane

Spinning PDMS onto the master mold results in thin membrane (approximately 6 microns, Fig. 3.1.1-1 right).
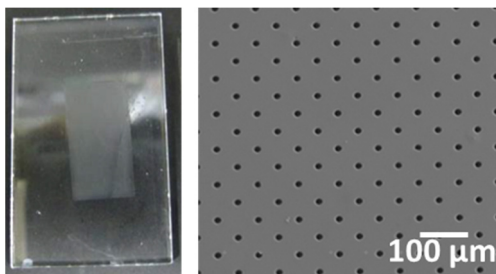

Fig.   3.1.1-1 Spin-coated PDMS membrane.

Left: membrane dried on a 4x3 cm acrylic board; right: membrane under a SEM microscope. The pore diameter is 10 microns.

Protocol: PDMS porous membrane

In order to reduce the viscosity of the PDMS membrane, the PDMS pre-polymer was diluted with hexane (Wako).

1. Mix the freshly made PDMS (refer to section 2.1.4 on how to make the working PDMS polymer) with hexane at w/w 2:1. Make sure there are no air bubbles.
2. Spin coat the PDMS/hexane mixture on the wafer at 500 RPM for 10 s then at 3500 RPM, for 300 s. Be careful of the air bubbles as it will generate defect in the resulting membrane. Heat the wafer and PDMS mixture at 120 C, 3 min.
3. Remove the wafer from the hotplate and place it in 100% ethanol to detach the PDMS membrane from the wafer. Place the peeled wafer onto an acrylic board to dry. The end product is a porous PDMS membrane (thickness ~10 um, pore diameter 10 um).

3.1.1.2 Two-layer microfluidic device assembly

Once the porous membrane and microchannels engraved PDMS slabs are ready, they can be bonded and assembled into the microfluidic device. The device is composed of identical upper and lower microchannels, sandwiching a porous membrane. Fig. 3.1.1-2 shows the exploded view of the microfluidic device.
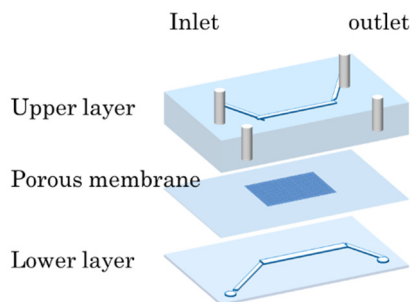
Fig.   3.1.1-2 Exploded view of the two-layer single-channel microfluidic device.

Protocol: microfluidic device assembly
1. Punch the inlets and outlets of a PDMS slab with a diameter 1.5 mm to make through-holes (4 in total). This is the upper channel of the device.
2. Tape the PDMS slab to remove dust and gently blow the PDMS membrane for the same reason. Place the PDMS slab and the membrane into an ozone cleaner for 45 s before bonding them together. Make sure the microchannel is covered by the porous part of a porous membrane. Place it in a 70 C oven for 1 h.
3. Remove the acrylic board to detach it from the porous membrane and the PDMS microchannel. Place the structure and another PDMS slab (no holes punched, i.e., lower channel) into the ozone cleaner for 45 s. Align the upper channel and lower channel under the microscope before moving it to a 70 C oven for 1 h.

4. Insert and glue a 18G needle to each of the in/outlet of the device and keep the device in an over to let it dry.
5. Sterilized the device under UV until use it for experiments.

3.1.1.3 Formation of the oBRB cell-cell model

Protocols: preparation for ARPE and HUVEC co-culture

1. Sterilize the device with 70% ethanol and place the device under UV for at least 30 min.
2. Immediately before being used, use the Corona Surface Treater – BD-20A (ELECTRO-TECHNIC PRODUCTS) to thoroughly treat the channels.
3. Wash the microchannels by flowing PBS, follow by filling them with Poly-L-Lysine (PLL). Incubate the device for 1 h. Next, wash the microchannels by flowing PBS, follow by filling them fully with fibronectin at 7.5 ug/ml (diluted in PBS). Incubate the device overnight.
4. Wash and fill the device with DMEM High glucose (10% FBS) and incubate for 1 h.
5. Load stained ARPE into the upper channel of the device at a density of approximately 3×10^7 cells/ml. Confirm that there are cells on the porous membrane by checking it under a microscope. Rest the device in an incubator for 5 hours or until the cells have attached on the membrane.
6. Prepare the perfusion system and run the syringe pump initially at 450 ul/hr until the flow is initiated before decrease the flow rate to 50 ul/h.
7. After ARPE is confluent on the membrane, load the stained HUVEC into the lower channel of the device and immediately turn the device upside down so that cells attached (seeding density of HUVEC is about 3×10^6 cells/ml). Return the device into an incubator and start the perfusion system once HUVEC has attached onto the porous membrane (approximately 30 min). Do not starve HUVEC without medium for longer than 2 h.

For analysis of co-cultures, ARPE-19 and HUVEC were dyed respectively with Cell TrackerTM Fluorescent Probes red and green (5 µM, each) according to the staining protocol. ARPE detachment and heterotypic interactions of the co-culture were analyzed. ARPE cells were conditioned in the media listed in Table 2-2 prior the start of co-culture experiments.

3.1.2 Characterization of the ARPE monoculture

3.1.2.1 Long-term culture of ARPE-19 and cell differentiation

Differentiation is the process during which a type of cell becomes a more specialized cell type. As an alternative to primary retinal pigment epithelial (RPE) cells, ARPE-19 is used widely due to higher proliferation rate and relatively undemanding culturing condition. However, its phenotype is dependent on culture conditions and many differentiation markers are usually absent. In an attempt to differentiate ARPE-19, which is said to take four months to differentiate, cells were grown in tissue culture plates and in a

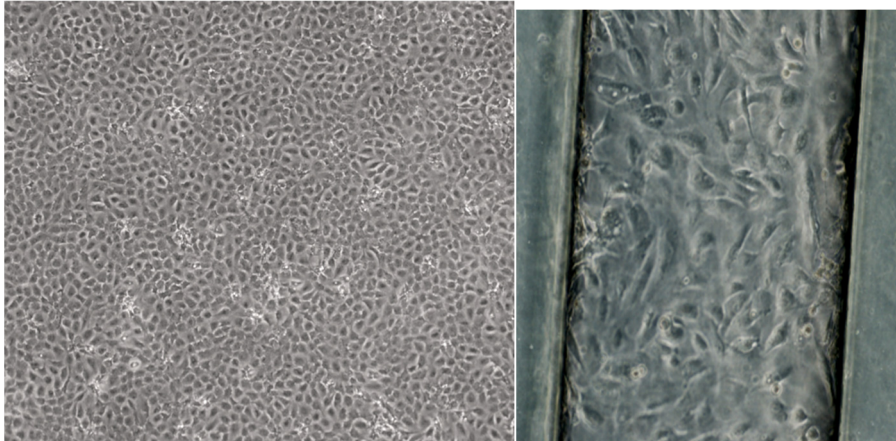microfluidic device with lower serum concentration (Fig. 3.1.2-1).

Fig.   3.1.2-1 ARPE-19 culture long-term culture.

Left: inside a tissue culture plate; right: a microfluidic device for over 2 months, viewed at magnification 40X and 100X. Cells were grown under DME high glucose supplemented with metabolic pyruvate and 1% serum.

Fully differentiated RPE cells are pigmented with hexagonal-shape morphology. VEGF secretion and markers such as RPE65 are also reliable indicators. The cells were cultured for three months but showed no observable signs of differentiation. As the phenotype is dependent on culture conditions, the medium, supplements and the origin of the cells were all possible reasons. In addition, epithelial and endothelial cells actively sense fluid flow. For example, it has been shown that fluid flow-mediated bending of the primary cilium elicits intracellular Ca^{2+} signaling (1). Fluid flow is also found to exert mechanical stresss on the actin cytoskeleton (1). Moreover, some studies hypothesize that fluid shear stress is required for complete differentiation of epithelia and endothelia, as they are subjected to constant fluid flow in vivo (1). The shear stress exerted on ARPE culture was way below physiological shear stress *in vivo*, which could be another possible reason to cells not differentiating inside the microfluidic device.

3.1.2.2 VEGF secretion

VEGF secretion, as introduced in the Introduction, fluctuated according to the microenvironment that cells are in. In addition to the disturbance of tight junctions, VEGF concentration was also analyzed in order to gauge the status of cells quantitatively.

Cells were deprived of serum (serum deprivation) 24 h prior the start of any experiments; thereafter, the media were changed (Chapter 2.2.1.2, ARPE-19) and samples were collected for analysis. ELISA kit was used in quantifying the VEGF in samples (Chapter 2.4, ELISA). The methodology was the same for experiments using both static (TC well-inserts) and microfluidic devices.

3.1.2.3 Trans-epithelial Electrical Resistance (TEER)

Evaluation of formation of ARPE-19 tight junctions

Tight junctions

Generally, epithelial cells assume a polarized architecture and are responsible for selective barrier and transport functions. Tight junctions control the paracellular pathway by sealing neighbouring together to control the passage of substances, resulting in 2 distinct plasma membrane domains: apical and the basolateral domain with no diffusive intermixing. The polarized distribution of transporters, carriers and channels is the basis for the vectorial transport, secretory and absorptive functions of epithelial cell layers [1]. Epithelial polarity is tightly controlled by a self-organizing network of polarity proteins and lipids, and a highly organized vesicular trafficking system [1]. This is underlined by the fact that malfunctions in epithelial polarity frequently lead to cancer formation [1].

Transepithelial electrical resistance (TEER) was used to determine the integrity of barrier functions. We can infer the differentiation degree of cells in vitro and how well they are growing by evaluating TEER. Multiple factors could influence TEER values, including the type of electrode, the type of the insert, or the human errors such as not resurfacing the electrode, ways of holding the chopstick electrodes, temperature of the cell culture, measure TEER after changing the medium, etc. One should be consistent in setting up experiments to reduce unnecessary variability in the results.

Quantification of ARPE detachment area

Corresponding images of ARPE-19 and HUVEC taken at the same time point were first converted to 8-bit before being merged into a colour composite image under Merge channels function in ImageJ. To calculate the detachment of ARPE-19 in co-culture experiments, images of ARPE-19 monolayer at each recorded time point were converted to 8-bit. The area of the channel was selected and cropped. Relative percentage of black and white pixels was then recorded after applying threshold values to the images from which the percentage of detachment was calculated for each sample.
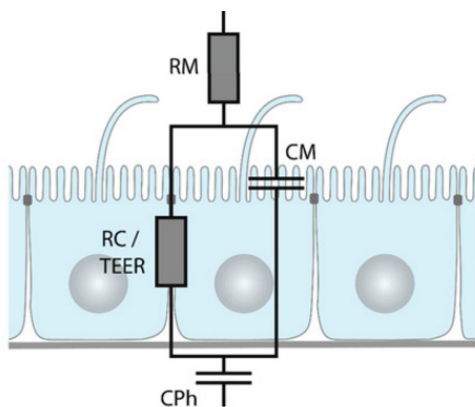
Reprint from [1].

Fig. 3.1.2-2 Electrical characterization of epithelial cell layers.

TEER is one of the indicators in evaluating the tightness of the tight junctions; in other words, the integrity of the barrier function of epithelial cells. Typically, TEER measurements are performed at low AC

frequencies (usually 12.5 Hz) but not at DC current which would have undesirable side effects on the cells and electrodes. The impedance of epithelia strongly depends on the AC frequency, which indicates that at higher frequencies the influence of the capacitance of the lipid bilayer of the cell membrane becomes dominant (Fig. 3.1.2-2). EVOM2 (World Precision Instrument) can be used to measure the voltage, but only resistance measurement is focused here.

Recording TEER of epithelial cells

The equipment required for the TEER measurement is shown in Fig.3.1.2-3.
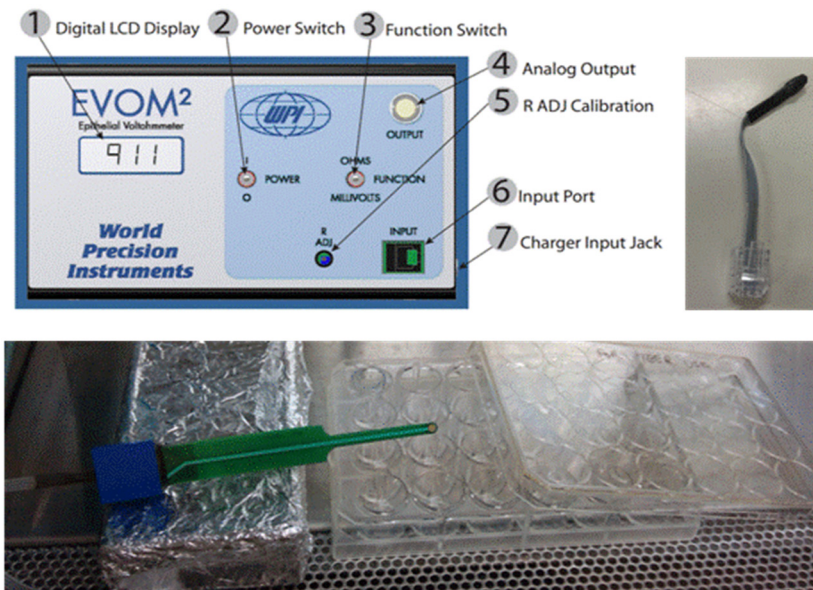
Fig.   3.1.2-3 EVOM machine, component for calibration and measurement.

Top right: the calibration resistor. Bottom: chopstick electrode and the cell culture plate. Reprinted from World Precision Instrument (2).

Preparation
- Calibrating the EVOM2 meter: in the **Ohms** mode, insert the 1000 ohm test resistor into the input port and calibrate the meter until 1000 ohm is displayed. Disconnect the meter from the AC power source when in use.
- Sterilization of STX2 electrode: immerse the electrode tips in 70% ethanol for *no longer* than 15 min. Rinse it with a sterile electrolyte solution similar to the experimental cell culture medium or in 0.1-0.15M KCl or NaCl solution. Handle the electrode aseptically, and store it inside a clean hood. Shield it from the UV light.

Protocol: TEER measurement (transwell)

1. Make sure the EVOM2 meter is charged and disconnected from the charger when it is used. Turn the Power on (I) and set the Function switch to Ohms.
2. Connect the electrode to the meter.

3. Add electrolyte to a blank cup (the cell culture insert without cells).

4. Place the electrode in the blank cup. Note the position of the electrodes - see Fig 3.1.2-4 A steady ohms reading of the solution resistance should result. This is the value of the blank resistance – it has to be measured for every new set of measurement.

5. In the same way as in step 4, take measurements of experimental samples. Rinse the electrodes with the experimental culture media between measurements to avoid carryover of one sample into the next.

6. After the measurements are all completed, wash the electrodes with a sterile 0.1 NaCl or KCl solution. Air dry and store the electrode inside the clean hood for future use.
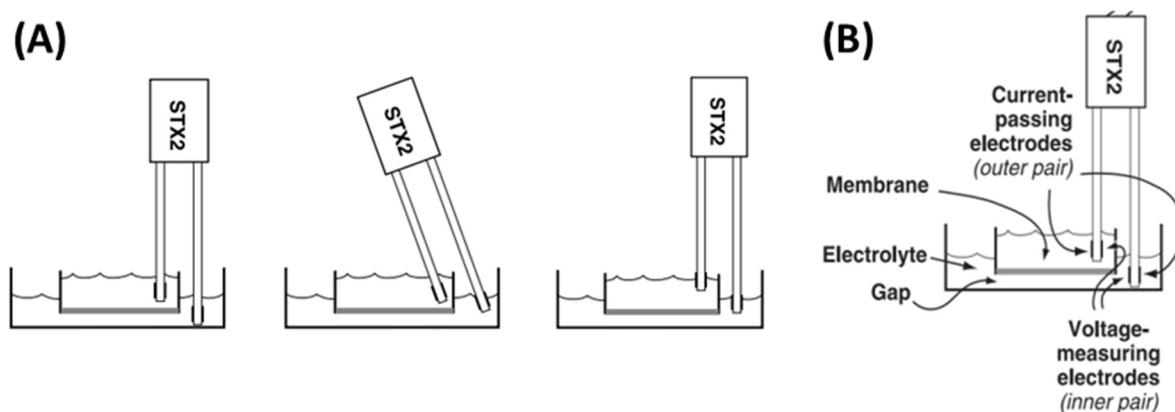
Fig. 3.1.2-4 TEER measurement: using the chopstick electrodes.

(A) Various position of a chopstick electrode inside a culture insert (correct measurement position, angle variance, depth variance). (B) Electrodes in solution. Reprint from World Precision Instrument (2).

Note 1: measure the TEER *before* medium change and make sure the volume in every insert (and well) is the same across all samples, i.e., be consistent in variables for reproducibility of results.

Note 2: TEER measurements are performed at room temperature – leave the samples in the clean bench for at least 30 min before taking the measurement.

Note 3: with use, the electrode surface can become coated with protein or other foreign materials. To address these issues, either (1) re-chloridize the electrode by soaking it in 5% sodium hpochlorite and rinsing it with water after soaking; or (2) resurface the electrode by lightly sanding the voltage electrode of STX2, which is the silver pellet on the inner surface near the electrode tips (Fig 3.1.2-4, B).

Resistance calculations and unit area resistance

The value of the blank always adds to the total resistance measured across a tissue culture membrane. The blank resistance must be measured and then subtracted from the resistance reading across the tissue in order to obtain the true tissue resistance. The calculated resistance for the tissue (R_{tissue}) is given by:

$R_{true\ tissue} = R_{total} - R_{blank}$

Where R_{blank} is the value from the blank resistance and R_{total} is the readings given the EVOM2 meter.

As the resistance is inversely proportional to the area of the tissue, typically the product of the resistance and the area is calculated and reported. The unit area resistance is independent of the area of the membrane used and may be used to compare data obtained from inserts of different sizes.

Note: resistance readings for 24 mm or larger diameter inserts obtained by using the EVOM2 with the STX2 electrode should *not* be converted to unit area resistance as recommended by the manufacture.

3.1.2.4 Permeability assay using FITC-dextran

Tissue culture well & inserts

The cell cultures were exposed to different medium conditions: DME High glucose, DME Low glucose, DME low glucose and $CoCl_2$. ARPE were exposed to respective conditions for 24 h and TEER were measured at certain time intervals.

Microfluidics

In the microfluidic system, the permeability to fluorescent particles was measured in order to determine the status of tight junctions. In this study, Fluorescein isothiocyanate-dextran (Sigma, FITC-Dextran, MW 70,000 Da) was used. FITC is a derivative of fluorescein; it is conjugated to dextran to be used as a fluorescent probe. The lower the permeability to FITC-dextran, the tighter the tight junctions among the neighbouring cells is. In the same way, a high permeability to FITC-Dextran indicates the leaky junctions (i.e., break down of intercellular connections). Fig. 3.1.2-5 illustrates an equivalent TEER measurement of microfluidic cell culture.

Following the same methodology, the cells cultured in microfluidic devices were exposed to different medium conditions (Chapter 2.2.1.2), fluorescent intensities were read by a microplate reader.
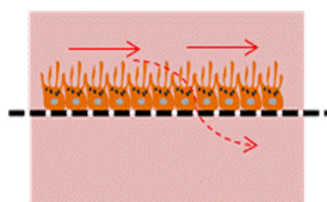
Fig. 3.1.2-5 Illustration of flowing FITC-dextran inside the microfluidic device. FITC was supplied in the upper channel (solid-line arrows); if the tight junctions are leaky, FITC molecule will leak through the membrane as shown in dashed arrows.

Note 1: protect the samples from light when working with FITC-dextran.

Protocol: evaluation of epithelial barrier function in the microfluidic device using FITC-dextran

1. After determining the duration of the experiments, the concentration of FITC-Dextran and the amount needed, of FITC-Dextran was measured by a precision weighing scale.
2. Dissolved the FITC-Dextran powder in pre-warmed DME medium completely. Filter the solution. Reserve 200 ul for fluorescent intensity measurement (this is the reading for input).
3. At the end of an experiment, collect the outputs (from upper and lower syringes from each device).
4. Subject the samples to microplate readers to measure fluorescent intensity immediately. Make sure

to have a blank (i.e., medium with no FITC-Dextran), input(s) and outputs.

5. Sorting the data: subtract the input(s) and outputs by blank. Standardize the output data by subtracting the input(s) to obtain the fluorescent intensity.

3.1.2.5 Effect of the pro-inflammatory cytokine and corticosteroids drugs

In an effort to investigate the effect of pro-inflammatory cytokines on ARPE-19 cells, the effect of TNF-alpha (Wako) was investigated against cells cultured in inserts of the transwell. The effect of corticosteroids drugs was also investigated. Steroids are given to treat inflammatory reactions and there are many corticosteroids drugs on the market that have been used in clinical trials. The sub-objective here was to first elicit inflammatory reactions in ARPE-19 cells and checked if the injured cells can be resurrected by using Dexamethoasone 21-phosphate disodium salt or DSP (Tokyo Chemical Industry), one of the steroid drugs. States of cells were judged by evaluating TEER and detachment percentage at different points throughout the duration of experiments. Steroids assessments were performed for no longer than 24 h due to the cytotoxicity from previous study.

The protocols below are written based on cells cultured in inserts of a transwell in 24-well format.

Protocol: elicit inflammatory reactions of ARPE-19 cells

1. Reconstitute TNF-alpha (2000 ng/ml) in PBS. Aliquot into vials; freeze at -20 C ~ - 70 C for long-term storage. For experimental uses, dilute further with cell culture medium/media.
2. Check the cells microscopically and measure TEER before changing the culture media.
3. Aspirate the cell culture media and replace them with the respective media as listed in Table 2-2 with dissolved TNF-alpha (0, 10, 30, 60 ng/ml).
4. Measure and record the TEER after certain time intervals (6, 24 h) after the start of experiments,

Protocol: investigating the effect of corticosteroids drugs

1. Impose inflammatory responses on ARPE-19 cells by resting cells in TNF-alpha containing medium for 24 h.
2. Aliquot DSP into desired concentrations (0.001, 0.01, 0.1, 1 mg/ml) in pre-warmed cell culture media.
3. Measured the TEER at certain time intervals throughout experiments to track the growth of cells.

3.1.2.6 Induction of hypoxia by cobalt chloride (II) in ARPE-19

When the oxygen level in blood is reduced much lower than a typically physiological range, human body is apt to respond and many molecular mechanisms are triggered. Hypoxia inducible factors (HIFs) are one of the key transcriptional activators that regulate oxygen homeostasis, which rely heavily on delivery of oxygen to tissues and cells. It is postulated that HIFs contribute to many diseases and pathogenesis including ocular neovascularization (3) – the angiogenic switch triggered by oxygen-deprived cells and tissues to induce vessel formation. It was also found that VEGF was directly induced by HIF-1alpha (4).

The optimal CoCl₂ concentration is the one that induces hypoxia on the cells, but not so toxic that it kills the cells. Fig 3.1.2-6 shows the cells exposed to CoCl₂ at 200 μM – it did impose some effect on the cells but they could not survive for over 48 h. The optimal concentration was then determined to be 150 μM.
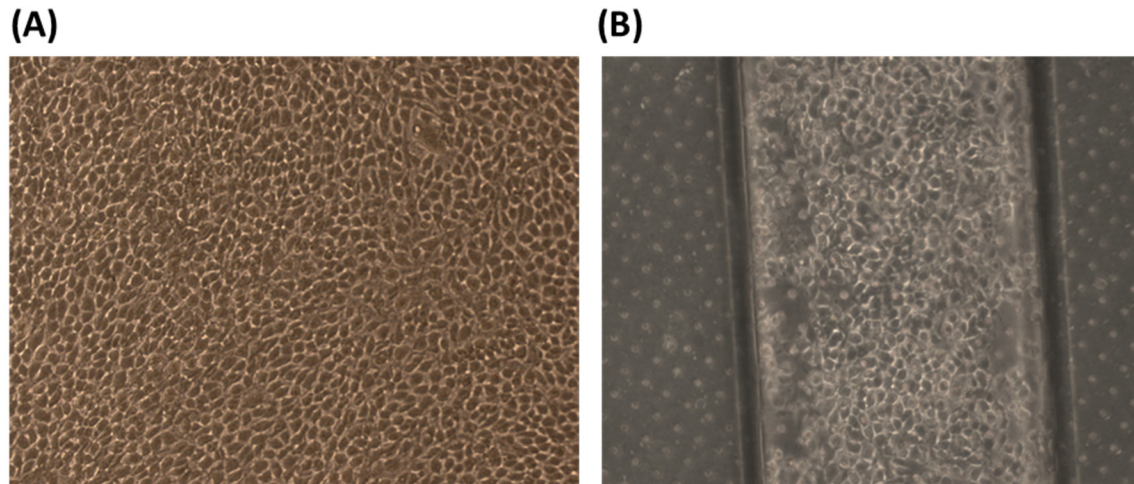
Fig. 3.1.2-6 ARPE exposed to an overly high concentration of CoCl₂.

(A) Cells cultured in a tissue culture flask and (B) microfluidic device 24 h after exposed to 200 μM of CoCl₂, viewed at 100X magnification. ARPE morphology changed, resembling cobblestone-like shape.

3.1.3 Image processing

Images were acquired using the fluorescence microscope (Olympus) or the confocal imaging system (LSM700, Carl Zeiss MicroImaging.Co., Ltd.). After obtaining raw data, they were trimmed and processed for analysis. All the processes were done in the software ImageJ (NIH).

Steps in overlay images in ImageJ

1. Open the first image to be overlaid in Image J.
2. Under the top panel, find Image, Color, then click Stack to RGB.
3. Convert the image to 8 bit under Image, Type. Choose 8 bit from the pullout menu.
4. Repeat the step 1-3 for the second image to be merged.
5. Go to Image, Color, Merge Channels…, choose the images corresponding to the appropriate filters will generate the overlaid image. Crop the resultant image if necessary.
6. To save the file, convert the resultant image back to RGB scale by going to Image, Type and click RGB color option.

3.2   Results and Discussion

3.2.1 Validity of the developed microfluidic device as the oBRB model

Microfluidic device fabrication

Photolithography process could be completed within 3 h. Once the master mold was made, multiple microchannels could be made in parallel, making device fabrication effective. The rapidity and mass production make micromachining promising in fabrication in vitro platforms that model tissue environments for studies of cellular interactions.

An understanding on the processes and materials that are used are important for one to adapt and create devices that suit the different applications.

In vivo epithelial cells within a monolayer receive their nutrients from the basolateral side (1); the porous membrane therefore allows access from the apical and basolateral side. However, it should not be thicker than a few ten micrometers in order to guarantee fast diffusive transport through the pores. In addition, pore diameters smaller than 1-2 µm prevent migration of individual cells through the pores which does not meet our experimental objectives. Other than customized PDMS membranes, commercially available porous membranes made of polyester, polycarbonate and polyethersulfone with different pore diameters are also available and has been utilized in microfluidic chips.
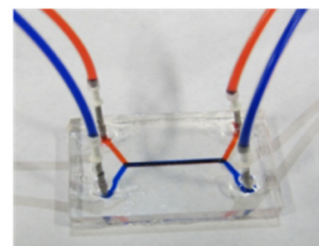
Fig. 3.2.1-1 The assembled two-layer single channel microfluidic device flowing with dye water.

The microfluidic device and its use in cell culture

The structure of the device is simple yet allowed co-culture (and possible tri-culture) of cells (Fig. 3.2.1-1). Judging its feasibility in culturing cells:

$$\tau = \frac{6\mu Q}{h^2 w} , \quad Q = v \times A$$

where τ: shear stress (Pa), μ: viscosity (kg/m.s), Q: flow rate (m3/s), h and w: height and width of a rectangular channel (both in m), v is the velocity of flow (m/s) for channels with a rectangular cross-section. At 37 C, the viscosity of the DMEM medium is estimated to be 0.78 x 10^{-3} Ns/m^2.

Based on the above numbers, a flow rate of 50 µl/h corresponds to a shear stress of 0.013 Pa, which is lower than the physiological shear stress in human vein (0.1 – 0.6 Pa) and way lower than the shear stresses in arteries (1 – 7 Pa) (5).

3.2.2   ARPE monoculture

Monolayer of ARPE was subjected to three tests: integrity of tight junctions, VEGF secretion and responses to TNF-alpha. The first two experiments aimed to characterize *in vivo* ARPE cells while the TNF-alpha and steroids drug were added to in an attempt to evaluate the effect of inflammatory cytokine (TNF-alpha) on ARPE-19.

Several studies were carried out on ARPE-19 monocultures to characterize the cells in both tissue culture

wells & inserts and the microfluidic device.

Static culture configuration

Cells were cultured in traditional tissue culture wells and inserts (BD Falcon), including 6, 12, and 24 well formats, which comes with inserts that are designed to be fitted into wells of the respective sizes (Fig 3.2.2-1).
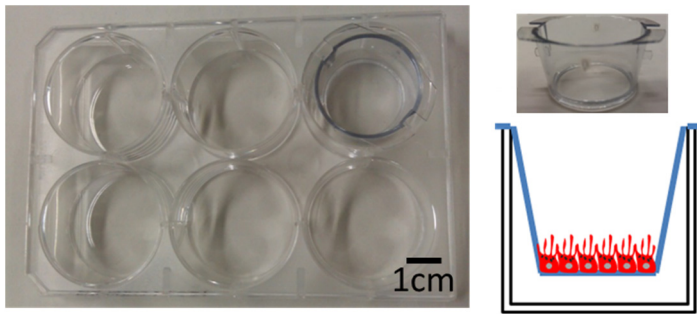
Fig. 3.2.2-1 Plate experiment: tissue culture plate (transwell and inserts).
The tissue culture well plate in 6-well format and an insert showing the top and side views; bottom right: schematics of the insert (blue) and cells (red) cultured on a membrane of an insert.

All the wells and inserts were sterile and tissue-culture treated (abbreviated as TC-treated); inserts membrane material were Polyethylene Terephthalate (PET). Depending on experimental purposes, cells were cultured in the wells in some experiments. If not specified otherwise, ARPE were cultured on the top of a porous membrane while HUVECs were cultured on the bottom of the membrane of an insert. The pore size of the membrane of the insert used was 8 µm for all the experiments.

3.2.2.1 Testing integrity of the tight junctions

Fig. 3.2.2-2 Evaluation of ARPE barrier properties in transwell and microfluidic device.
Evaluation of tight junctions of ARPE cells cultured in tissue culture inserts (left) and in microfluidic devices (right). TEER was measured from cultures in transwell while fluorescence intensity was analyzed from microfluidic cell cultures.

Figures 3.2.2-2 show the TEER of culture insert and microfluidic device respectively. ARPE-19 monolayers were subjected to different media over 24 h and the TEER was measured. FITC intensity was measured for over 24 h period of time.

Tissue culture insert sample

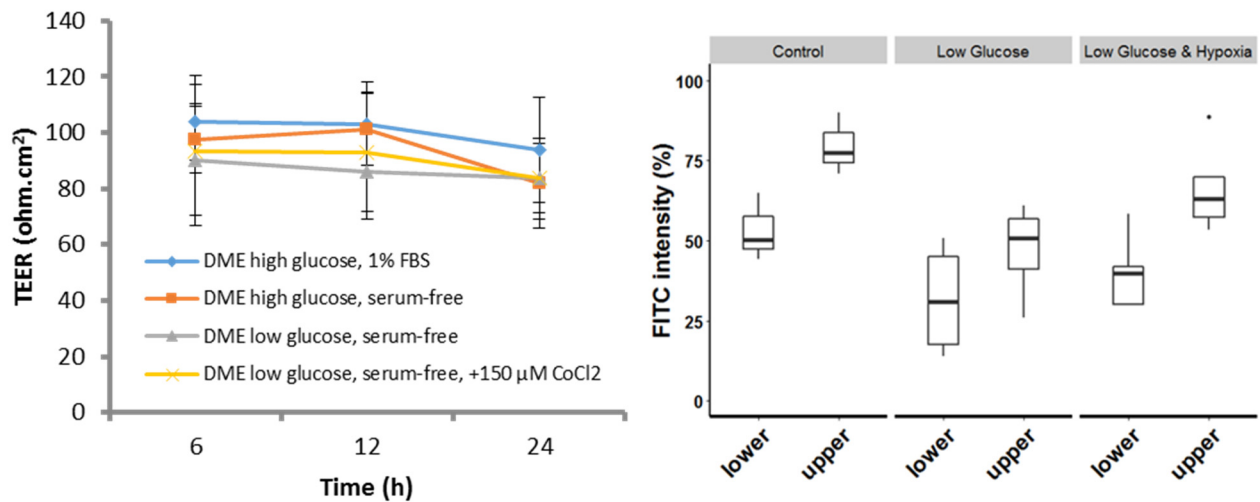The effect of time and the difference between medium conditions were analyzed statistically. The TEER dropped slightly by $t = 24$ ($p = 0.0237$) but the difference between the control, low glucose and hypoxia cases were insignificant.

Microfluidic cell culture

As mentioned before, the integrity of microfluidic cell culture was determined by flowing fluorescent molecules in only one channel. TJs serve as an indication on how tight the barrier function is and is of particular importance in the blood-retina barrier (BRB). As the outer BRB prevents transport of molecules larger than 300 kDa into and out of the retina (6), we do not anticipate 70 kDa FITC-dextran to be obstructed by monolayers in our permeability test. Samples from both channels were collected and analyzed. There was an overlap in results between the upper and lower channels in the low glucose case, but the differences between different conditions were not significant. The upper channel across all cases had a higher FITC-Dextran intensity ($p = 0.00047$), indicating that the tight junctions were not leaky but relatively stable under low glucose and hypoxic conditions. The inter-fluorescence intensities (i.e., between control, low glucose and hypoxia cases) were insignificant.

The results above indicated that ARPE monolayer remained relatively stable under low glucose and/or hypoxia conditions.

3.2.2.2 VEGF secretion

Innate RPE cells secrete VEGF predominantly from the basolateral side to help regulation of the metabolism of the choroid vessels (7,8). However, RPE cells are prone to secrete an even higher concentration of VEGF if there is slight alteration to the microenvironment that induces DNA damage as non-lethal levels of DNA damage are postulated to activate stress-induced premature cellular senescence (SIPS) of cells (9). Increasing non-hexagonal RPE cell shapes, reminiscent of the SIPS characteristic alterations of cell shape, has been described in aging retinas and AMD donor eyes (9).

Tissue culture insert sample

ARPE was induced and secreted a significantly higher concentration of VEGF under low glucose and hypoxic cases (1.28 and 1.86 times higher, respectively). However, the results (Fig. 3.2.2-3) did not show basolateral-dominant secretion, but align with a study that found net secretion from the apical side of the cells (10).

Microfluidic cell culture

From the VEGF outputs (Fig. 3.2.2-3), ARPE-19 responded to lowered glucose and hypoxic microenvironments by increasing VEGF secretion (68.1% and 77.1%, respectively, compared to the control in the upper channel). Studies have found that the expression of VEGF-C and VEGFR-3 is upregulated in ARPE-19 cells after being exposed to hypoxia *in vitro*, consistent with the increased concentration of VEGF detected in the extracellular medium (11).

Another study pointed out that polarized secretion was toward the apical side only when RPE cells were exposed to light damage (7). There are many possible factors contributing to these observations including density of the porous membrane, origin of the cells and whether it is a cell line. As the ARPE-19 cells used in our experiments were not fully differentiated, we also considered this as another factor contributing to the unexpected behaviour.
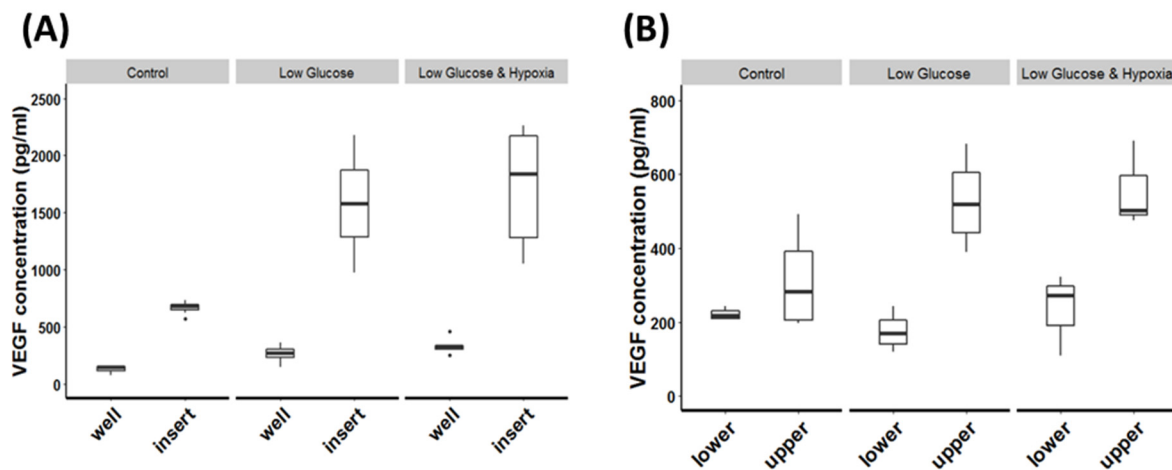
Fig. 3.2.2-3 VEGF secretion from cells cultured in tissue culture well & inserts and in microfluidic devices. (A) transwell culture; (B) microfluidic culture. Well – insert corresponds to lower channel – upper channel from the static and microfluidic system.

3.2.2.3 Effect of the TNF-alpha and corticosteroids drugs

As a pioneering test on the potential steroid drugs to eye diseases and use the microfluidic cell culture as a mean of drug discovery, we first wish to characterize the response of ARPE-19 to steroid drugs that are on the market. To test the effectiveness of the drugs, ARPE-19 was first exposed to TNF-alpha, one of the pro-inflammatory cytokines that elicit inflammatory reactions in cells. Glucocorticoid steroids are a class of steroids that bind to the glucocorticoid receptor which regulates inflammation and have been used extensively to treat inflammatory conditions. Dexamethasone, a synthetic glucocorticoid steroid, has been shown to regulate pro-inflammatory cytokines in two ways: 1) the glucocorticoid receptor interacts directly with glucocorticoid response elements in the promoter region of genes, thereby inhibiting gene expression, 2) by interfering with transcription factors nuclear factor kappa-light-chain-enhancer of activated B cells(NF-κB) and Activator Protein 1 (AP-1) (12). In human monocytes, dexamethasone has been shown to induce a specific anti-inflammatory subtype marked by the up-regulation of many anti-inflammatory genes and the down regulation of pro-inflammatory genes (12).

Effect of TNF-alpha

ARPE cultured in tissue culture inserts were exposed to TNF-alpha of various concentrations, under different medium conditions. From Fig. 3.2.2-4, by t = 24 h, the TEER across cultures decreased compared to t = 6h, regardless of TNF-alpha concentrations. However, there were initial surges in TEER values during the first 6 h after the start of the experiment. As the cultures were conditioned to the respective medium, the increased resistance values were not accounted for. The most likely reason was due to the instability associated to addition of TNF-alpha. In addition, the resistance values under the effect of hypoxia and TNF-alpha were the lowest of all.

Looking at the TNF-alpha concentrations, TNF-alpha concentration above 30 ng/ml caused substantial decreased in TEER and death of cells as observed from the morphology.
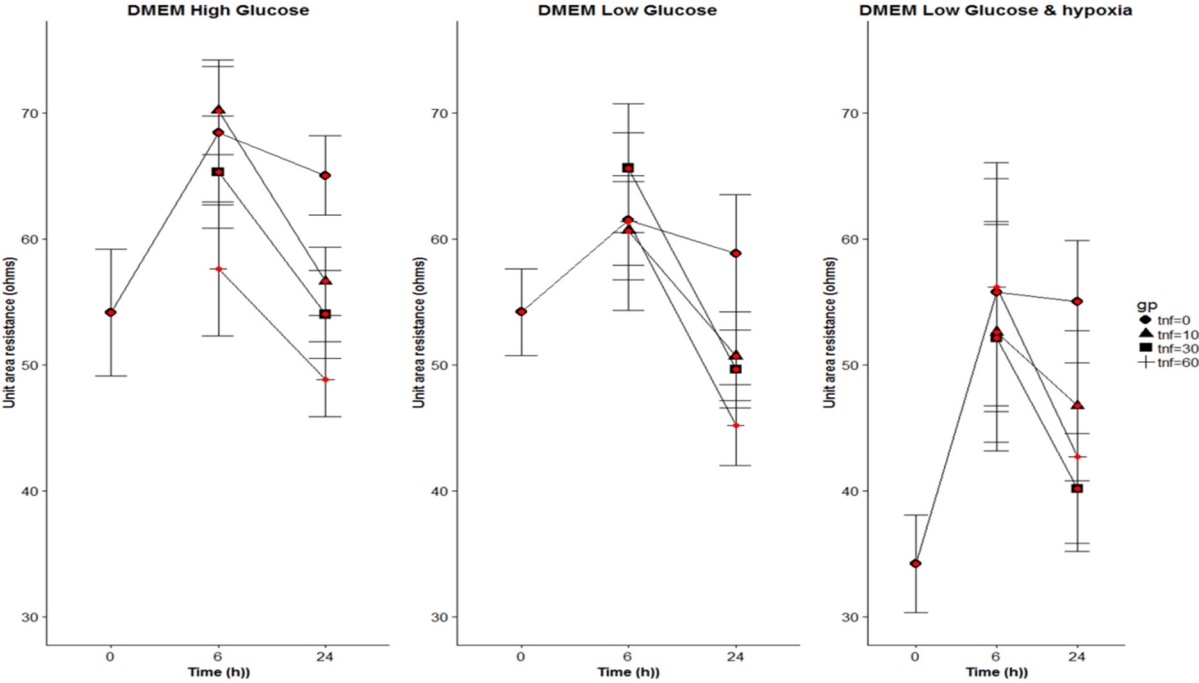

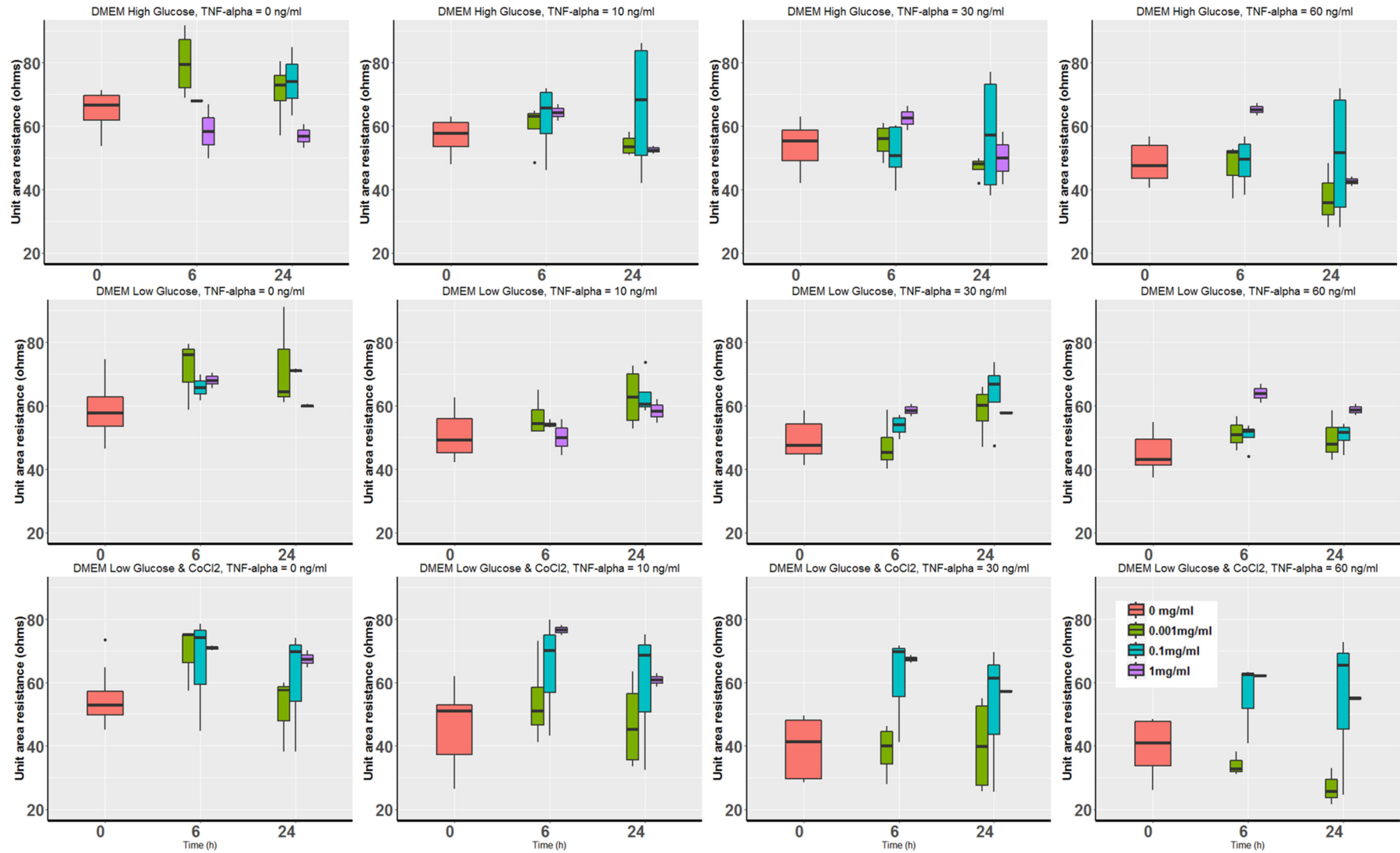**Fig.   3.2.2-4 TEER measurement of ARPE under pathological microenvironments.**

Fig. 3.2.2-5 Effect of corticosteroids drug (DSP) on ARPE treated with TNF-alpha.

Cells were cultured in high glucose (top row), low glucose (middle row) and low glucose & hypoxia (last row).

Dexamethoasone 21-phosphate disodium salt, DSP

Research has found that an overly high concentration (> 1 mg/ml) is harmful to the cell culture hence DSP concentration was tested from 0.001 mg/ml – 1 mg/ml. From the results, if the cells were not treated with TNF-alpha, the TEER increased by t = 6 for low glucose and hypoxia cases (Fig 3.2.2-5). In addition, TEER for cell cultures in low glucose and hypoxia exposed to TNF-alpha all increased by t = 24 h, although the difference was found to not be significant.

In the future, TNF-alpha concentration will be experimented between 10- 30 ng/ml; it is anticipated to be mixed together with DSP in accessing the TEER. The experiments are expected to be repeated for higher reproducibility and a more confirmed conclusion.

3.2.3 HUVEC monoculture

Additional to analyzing ARPE monolayer, the angiogenic property of HUVEC monoculture was also observed. Cells were cultured on the bottom of a membrane in both culture inserts and microfluidic devices. For all experiments, VEGF-A165 (Wako) at 50 ng/ml and controls (no VEGF-A165 addition) were observed, where VEGF was added to the upper channel or in the inserts. Fig 3.2.3-1 shows the schematics of this approach. As discussed in Introduction, angiogenic abilities of HUVECs propel them to grow towards the source of the growth factor. Thus, it was anticipated that HUVECs would migrate over the pores of membranes to the source of VEGF in this case.

To culture HUVEC, culture inserts were turned upside down to allow seeding of cells. Once the cells attached (30 min), inserts were turned back to the original position (upright) and medium was supplied. The same approach was employed for microfluidic cultures except attachment was not strictly limited to 30 min as in culture insert case (no longer than 1.5 h is recommended).

Monoculture of HUVEC in the microfluidic device

The device is designed in such a way that ARPE-19 cells and HUVEC are separated by a porous membrane, similar to the *in vivo* anatomy where retinal cells are separated from the choroids by Bruch's membrane (BM). Bruch's membrane supports fundamental cellular functions and cell-cell communication while being formed and maintained from both the RPE cells and choroids in a coordinated fashion (6). Cells in our device are separated by a fibronectin-coated 6.5 um-thick membrane which closely mimics the anatomical structure of BM. On the other hand, the PDMS membrane lacks the 3D space for the capillary tube formation. As a result, we used endothelial cell migration as a surrogate for the first step in angiogenic tube formation. VEGF was experimentally supplied to the upper channel of the device. This approach is comparable to the well-known Boyden assay except cells were under a constant flow inside the device.

70
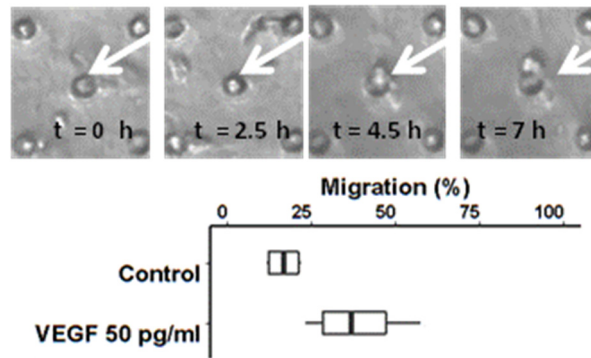
Fig.   3.2.3-1 HUVEC migration under culturing and angiogenic environment.

There was a 21.9% increase in the number of HUVEC migrating through the porous membrane compared to the control where no VEGF was added (Fig. 3.2.3-1). Results indicated that under constant shear stress, HUVEC responded and moved through the pores, toward the source of VEGF.

3.2.4 Co-culturing ARPE-19 and HUVEC inside a microfluidic device

Thus far, properties of ARPE-19 and HUVEC were investigated and confirmed individually using the transwells or/and microfluidic devices. Once the in vitro characteristics were confirmed to be aligned to the in vivo characteristics, co-cultures were performed to work further towards an ocular fundus tissue model. In essence, the goal was to combine previous objectives where abnormal VEGF secretion by ARPE-19 caused by changing medium conditions was enough to stimulate the migration of HUVEC. In other words, the VEGF was not exogenously supplied but came from secretion by ARPE-19 cells alone.

3.2.4.1 Analysis of co-culture

The analyses presented here regarded ARPE-19 and HUVEC co-cultured inside the microfluidic device. The detachment of ARPE was calculated and the interactions were analyzed qualitatively.

Fig. 3.2.4-1 Interactions of ARPE-HUVEC cell-cell co-culture.

(A) anticipation of what happened in the heterotypic interactions; (B) microscopic images of cells in control (top), low glucose (middle) and low glucose and hypoxia (last row) at different time points; (C) ARPE detachment area under different medium conditions.
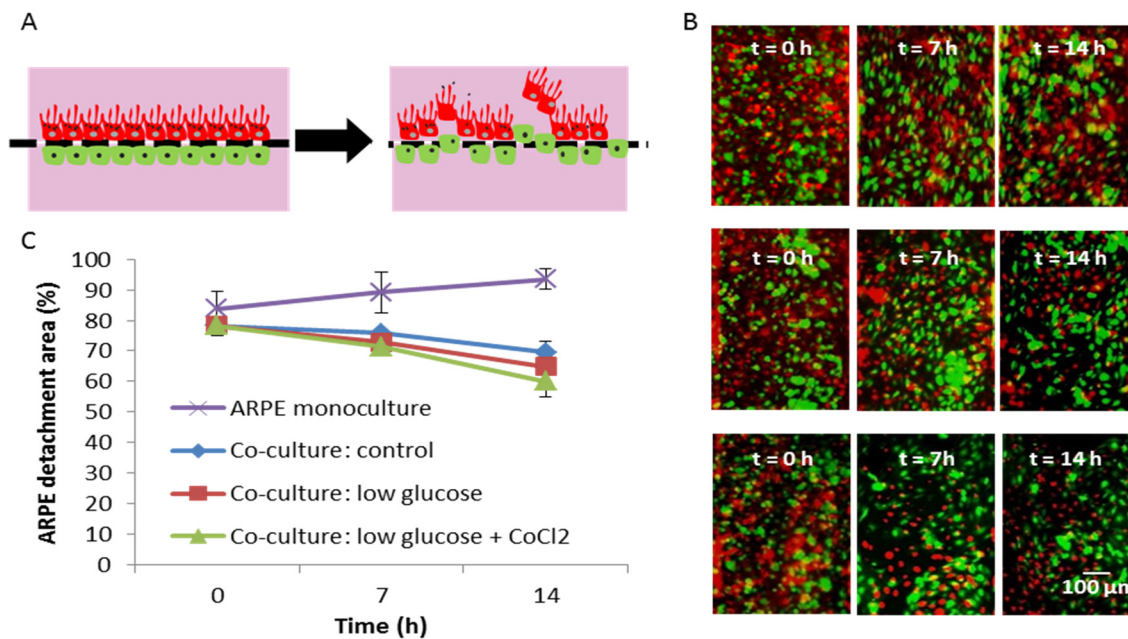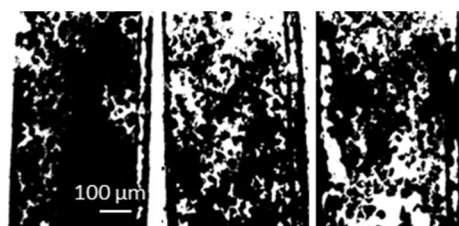

Time (h)	t = 0	t = 7	t = 14
Black:white pixel (%)	80.50	72.18	68.73

Fig. 3.2.4-2 Quantification of ARPE detachment area (raw data and calculation).
ARPE images were processed in ImageJ and the relative pixel intensities were calculated and plotted.

Having confirmed the characteristics of individual cells, we investigated if the VEGF produced by ARPE-19 (rather than exogenously supplied) would elicit behavioral changes in HUVEC with co-culture (schematic representation, Fig. 3.2.4-1 A). As an assessment of the interaction, we overlaid fluorescent images of ARPE-19 and HUVEC at different time points. Judging the results qualitatively (Fig. 3.2.4-1 B), HUVEC (green) attached and proliferated the best for a certain time period (approximately 7-10 h after the start of the experiment); the numbers then gradually decreased under all conditions. On the other hand, ARPE-19 cell numbers reduced as the time progressed, with the highest detachment rate 7 hours after the start of the experiments (initiation of the co-culture). Fig. 3.2.4-1 (B) shows that imposing a combination of low glucose concentration and hypoxia induced the highest loss of ARPE-19 and that the HUVEC grew better (up to certain

72

time point) under such corresponding conditions. We speculate that when ARPE-19 secreted an abnormally higher concentration of VEGF, HUVEC responded by migrating through the pores, causing the detachment of ARPE-19. However, in response to the breakdown of the ARPE-19 monolayer, the media supplied to ARPE-19 diffused into the lower channel and weakened the HUVEC. From observation, the proliferation rate of HUVEC was slow and gradual unlike other angiogenic studies where high invasion of HUVEC was observed (13). Based on observations from the permeability testing, ARPE-19 maintained the monolayer under lowered glucose and/or hypoxic conditions. Thus, it suggests that the loss of the ARPE-19 was less likely to be the culturing conditions but due to heterotypic interactions between HUVEC and ARPE-19. In other words, the superimposed images of the co-culture indicate the possible invasion of HUVEC and subsequent detachment of ARPE-19. To quantify these interactions, we further analyzed the area occupied by the ARPE-19 monolayer over time. Fig. 3.2.4-1 (C) showed the calculation of the detachment area of ARPE-19 cells (the binary images can be found in Fig. 3.2.4-2). We had characterised the monoculture of HUVEC in order to distinguish the invasion from the non-directional proliferation of HUVEC. VEGF is one of the first pro-angiogenic factors found, and our results, along with many studies, have proven its effect on HUVEC. Although we did not examine the effect of VEGF antagonists, HUVEC did respond positively to VEGF-A. Furthermore, the ARPE-19 monolayer in low glucose and/or hypoxic environments secreted 234.84 pg/ml of VEGF from the lower channel which is comparable to the 50 pg/ml of VEGF that we added to HUVEC monoculture. Combining both results led us to conclude that ARPE-19 secreted excessive VEGF due to the changes in glucose and/or oxygen level which induced directional growth of HUVEC.

There are 2 prime concerns in the choices of the supplements in the media: (1) whether to mix culture media of each cell line in the co-culture experiments; (2) the use of serum and growth factors in the experimental stage. Different cell types are cultured in their most suitable type of media to optimize the cell growth. Arguably, the medium for the co-culture should be the same to standardise the culturing conditions. However, the composition of a culture medium is optimized to a particular cell type and replacing it for the other could stress cells and deprive them of their essential *elements* therefore exposing them to less than optimal conditions. Previous studies on co-culture and tri-culture had also adopted the same approaches by supplying different cell lines with their respective culture medium (14,15), utilizing the advantages offered by the microfluidic systems.

We removed the serum component when conducting ARPE-19 monoculture VEGF analysis as VEGF concentrations of serum could considerably bias the results obtained. For a different reason, we removed the serum in the co-culture experiments; serum starvation has been used as a tool to study various molecular mechanisms such as cellular stress response, protein degradation, apoptosis and to simulate particular pathological conditions (16)   as removal of serum is believed to synchronize the cell cycle (i.e., bring them to one phase of cell cycle) (17,18). Serum free media synchronizes cells in G1 phase. We have adopted this approach to be consistent with previous neovascularization studies (19).

3.2.4.2 Discussion on model validity

This study integrated microfabrication techniques and cell culturing in an attempt to tackle medical problems,

angiogenesis and neovascularization.

The microfluidic platform was simple yet elegant; ARPE-19 monocultures, HUVEC monocultures and their co-culture were characterized. Utilizing the fact that multi-channels can be segregated from each other within a microfluidic platform, the co-culture platform was used in studying the role of medium conditions on ARPE-19 and the consequent response of HUVEC. Due to limitations mentioned in the discussion, observing the complete angiogenesis process was not anticipated but this was probably the first step in elucidating molecular mechanisms of angiogenesis within the microfluidic device using ARPE-19 and HUVEC co-cultures.

Capabilities of microfluidic systems have been widely applied for years; we seek to further build on the on-chip model of the retina by looking at effects of specific soluble factors and evaluating potential treatments. Because viable RPE cells from AMD patients do not grow well in culture (6), the process of wound healing appears to be disturbed in AMD patients. The preliminary results of corticosteroids showed that the drug did seem to resurrect the ARPE cell culture under inflammation. In the future, the experiments are expected to be repeated on the ARPE-19 monolayer and co-cultures to get a more confirmed conclusion. Further, the development of hydrogel-based angiogenesis model will be improved concurrently to get develop in vitro angiogenesis model. It is to be hoped that a robust angiogenesis model be used for disease modelling and drugs discovery.

The consequences of angiogenesis and neovascularization are devastating, and much time and effort has been invested in an attempt to better understand the progression of the unwanted vessel growth. Looking at an even broader scope, microfluidics provide customizable platforms to study development of treatments for cancer and other diseases associated with angiogenesis through identification of compounds that stimulate or inhibit the angiogenesis process.

3.3   Summary of the oBRB cell-cell model

We have presented a simple but elegant microfluidic platform where we characterised ARPE-19 and HUVEC monocultures and their co-culture. Utilizing the fact that multi-channels can be segregated from each other within a microfluidic platform, the co-culture platform was used in studying the role of medium conditions on ARPE-19 and the consequent response of HUVEC. Due to limitations mentioned in the discussion above, we did not anticipate observing the complete angiogenesis process but we believe we have taken the first step in elucidating molecular mechanisms of angiogenesis within the microfluidic device. Capabilities of microfluidic systems have been widely applied for years; we seek to further build on the on-chip model of the retina by looking at effects of specific soluble factors and evaluating potential treatments. Because viable RPE cells from AMD patients do not grow well in culture (6), the process of wound healing appears to be disturbed in AMD patients. In the future, we plan to impose angiogenic regulators such as TNF-alpha on the ARPE-19 monolayer and evaluate the interactions of cells. The consequences of wet AMD are devastating, and much time and effort has been invested in an attempt to better understand the progression of this type of AMD.

Looking at an even broader scope, microfluidics provide customizable platforms to study development of treatments for cancer and other diseases associated with angiogenesis through identification of compounds that stimulate or inhibit the angiogenesis process.

References

1. Thuenauer R, Rodriguez-Boulan E, Römer W. Microfluidic approaches for epithelial cell layer culture and characterisation. Analyst. 2014 Jul 7;139(13):3206–18.

2. Laboratory Equipment And Supplies : World Precision Instruments [Internet]. [cited 2017 Jan 25]. Available from: https://www.wpiinc.com/

3. Oxygen Sensing, Hypoxia-Inducible Factors, and Disease Pathophysiology. Annual Review of Pathology: Mechanisms of Disease. 2014;9(1):47–71.

4. Weidemann A, Johnson RS. Biology of HIF-1α. Cell Death Differ. 2008 Feb 15;15(4):621–7.

5. Chiu J-J, Chien S. Effects of Disturbed Flow on Vascular Endothelium: Pathophysiological Basis and Clinical Perspectives. Physiol Rev [Internet]. 2011 Jan [cited 2017 Jan 15];91(1). Available from: http://www.ncbi.nlm.nih.gov/pmc/articles/PMC3844671/

6. Booij JC, Baas DC, Beisekeeva J, Gorgels TGMF, Bergen AAB. The dynamic nature of Bruch's membrane. Progress in Retinal and Eye Research. 2010 Jan;29(1):1–18.

7. Cachafeiro M, Bemelmans AP, Samardzija M, Afanasieva T, Pournaras JA, Grimm C, et al. Hyperactivation of retina by light in mice leads to photoreceptor cell death mediated by VEGF and retinal pigment epithelium permeability. Cell Death Dis. 2013 Aug 29;4:e781.

8. Blaauwgeers HG, Holtkamp GM, Rutten H, Witmer AN, Koolwijk P, Partanen TA, et al. Polarized vascular endothelial growth factor secretion by human retinal pigment epithelium and localization of vascular endothelial growth factor receptors on the inner choriocapillaris. Evidence for a trophic paracrine relation. Am J Pathol. 1999 Aug;155(2):421–8.

9. Marazita MC, Dugour A, Marquioni-Ramella MD, Figueroa JM, Suburo AM. Oxidative stress-induced premature senescence dysregulates VEGF and CFH expression in retinal pigment epithelial cells: Implications for Age-related Macular Degeneration. Redox Biology. 2016 Apr;7:78–87.

10. Ablonczy Z, Dahrouj M, Tang PH, Liu Y, Sambamurti K, Marmorstein AD, et al. Human retinal pigment epithelium cells as functional models for the RPE in vivo. Invest Ophthalmol Vis Sci. 2011 Nov 4;52(12):8614–20.

11. Zhao J, Geng YU, Hua H, Cun B, Chen Q, Xi X, et al. Fenofibrate inhibits the expression of VEGFC and VEGFR-3 in retinal pigmental epithelial cells exposed to hypoxia. Exp Ther Med. 2015 Oct;10(4):1404–12.

12. Keeler GD, Durdik JM, Stenken JA. Localized Delivery of Dexamethasone-21-Phosphate via Microdialysis Implants in Rat Induces M(GC) Macrophage Polarization and Alters CCL2 Concentrations. Acta Biomater. 2015 Jan;12:11–20.

13. Staton CA, Reed MWR, Brown NJ. A critical analysis of current in vitro and in vivo angiogenesis assays. Int J Exp Pathol. 2009 Jun;90(3):195–221.

14. Theberge AB, Yu J, Young EWK, Ricke WA, Bushman W, Beebe DJ. Microfluidic multiculture assay to analyze biomolecular signaling in angiogenesis. Anal Chem. 2015 Mar 17;87(6):3239–46.

15. Sellgren KL, Butala EJ, Gilmour BP, Randell SH, Grego S. A biomimetic multicellular model of the airways using primary human cells. Lab Chip. 2014 Sep 7;14(17):3349–58.

16. Pirkmajer S, Chibalin AV. Serum starvation: caveat emptor. American Journal of Physiology - Cell Physiology. 2011 Aug 1;301(2):C272–9.

17. Chen M, Huang J, Yang X, Liu B, Zhang W, Huang L, et al. Serum Starvation Induced Cell Cycle Synchronization Facilitates Human Somatic Cells Reprogramming. PLoS One [Internet]. 2012 Apr 18 [cited 2016 Oct 24];7(4). Available from: http://www.ncbi.nlm.nih.gov/pmc/articles/PMC3329488/

18. Kues WA, Anger M, Carnwath JW, Paul D, Motlik J, Niemann H. Cell cycle synchronization of porcine fetal fibroblasts: effects of serum deprivation and reversible cell cycle inhibitors. Biol Reprod. 2000 Feb;62(2):412–9.

19. Kumar R, Harris-Hooker S, Kumar R, Sanford G. Co-culture of Retinal and Endothelial Cells Results in the Modulation of Genes Critical to Retinal Neovascularization. Vascular Cell. 2011;3:27.

4   Cell-vessel model of the outer blood-retina barrier

Previous chapter focused on mimicking oBRB using the cell-cell model and cell-cell interactions were elucidated. It is however, not a fully representative model as in vivo RPE is sustained by the choroids (microvessels). The aim of this chapter is therefore to build a more realistic oBRB model by first making and characterizing the model of microvessels in a single-layer microfluidic device; thereafter, the RPE cell-vessel co-culture is characterized in a top-down two-layer microfluidic device. In order to sustain the growth and remodeling of microvessels, normal human lung fibroblasts (NHLF) is also used, making a tri-culture of the oBRB model. Finally, the developed model is modified to allow insertion of platinum (Pt) electrodes for TEER measurement. Thus, the model described in this chapter builds on the same concept but serves as an improvement of the oBRB cell-cell model.
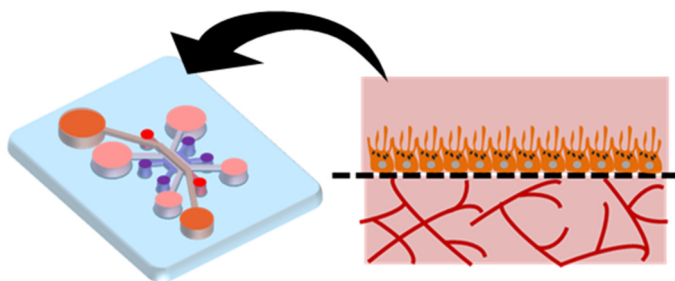
Graphical abstract of the aim of this chapter.

4.1   Materials and Methods

4.1.1   Experimental conditions

ARPE-19, HUVEC/ GFP-HUVEC and NHLF are used in building the oBRB model while HUVEC and NHLF are used in building the microvascular model. Cell culture conditions are described in Chapter 2.2.1. Conditions for ARPE and HUVEC under serum starvation and experiments are the same as in the cell-cell model (Chapter 3). When co-culturing HUVEC and NHLF, NHLF was cultured and conditioned in the same medium/media as HUVEC. Specific eexperimental conditions for the disease model are described under Chapter 2.2.1.2.

4.1.2   One-layer multichannel microfluidic device and the microvascular model

This section outlines the fabrication of the one-layer multichannel microfluidic device and the application on building a model of microvessels. Morphology and functionality of the microvascular model were evaluated.

4.1.2.1 Device specification

Methods on fabrication is described in Chapter 2.1. As such, only the design of the mask and the dimension are given here (Fig. 4.1.2-1).
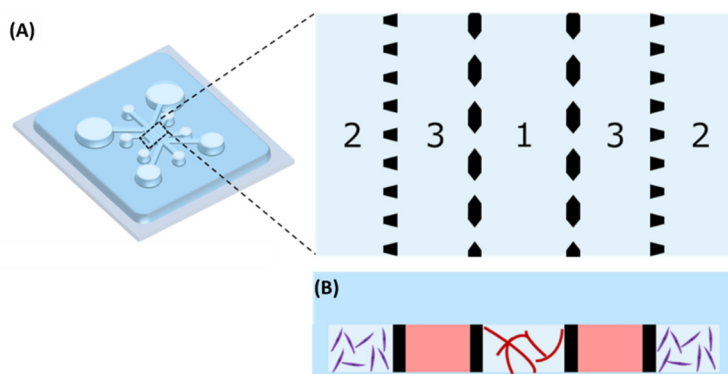

Fig. 4.1.2-1 Schematics of the one-layer microfluidic device.

(A) top view and the magnified view showing the multi-channel structure. (B) Cross-section showing medium chambers (channel 3, pink) and side channels (channel 2, purple, NHLF) and the central channel (channel 1, red microvessels, HUVEC). Device dimension is in Fig. 5.1.3-1.

4.1.2.2 Formation of microvascular model using one-layer multichannel microfluidic device

The one-layer multichannel device allows multiple culturing of different cell types in a single device. In making the microvascular model, HUVEC is co-cultured with NHLF. Fibroblasts are specialized in secreting collagenous extracellular matrix (ECM), and secretes several growth factors, of which VEGF, and bFGF are potent pro-angiogenic factors, stimulating growth of the vascular network. Vascular networks from HUVEC monoculture and HUVEC-NHLF co-culture were compared.

Formation of vascular models rely on self-organization of HUVEC; hence, a 3D culturing space mimicking in vivo ECM is necessary. Fibrin has been characterized in many vasculature model, and is adopted in all subsequent 3D cell culture. In the model, HUVEC and NHLF were embedded in fibrin gel, insoluble strands of protein. Fibrin is formed from fibrinogen, a soluble protein, and polymerized (cross-linked) by thrombin, a protease enzyme. The following three components are required for preparation of the fibrin gel. Aprotinin is a serine protease inhibitor, used to slow fibrin degradation (fibrinolysis). A multitude of protease inhibitors (aprotinin, MMP-inhibitors) act to inhibit various protease classes (serine and cysteine proteases, aminopeptidases, acid proteases and metalloproteases) to preserve proteins from endogenous and exogenous proteolytic cleavage.

- Fibrinogen, Sigma F8630

Reconstitute in PBS(-) at 10mg/ml. Solution was filtered through 0.45 um milipore before use. Make fresh before use in experiments.

- Thrombin, Sigma T7513

Reconstitute in PBS(-) to 50 U/ml and aliquot at 100 ul per tube, stored at a -30 degree freezer.

- (optional) Aprotinin, Sigma

Use as is supplied, supplementing it to the culture medium at 1/1000 (v/v).
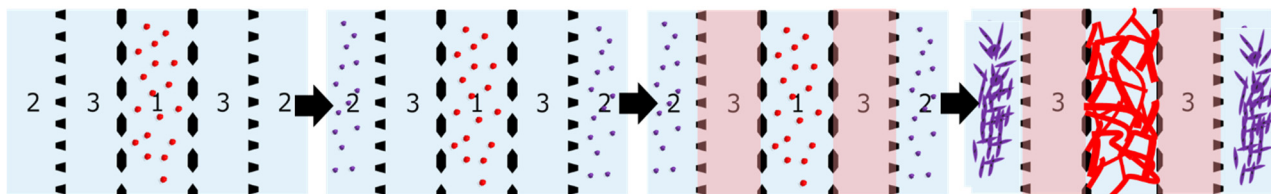

Fig. 4.1.2-2 Schematic showing vasculature formation from HUVEC-NHLF co-culture.

Protocol: microvascular model of HUVEC monoculture

Below lists the steps for building the microvascular model of HUVEC using the one-layer microfluidic device, with the schematic shown in Fig 4.1.2-2, skipping intermediate step of seeding NHLF (purple).

The formation of microvasculature was based on published work from previous studies (1,2). Briefly, GFP-HUVECs were detached from the culturing surfaces and made into suspensions of $7*10^6$ cells/ml. Fibrinogen precursor (Sigma F8630) 10mg reconstituted in 1ml of PBS(-) and filtered through 0.45 µm milipore was mixed with 3 times volume of GFP-HUVECs suspension (at $7*10^{\wedge 6}$ cells/ml) thoroughly. Thrombin (Sigma T7513) pre-aliquoted at 50 U/ml (two µl for 0.25mg fibrinogen used) was mixed thoroughly with the cell-fibrinogen mixture which were immediately loaded into the central microchannel (Fig 4.1.2-2, channel 1). The devices were kept in the 37 C incubator for 5 min for the fibrin gel to polymerize, resulting in GFP-HUVECs dispersed in 2.5 mg/ml fibrin. After confirmation of the gelation, EGM supply was initiated by filling the inlet reservoirs and aspirating the medium from the outlets using a tip-cut 1ml pipette. Fully supplemented EGM was used and changed 24 h after seeding. Thereafter, it was changed every 48 h.

Protocol: microvascular model of HUVEC & NHLF co-culture

The formation of microvasculature is the same as the HUVEC-only vascular model, with extra steps seeding NHLF into both side channels. Briefly, GFP-HUVECs and NHLF were detached from the culturing surfaces and made into suspensions of $7*10^6$ cells/ml. Fibrinogen precursor (Sigma F8630) 10mg reconstituted in 1ml of PBS(-) and filtered through 0.45 µm milipore was mixed with 3 times volume of GFP-HUVECs (at $7*10^6$ cells/ml) thoroughly. Thrombin (Sigma T7513) pre-aliquoted at 50 U/ml (two µl for 0.25mg fibrinogen used) was mixed thoroughly with the cell-fibrinogen mixture which were immediately loaded into the central lower microchannel (Fig 4.1.2-2, channel 1). The devices were kept in the 37 C incubator for 5 min for the fibrin gel to polymerize. Thereafter, NHLF (at $7*10^6$ cells/ml) mixed with fibrinogen was loaded into both side channels (Fig 4.1.2-2, channel 2) following the same procedure, resulting in GFP-HUVECs and NHLF dispersed in 2.5 mg/ml fibrin. After confirmation of the gelation, EGM supply was initiated by filling the inlet reservoirs (4.1.2-2, channel 3, cross reference the top view in 4.1.2-1) and aspirating the medium from the outlets (4.1.2-2, channel

3, cross reference the top view in 4.1.2-1) using a tip-cut 1ml pipette. Fully supplemented EGM was used and changed 24 h after seeding. Thereafter, it was changed every 48 h.

4.1.2.3 Response of the vascular network to stimulants in one-layer multichannel microfluidic device

In order to evaluate the functional response of the vascular network and use it as a disease model, angiogenic factor VEGF (100 ng/ml) and pro-inflammatory cytokine TNF-alpha (10 ng/ml) were supplied to the inlets of the device and images of the 3D vascular network were observed using a confocal microscope. Images were processed as outlined below.

4.1.2.4 Evaluation of the vascular network

Quantification of the vascular parameters (characterization of the vascular morphology)

In order to do a systematic evaluation of the vascular network, relevant parameters are quantified based on plugins in ImageJ. DiameterJ is a plugin published by Nathan Hotaling, originally developed for analysis of nanofibers (3). The plugins compile available libraries in ImageJ into a source file to quantify parameters such as orientation angle, diameter and length of fibers and the porosity of an input image. The code was modified to fix bugs and to made appropriate for vessel analysis in this project, namely to quantify vascular parameters of interest (diameter, number of branch segments, branch length and vascular area). The full code is available upon request.
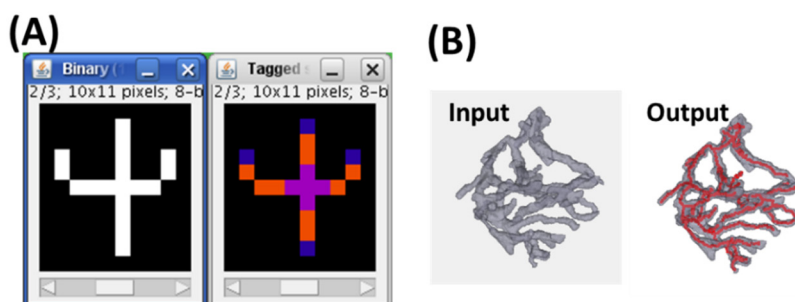

Fig.   4.1.2-3 Image processing: definition for quantification and the sample output.
(A) Definition of pixels showing slab pixels, end-point pixels and intersections. Reprint from (3). (B)
Skeletonization example showing an input and the output in red ('skeleton'). Images were generated from
MATLAB.

The general procedure in words is as followed (Fig. 4.1.2-4):

- Pre-processing input images: remove noise using despeckle filtering and improve contrast if necessary
- Determine a global threshold by trying on representative images then segment the input files into binary images (background and object).

Following libraries were used to extract different vascular parameters (Fig. 4.1.2-5) :

- Vascular area: the number foreground pixels (object) after segmentation is used to represent the 2D projected vascular area.
- Vessel length: the center-lines are extracted by two algorithms: Voronoi tessellation and axial thinning algorithm developed by Zhang and Suen (4).
- Vascular diameter: vascular area divide by the average of vessel length calculated from the two algorithms
- Node numbers: identified by counting number of intersection points (three-point, four-point intersections) using the algorithm developed by Arganda-Carreras et. al. (see Fig. 4.1.2-3, A) (3).
- Characteristic branch length: defined as mean length of vessel between intersections and is calculated by dividing the total length of vessels by number of intersections (node numbers)
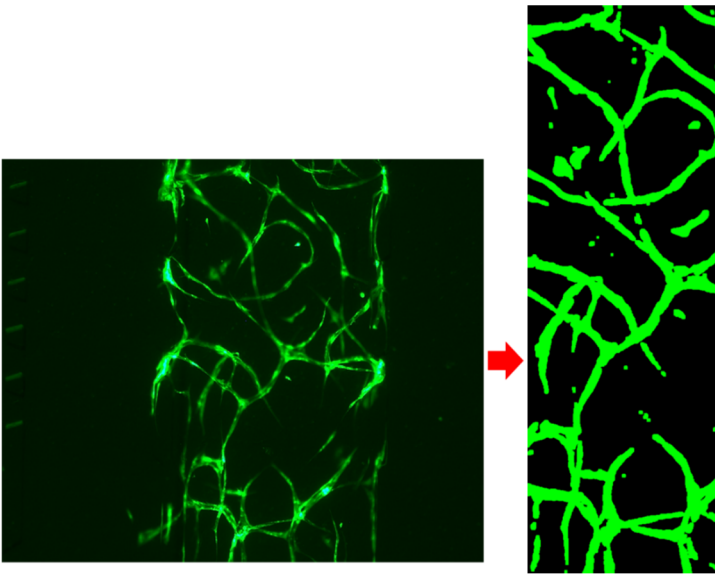

Fig.   4.1.2-4 Image processing: pre-processing.

Left: raw image taken by a fluorescence microscope. The raw input was cropped for a defined region of interest (vascular area), enhanced contrast, remove noise, and finally segmented (right).
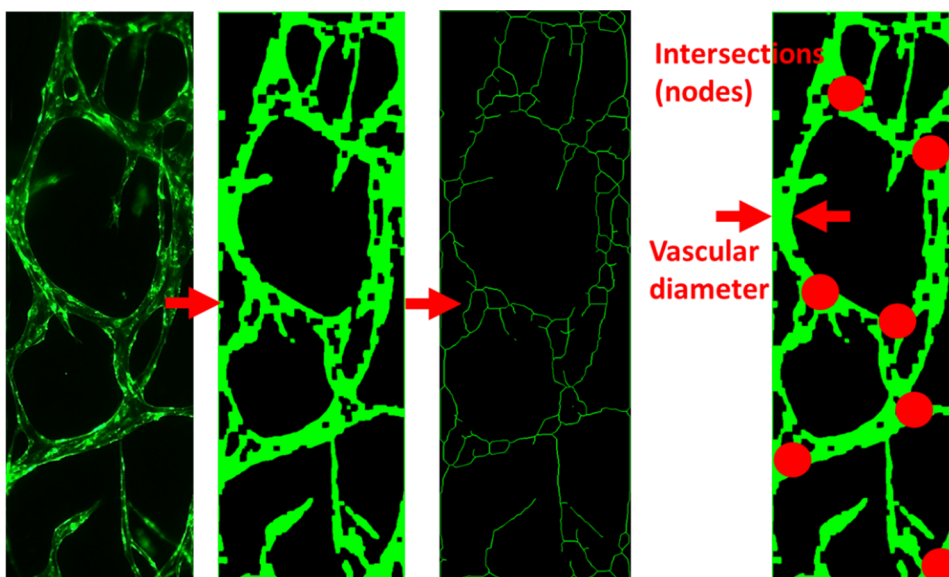

Fig.   4.1.2-5 Image processing: skeletonization and vascular parameters.

Functionality evaluation of formation of vessel lumen

Formation of lumens was tested by perfusing 5 µl of fluorescent microbeads (Fluoresbrite, φ3.0 µm, Polysciences) into one of the inlets. Fluorescent-labelled carbohydrate (FITC-dextran 70kDa, Invitrogen) at 0.5 mg/ml (50 µl) was also used to observe the perfusion of molecules into the vascular lumen and into the gel. The device was positioned on a confocal microscope throughout the observation and video was recorded.

4.1.3 The two-layer multichannel microfluidic device towards the oBRB model

Previous section described the fabrication and evaluation of the vascular network. After characterization of the vascular network, this section described the development of the two-layer microfluidic device to build the oBRB cell-vessel model. A single-layer microchannel is overlaid onto the central channel of the one-layer microfluidic channel, making it a two-layer multichannel microfluidic device. Similar to the oBRB cell-cell model, ARPE monolayer was cultured in the two-layer microfluidic device before proceeding onto the co-culturing ARPE and HUVEC in the device.

4.1.3.1 Device specifications and assembly of components into a two-layer microfluidic device

General steps of photolithography and soft lithography are described in details in Chapter 2.1. This section describes the dimension of the device and the steps in assembly of components to make a two-layer model (Fig. 4.1.3-1).

The microfluidic device used in the study has an upper microchannel and multiple lower microchannels, separated by a polyethylene terephthalate (PET) porous membrane of 8 µm in diameter (Falcon #353093). The device was made by conventional photolithography: the photomasks for the upper microchannel were designed in LayoutEditor (justpertor GmbH, Unterhaching, Germany) and patterned by the Heiderlberg DWL66 laser writer. Thereafter, a master mold was made by spincoating a 200 µm thick layer of SU-8 2100 (Microchem) on a silicon wafer and patterned by UV-lithography. Microchannels were made by liquid poly(dimethylsiloxane) (PDMS; Dow Corning, Sylgard 184) mixed at 10:1 ratio (wt/wt) of base polymer to curing agent, poured over the silicon master mold, degassed under vacuum pressure and cured in a 70 C oven for at least 3 hours. The cured PDMS were then cut into slabs and removed from the mold. Creation of the master mold and PDMS soft lithography for the lower microchannel followed the same procedure, except the lower PDMS slabs were made thin (2 mm in thickness) as opposed to the upper PDMS slabs. The thin lower PDMS slab was for microscopic observation while the upper PDMS slab was made thick to hold cell culturing media. The inlets and outlets of PDMS slabs were punched with the respective dimensions (Fig. 4.1.4-1), tapped to remove dust and impurities.

The membrane for the device was cut into 7 mm x 10.5 mm (width * length) out of the conventional PET membrane from Falcon transwell inserts (Falcon #353093). The membrane was bonded to the upper PDMS following the protocol developed previously (5). Briefly, the laser cut membranes were immersed in 5% of 3-

Aminopropyltrimethoxysilane, APMS (Sigma) in distilled water at 80 degree for an hour. Thereafter, the membranes were washed with distilled water twice, and bonded onto plasma treated PDMS upper channel. The membrane-bonded PDMS slabs were heat at 120 C for an hour. For device assembly, the upper and lower channels treated with oxygen plasma were bonded. After a device was assembled, it was kept in a 120 C oven for at least an hour. The bonding between the upper and lower PDMS slabs was checked (no leakage of ethanol) before use.
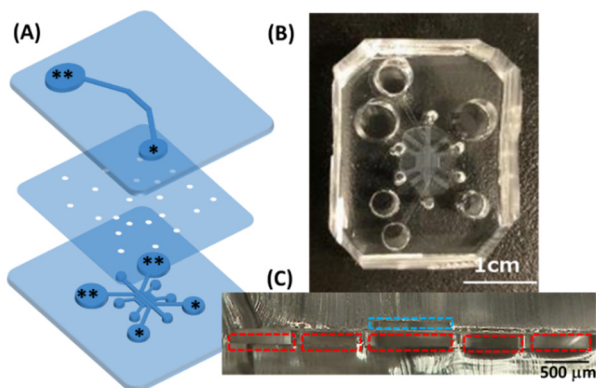

Fig. 4.1.3-1 Configuration of the two-layer multichannel microfluidic device.

(A) Exploded view; medium reservoirs are marked with asterisks (** as inlets, * as outlets when loading cells or media). (B) Top view of the assembled device. (C) Microscopic cross-sectional view of the assembled two-layer device. Dashed blue line indicated the top microchannel; each dashed red box indicated the lower microfluidic channels separated by micropillars. Detailed dimension is in Fig. 4.1.4-1.

4.1.3.2 Characterization of ARPE monolayer in the two-layer multichannel microfluidic device

Fig 4.1.1-1 shows the schematic representation of the oBRB and the model built using the proposed model. Before proceeding onto the co-culturing ARPE and HUVEC microvdssels, ARPE monoculture cultured in the device was first evaluated to ensure cells retain the RPE cell physiology and maintain the tight barriers. ARPE was cultured in the upper channel as indicated in Fig. 4.1.3-1 C, blue box.

Protocol: culturing ARPE in the two-layer microchannel device

1. The upper channel was coated with fibronectin at 10 ug/ml and kept at a 37 C incubator for at least 2 hours (or overnight).
2. Load 2.5 mg/ml of fibrin (reconstituted in PBS (-)) to the side channels and the central channel. Preparation of fibrin is the same as described in Fig. 4.1.2-2.
3. Before loading cells, wash the device with PBS(-) and extra solution in the in/outlets and the channel was aspirated completely. 5 ul of ARPE suspension at 10^7 cells/ml was pipetted into the upper channel.
4. After confirming the successful seeding, the cells were let attach in a 37 degree incubator for 4 h before washing away the unattached cells and supplying ARPE culturing medium in the upper and lower channels. Medium was supplied in the same way as the one-layer device as outlined in Chapter 4.1.2.2.

Evaluation of the ARPE monolayer in the two-layer microfluidic device

As outlined in Chapter 3, ARPE cultured in the two-layer microfluidic device was subjected to evaluation of the tight junctions and VEGF secretion.

One of the most important functions of the BRB is the tightness of the barrier in guarding the retina from the systemic circulation. In the oBRB, RPE cells form tight junctions to their neighbouring cells, forming a monolayer sheet-like structure. The barrier becomes leaky under inflammatory conditions, as found compromised in the patients of age-related macular degeneration. In order to characterize the response of ARPE to different stimulations, the barrier integrity was evaluated by flowing FITC-dextran 70 kDa (Sigma) over the monolayer, and the fluorescent intensity at the lower channels was measured (Gemini EM, Molecular Device). The methods and the conditions (high glucose and hypoxia) for the barrier integrity test was the same as described in Chapter 3.1.2.4. In conjunction to analysing permeability of fluorescent molecules, one of the types of tight junctions (ZO-1) were stained for qualitative measurement.

As an additional evaluation to the RPE barrier integrity, the functional response of ARPE to stimulations was also evaluated. In the same way in Chapter 3.1.2.2, VEGF secretion under high glucose and hypoxia were measured and evaluated. Methods for quantification using ELISA and FACS were described in Chapter 2.4.

4.1.3.3 Formation of the oBRB cell-vessel model and the disease model

After confirming the successful culturing of ARPE in the microfluidic device, the tri-culture of ARPE-HUVEC-NHLF of oBRB model was attempted. ARPE monolayer was cultured in the upper channel while HUVEC-NHLF were cultured in the respective lower microchannels as aforementioned (Chapter 4.1.2.2). Different stimulations were imposed on the developed model to use it as a disease model of the oBRB.

Protocol: outer blood-retina barrier model

1. The microfluidic device is sterilized and used under hydrophobic condition, i.e., no immediate plasma treatment prior use or wash with PBS(-).
2. Day 0*: First build the model of the vasculature in the lower channel following the same protocol for microvasculature formation using HUVEC-NHLF in the one-layer multichannel microfluidic device ( ). The upper channel was kept non-wetted.
3. The microvasculature was cultured for 24 h** before ARPE-19 were seeded. Prior to seeding ARPE, coat the upper channel with FN 10 ug/ml for 2 h. Wash the upper channel with PBS(-).
4. In seeding ARPE-19 into the upper channel, the solution in the upper channel was aspirated before cell seeding (at 10^7 cells/ml, 8 µl per device). The devices were left in a 37 C incubator for 2 hours for ARPE-19 to attach, after which 100 µl of DMEM was supplied to the upper inlet and aspirated from the upper outlet to wash out unattached ARPE-19. The devices were then returned to the incubator for an additional 2 hours before loading the medium. The culture media (DMEM for the upper channel, EGM for lower channels) were refreshed every 48 h. Continue culturing until maturation, where ARPE

maintains a confluent monolayer and HUVEC forms a mature microvascular network (typically on day 3 or day 4, following the above conditions and parameters).

Note *: Culturing time for the model is defined based on the day when HUVEC was seeded, i.e., day 0, seeding HUVEC; day 1, first day after seeding HUVEC. In this fashion, ARPE seeding is on day 1.
Note **: culturing time for microvessels can be 48 h (pending on the maturation and HUVEC seeding density)

Protocol: oBRB model as a disease model
Prerequisite: the oBRB model where ARPE maintains a confluent monolayer and HUVEC forms a mature microvascular network.

1. 24 h prior experiments, condition the ARPE and HUVEC (and NHLF) using the respective media described in Chapter 2.2.1.2. Flow warm basal media (respective to each cell type) twice to wash out serum present in the media.
2. Impose the experimental conditions on to the model and observed at the designated time points. Initial time (t0) refers to the time when experimental media were imposed onto the model. See Chapter 2.2.1.2 for formulating experimental media for ARPE and HUVEC. Each cell type is supplied with its respective medium.

4.1.4 The two-layer microfluidic device for TEER evaluation

The two-layer microfluidic device was modified for TEER measurement of ARPE monolayers. The design and dimension are the same as the two-layer multichannel uFD outlined in the previously, with addition microgrooves for insertion of electrodes as shown in Fig 4.1.4-1.
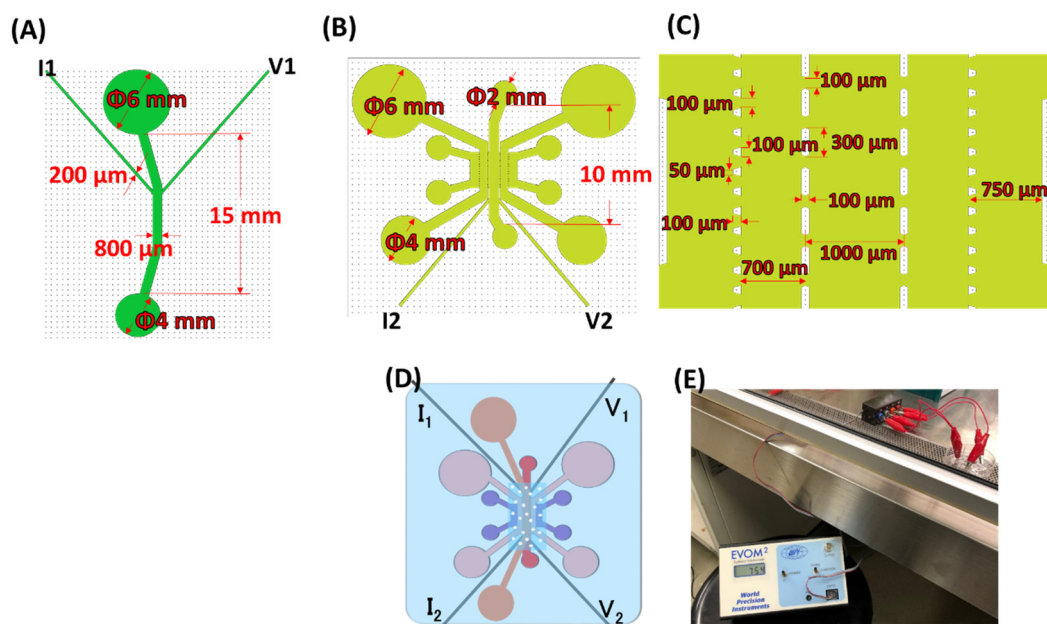

Fig. 4.1.4-1 Two-layer multichannel microfluidic device dimension.

Dimensions of the microchannels for trans-epithelial electrical resistance (TEER) measurement. (A) Upper channel. (B) Lower channel. (C) Magnified view of (B), showing dimensions of multi-channels. (D) Top view of

the assembled TEER device. (E) Experimental set-up for TEER measurement showing the connection between the microfluidic device and the EVOM instrument.

4.1.4.1 Modification of the device for TEER measurement.

The masks of the upper and lower channels were redesigned with four microgrooves for placement of two electrodes in each of the upper and lower channel (Fig. 4.1.4-1 A, B). The microgrooves for platinum (Pt) wire were designed and made at 200 μm in width, but Pt wire of 300 μm in diameter was used as it fit firmly inside the PDMS microgroove. In the last step of fabrication, four pieces of 3 cm long Pt wires were inserted into one device. The protrusion of wire inside the microchannel is approximately 1 mm (Fig. 4.1.4-1 D). After insertion, a drop of uncured PDMS was applied to the electrode channel's entrance and cured in order to minimize potential displacement of electrodes during handling alligator clippers for measurement (Fig. 4.1.4-1 E). Each microfluidic device underwent quality checks for the following: (1) porous membrane covered the entire lower microchannel length, except inlets and outlets, (2) the tip of an electrode protruded 1 mm into the microchannel, (3) the upper and the central lower channel were properly aligned. Devices that met the criteria were then kept sterilized until being used for experiments. Individual layer and the assembled device are shown in Fig 4.1.4-1.

4.1.4.2 TEER measurement setup

The Pt wires from the device were connected to four ports of an adaptor (Fig. 4.1.4-1 E) which was connected to the EVOM (World Precision Instruments) set to Ohm mode. To be consistent in the approach, the Pt wires were connected to current (I) and voltage (V) ports in the order shown in Figure 4.1.4-1 D for all the devices. Due to variability in TEER readings between devices, the blank (acellular device filled with culture media: DMEM in the upper channel, EGM in the lower channel) for each sample was recorded before every experiment. Culture media were equilibrated to room temperature (kept 20 min in the clean bench) and readings were recorded in all cases to minimize variations in results.

4.1.4.3 Data collection and analysis

Samples (devices) used for experiments were individually labelled and the TEER readings and microvasculature morphology specific to each device were recorded. The number of samples is indicated in the corresponding figure captions. Due to a relatively small sample size, we did not test for statistical significance of difference in TEER readings between different days of culture. TEER values were extracted and reported as unit area of resistance (ohm·cm^2) by first subtracting the raw values from the blank, and multiplied the resulting value by area in cm^2. The area was calculated as width * length between electrodes (0.08 cm * 0.5 cm). Readings from gel-free, acellular devices was taken as the blank for ARPE monolayers, while the blank for HUVEC-NHLF and ARPE-HUVEC-NHLF cultures was taken as the readings 30 minutes after seeding (ie., cells-embedded in fibrin gel) to take the effect of gel contributing TEER into account. The device was individually labelled and the blank and readings specific to each device were used in calculation.

4.1.5 Fabrication of single microvessels as an alternative angiogenesis model

Other models that are feasible in evaluating angiogenesis have been developed, in attempt to provide a closer *in vivo* environment of microvessels so that tubule formation is more realistic. Various methods have been actively engaged; the subtractive method and embedded method in fabricating microchannels were attempted. The promising one seems to be the hybrid model incorporating hydrogel inside a microfluidic device.

4.1.5.1 Hydrogel-embedded model

This model involved a sacrificial element embedded inside hydrogel until it is cross-linked, after which the sacrificial element is eliminated in other means (Fig. 4.1.5-1). The sacrificial elements chosen were carbohydrate sugars and gelatin due to the biocompatibility.
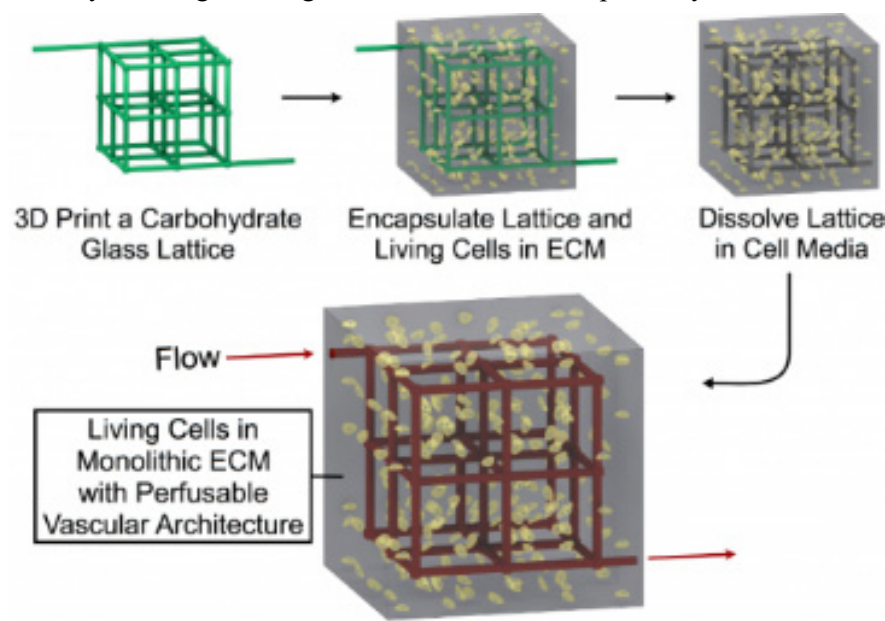

Fig. 4.1.5-1 Tissue engineering microvessels: hydrogel-embedded model.
Schematic of hydrogel-embedded model. The sacrificial element used in this case is carbohydrate glass printed by a 3D printer. Reprint from (6).

Carbohydrate sugar template tentative protocol

Carbohydrate sugar (dextran, Sigma-Aldrich) were heated until it was dissolved in water. As soon as it was soft, it was loaded inside a syringe to form the template onto a glass slide. Once it was treated with chloroform (Wako), it was embedded inside collagen (6 mg/ml, Corning). The embedded carbohydrate template was dissolved by placing the hydrogel model inside an incubator at 37 C. HUVEC were introduced into the vessel thereafter.

Gelatin template tentative protocol

The PDMS slab was treated with Pluronic F-127 (Sigma-Aldrich) for 1 h then lightly bonded onto a glass slide (reversible bonding). The microchannel from a PDMS slab was used in which gelatin mixture (3% in distilled water) was molded. Once the gelatin solidified, the PDMS slab was removed, leaving the gelatin-made microchannel on the glass slide. It was then embedded in collagen (6 mg/ml). Once the collagen gel cross-

linked, the gelatin was dissolved by heating the model at 37 C, leaving the hollow microchannel inside the collagen gel.

4.1.5.2 Subtractive method

Similar to the embedded method, the microvessel was patterend using a wire or a needle, onto which hydrogel was loaded and cross-linked. The wire or the needle was removed, leaving the microvessel within the hydrogel. See schematic illustration in Fig. 4.1.5-2.
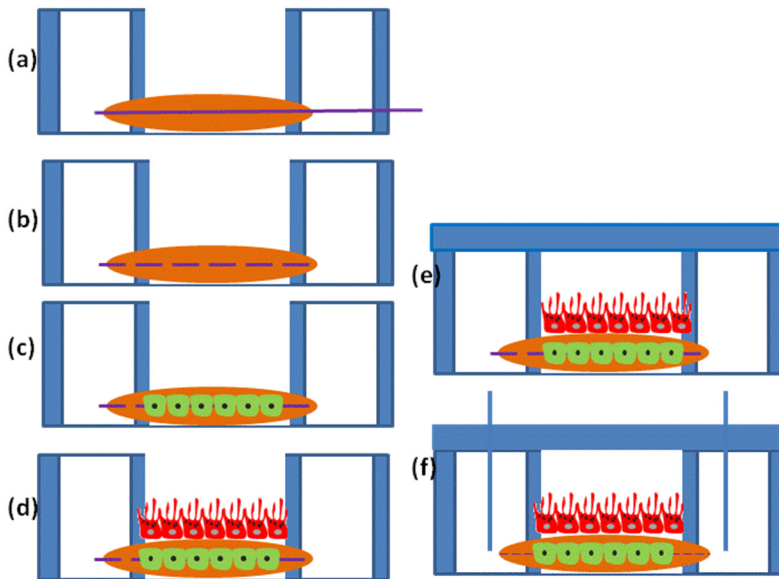

Fig.   4.1.5-2 Tissue engineering microvessels: subtractive method.

Fabrication process of the subtractive method. In (a), collagen is placed around a needle which is already treated with BSA and inserted into the device. (b) the needle is removed, HUVEC seeded as shown in (c). For co-culture, ARPE is seeded on the top of collagen (d), and lid is attached (e), needles inserted for perfusion (f).

Protocol: subtractive method using a needle as the sacrificial element

1. After sterilization, the needle (27G) is treated with Bovine Serum Albumin (BSA, 1% in PBS) for 1 h in room temperature. After being washed in distilled water and dried, insert it inside the device.
2. Formulate the collagen (6 mg/ml) and load it into the well and surrounded the needle completely. Tap the device to make sure that collagen has completely filled every corner inside a well. Drop a few PBS around the dish, and incubate the device in an incubator (37 C) for 30 min.
3. Once the collagen gel has cross-linked, remove the needle horizontally (avoid jig-jag movement). At the mean time, make sure that inlet and outlet wells are covered with PBS. The flow is apparent once the needle is pulled out immediately.
4. For cells to be seeded inside the microvessel, load the cells into the inlet well. Slightly tilt the device to facilitate movement of cells inside the microvessel. Incubate for 30 min, then turn the device upside down for cells to attach at the upper side of the microvessel. Make sure to keep the hydrogel hydrated all the time.

5. Once cells are attached inside the microvessel, fill the wells with culture medium. Change the medium at least once per day.

6. For co-culture, the second type of cells are loaded on the top of the hydrogel (Fig 4.1.5-2, f.). Bonded a lid on the top of the device and start the perfusion.

4.1.5.3 Hybrid model of hydrogel and the microfluidic device

This method involves introducing hydrogel inside a microfluidic device. Here, 5 parallel channels were separated by trapezoidal microposts (similar to the one in Fig. 4.1.2-1). The device was designed in such a way so that extra channels were made for seeding of fibroblast (human lung origin). HUVEC, and fibroblasts embedded inside fibrin/collagen mixture were separately seeded inside microchannels. As the typical cross-link time for fibrin is on a scale of seconds, leakage is not a problem.

Protocol

1. Sterilize the device. Prepare the hydrogel mixture: mix fibrin precursor and thrombin and collagen (3 mg/ml). Left it on ice. At the same time, passage HUVEC and fibroblast accordingly.

Mix the HUVEC into fibrin precursor/collagen mixture. Be careful of generation of air bubbles. Once cells are dispersed homogenously inside the mixture, mix in aprotinin. Load the solution into the device immediately. Repeat for second cell-type.

2. Inspect under a microscope that cell were embedded inside the gel and that there are no air bubbles injected inside the microchannel. Incubate the device at 37 C until cells attach inside the microchannel.

3. Add in culture medium and continue the experiments.

Note: cells are stained prior experimental uses if necessary.

4.2 Results and Discussion

4.2.1 Microvasculature formation in the one-layer multichannel microfluidic device

3D culture of HUVEC is necessary as demonstrated (Fig.4.2.1-1) showing an elongated morphology of HUVEC when embedded in hydrogel compared to 2D cell culture surface. Microvascular model is developed, embedding HUVEC in fibrin gel and cultured in the fabricated one-layer multichannel microfluidic device. As NHLF secrete growth factors (out of all, bFGF) that sustain the growth and remodeling of HUVEC microvessels, microvessels formation using HUVEC monoculture and HUVEC-NHLF co-culture were investigated. After coming up with the model prototype, microvessels were imposed with pathological conditions and results were evaluated.
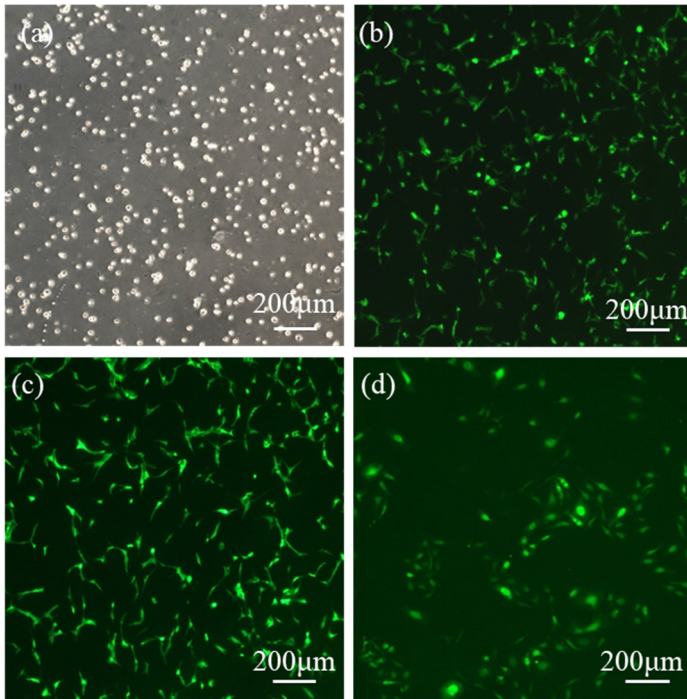
Fig. 4.2.1-1 3D culture of HUVEC in comparison to 2D culture.

Changes in morphology of HUVEC cultured in different microenvironment. (A-C) Monoculture of HUVEC embedded in hydrogel (3D culture). (A) immediately after seeding. (B) Day1, (C) Day 2 after seeding. (D) HUVEC cultured on the flask (2D).

4.2.1.1 The role of NHLF in microvasculature formation

Fig. 4.2.1-2 compares the microvasculature form with HUVEC monoculture and HUVEC-NHLF co-culture. Qualitatively assessing the images, microvessels formed with HUVEC monoculture appear to be thinner and less robust, compared to the HUVEC-NHLF co-culture microvessels. Although the cytokines secreted by NHLF were not quantified here, previous studies had shown that NHLF secreted multiple angiogenic cytokines that play a role in the proliferation and remodeling of the HUVEC vasculature. The presence of the angiogenic gradient is also confirmed in the angiogenic sprouting model, discussed in the next chapter.

HUVEC microvasculature was immunostained for ZO-1, a type of tight junctions, and counterstained for DAPI (nucleus) for close-up assessment (Fig. 4.2.3-1 B). shows the confocal image and the cross-section of the stained microvessels on day 4 after vascular formation. There appears to be luminal structure; in order to test if the lumen actually formed, fluorescent microbeads were perfused as shown in the next section.
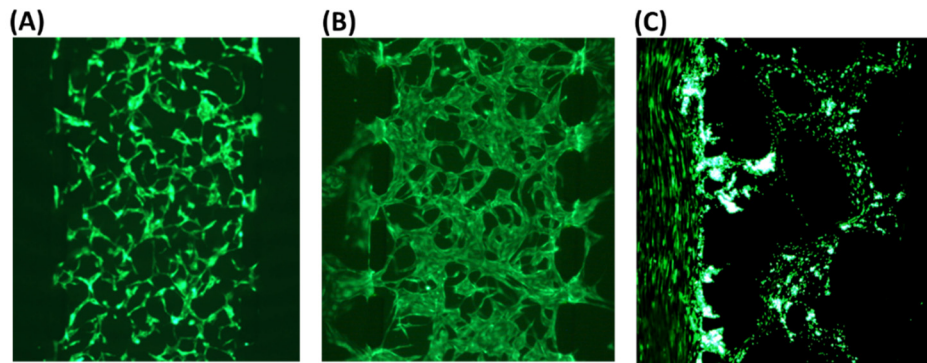
Fig. 4.2.1-2 Comparison of microvasculature model from mono- and co-culture.
(A) HUVEC monoculture. (B) HUVEC-NHLF co-culture. Both were at day 3 culturing. (C) A snapshot of lumens with microbeads.

4.2.1.2 Evaluation of the vascular lumen formation

5 ul of microbeads diluted in 100 ul PBS(-) was loaded into one of the inlet of the model. The flow from the inlet to outlets was induced due to the hydrostatic pressure. As shown in Fig. 4.2.1-2 the microbeads flow from the medium channel, through the microposts, into the vascular lumen. This is confirmed using a fluorescent microscope and a confocal microscope.

As a separate experiment, 70 kDa FITC-dextran (1 mg/ml) was perfused in a similar fashion as the microbeads. Fig 4.2.3-1 B2. shows that the FITC-dextran illuminating the luminal structure. However, 30 minutes after loading the fluorescent molecules, FITC-dextran diffuse into the hydrogel.

4.2.1.3 Response of the vascular network under stimulations in the one-layer multichannel microfluidic device

As a preliminary screening to test if the HUVEC microvessels in the device respond to stimulations, exogenous VEGF at 75 ng/ml was supplied daily to the top microchannel and the confocal image was taken. As can be seen from the images, microvessels remodelled the matrix and grew in diameters, demonstrating the response to stimulants (VEGF). Noted that microvessels sprouted upwards, as shown in the cross-section of Fig 4.2.1-3.
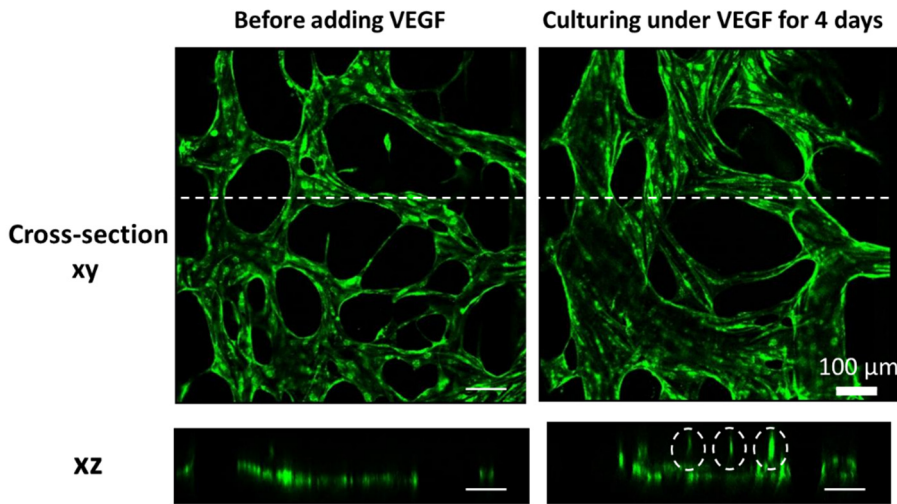
Fig. 4.2.1-3 HUVEC-NHLF microvessels under VEGF stimulation.

(A) Before stimulation. (B) 3 days under VEGF stimulation.

4.2.1.4 Quantification of the vascular network

HUVEC-NHLF co-culture microvessels under TNF-alpha stimulation (10 ng/ml) 24 h and the control (in the condition medium) were compared. TNF-alpha stimulations resulted in decreased huvec vascular diameters (Fig. 4.2.1-4) and vessel regression and disconnected vessels fragments (Fig. 4.2.1-5). Along with vascular diameters, above vascular parameters indicate regression of the vascular network.
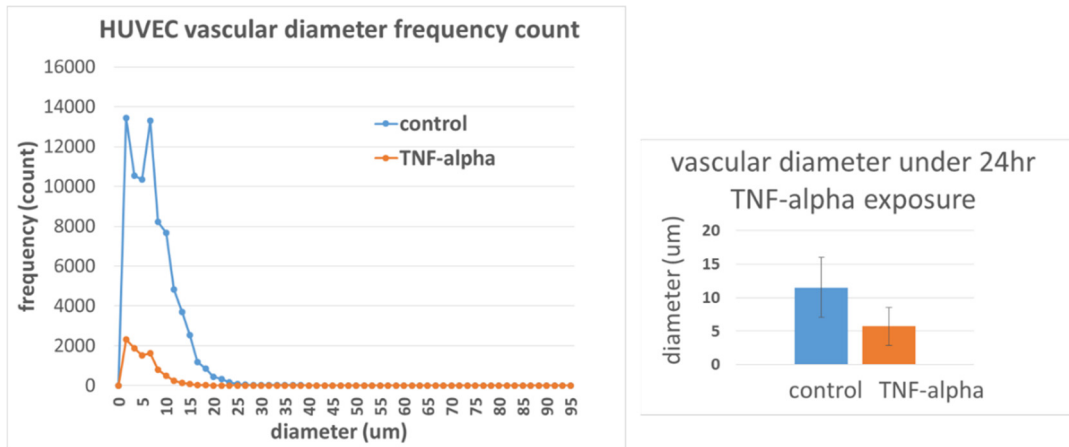

Fig. 4.2.1-4 Quantification of HUVEC microvessel under TNF-alpha: vascular diameter.
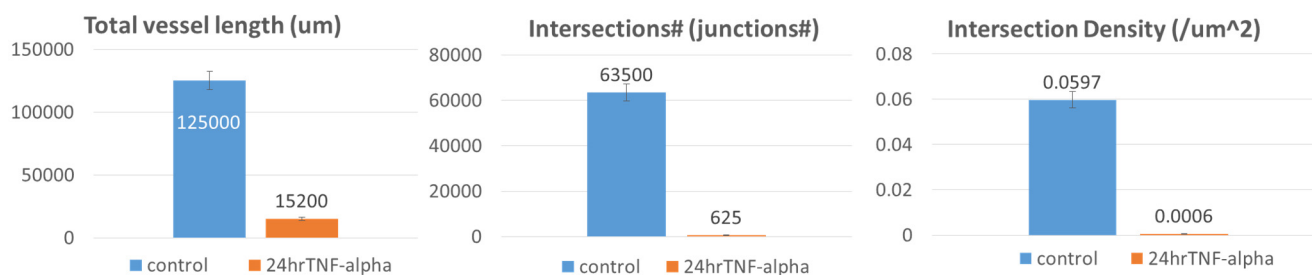
Fig. 4.2.1-5 Quantification of HUVEC microvessel under TNF-alpha: vessel length and intersections.

4.2.2 ARPE monolayer in the two-layer microfluidic device

In order to evaluate if fibronectin could be coated in the device, rhodamine-labelled fibronectin was used. Fig. 4.2.2-1 shows the microscopic image of the upper channel after coating (and washing with PBS(-)). Red part of the microchannel indicated the presence of the fluorescently labelled fibronectin. White lines indicated the border of the microchannel.
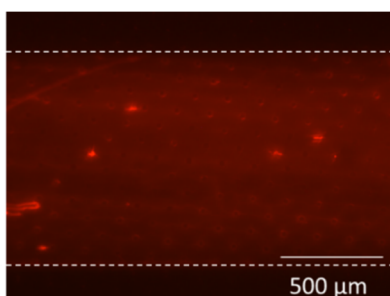

Fig. 4.2.2-1 Rhodamine-labelled fibronectin coating in the microchannel.

After seeding ARPE into the upper microchannel, no cells were found in the lower channels, indicating the feasibility of using 8 um porous membrane in the device, albeit anatomically larger than the 3 um pores in the in vivo Bruch membrane. Thereafter cells were fixed and stained for tight junction to evaluate the formation of monolayers.

4.2.2.1 ARPE response to stimulations

Instead of physically altering the O_2 concentration, $CoCl_2$ was used chemically, due to the same logic discussed in the previous chapter. $CoCl_2$ has been used to induce hypoxia in the cells, as it upregulates the expression of Hypoxia-inducible factor-1 (HIF-1), the major transcription factor specifically upregulated during hypoxia. Fig. 4.2.2-2 shows the morphological change of ARPE ((A) in the flask and (B) microfluidic device) when exposed to an overly high concentration of $CoCl_2$. The CoCl2 concentration being imposed onto ARPE was first optimized (data not shown) by trials and errors, ranging from 50 uM to 300 uM for 24 h. It was found that $CoCl_2$ above 200 uM induced cell death 24 h after imposing the condition. Therefore, 150 uM was chosen as the parameter to induce hypoxia to be applied to the model. Glucose concentration was also optimized. As an

osmolarity control to the additional glucose molecules, mannitol at the same concentration as the glucose was used and changes to ARPE was observed. Under elevated glucose concentration, there was no obvious morphological changes to cells.
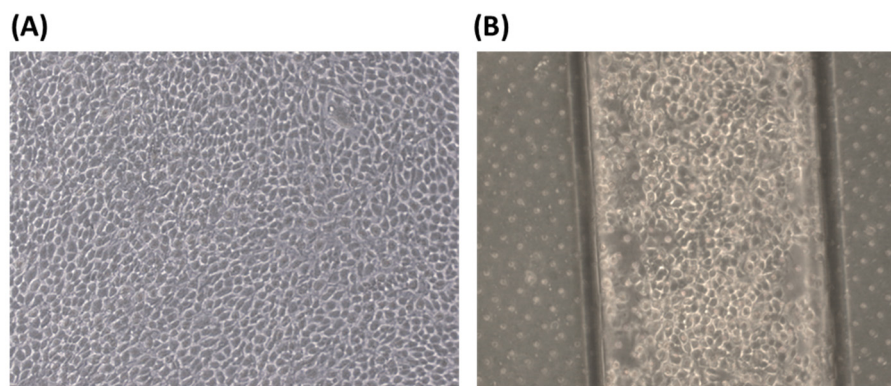

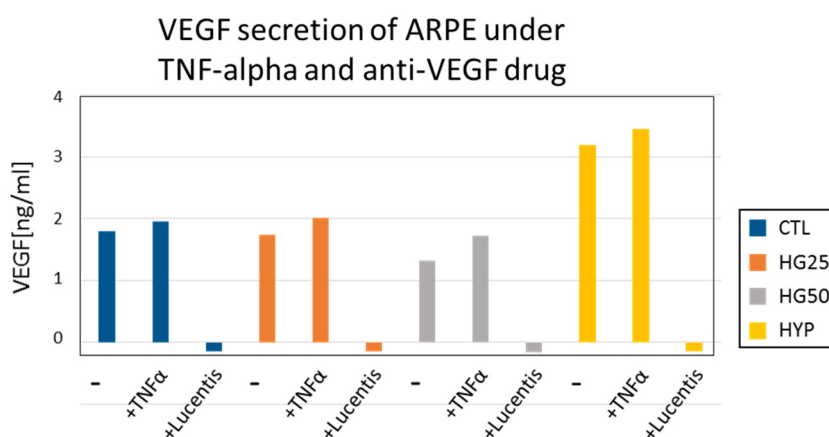**Fig. 4.2.2-2 Morphological change of ARPE exposed to CoCl2 300 uM.**

Fig. 4.2.2-3 Quantification of VEGF secretion of ARPE under TNF-alpha and Lucentis.

After the qualitative assessment of the cells under stimulation, VEGF, a type of growth factor secreted by ARPE, was quantified in order to evaluate the functional response of APRE cells (Fig. 4.2.2-3). It has been found that in vivo RPE cells has a polar response; VEGF secretion is from the basolateral side and the VEGF concentration is further elevated under oxidative stress and inflammatory conditions. The polarity of ARPE was discussed in the previous chapter. Here, the experiments was reproduced with additional TNF-alpha (a pro-inflammatory cytokine) or Lucentis (anti-VEGF) to mimic an inflammatory microenvironment or to test the effect of drug (anti-VEGF) on ARPE.

As the final part of assessment of ARPE under stimulations, the tight junctions were quantitatively evaluated using permeability of fluorescent molecules as well as TEER changes was described in the previous chapter.

4.2.3 Triculture of ARPE-HVUEC-NHLF as the model of the oBRB

In building the model, we first evaluated the formation of ARPE monolayer in the device (Fig. 4.2.3-1 A). Separately, the formation of lumens of the HUVEC vasculature was confirmed by immunostaining of tight junction (Fig. 4.2.3-1 B1) and loading a diameter 6um micorbeads in one side of the inlet of the device. Images of microvascular network focused on a z-plane in figure 4.2.3-1 B2 were captured after flowing FITC-dextran 70 kDa at 0.5 mg/ml in one side of the lower channel inlet. Figure 4.2.3-1 B shows the schematic cross-sectional view of the multi-channel microfluidic device in which endothelial cells (HUVEC) and the supporting cells (NHLH) in two side channels were cultured (media channels were indicated M in Fig. 4.2.3-1). After confirming the ability of culturing epithelial cells and the vasculature, we attempted to demonstrate the feasibility of multi-culture of cells and/or vessels using our proposed device and built a model of the outer blood-retina barrier (oBRB). The design of the microfluidic device was an extension based on previously developed models by Noo Li Jeon and Roger Kamm research groups where models have been used to study microvessels. Here, we further modified it to enable culturing of the ARPE-19 directly on the top of HUVEC microvasculature, mimicking oBRB where in vivo RPE and the juxtaposed choriocapillaries are separated by the Bruch membrane (Fig. 4.2.3-1). We adopted a larger pore size here as a demonstration of the model; the diameter of the pore, however, is customizable by using commercial membranes of different diameters. We had previously built the cell-cell oBRB model using ARPE-19 and HUVEC cells (7), characterizing the behavior of cells under pathological angiogenesis. We anticipate the prototype we proposed here to be used to characterize epithelial monolayer – microvasculature such as BRB or BBB, under pathological microenvironments.
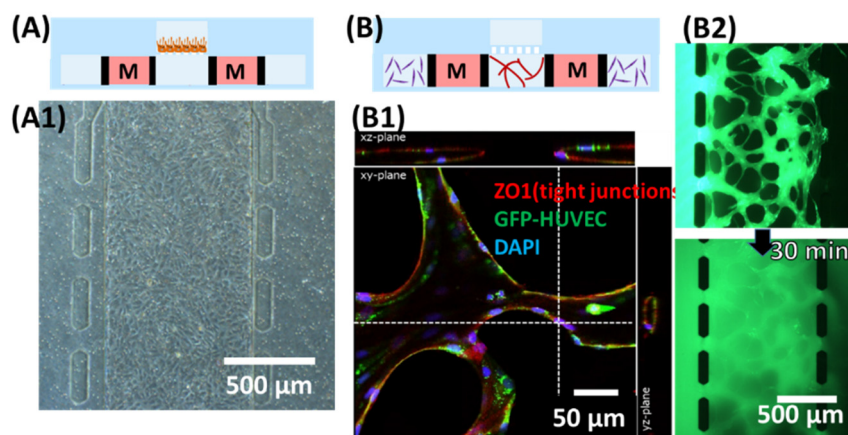

Fig. 4.2.3-1 Individual characterization of ARPE and HUVEC in two-layer multichannel microfluidic device. Demonstration of individual culturing chambers. (A) Culturing the human retinal pigmental epithelial cell (ARPE-19) monolayer in the upper channel. (A1) Microscopic view focusing on the upper channel, showing monolayer of ARPE. (B) Formation of microvascular lumens in the lower channels. "M" (medium channels) corresponded to * (lower channel) in Figure 4.1.3-1 A. (B1) Confocal microscopic image staining for zonula occludens-1 (ZO1) and 4′,6-diamidino-2-phenylindole (DAPI). (B2) Snapshots taken after loading 70 kDa of FITC-dextran into one side of the lower channel immediately (top) and 30 min after (bottom).
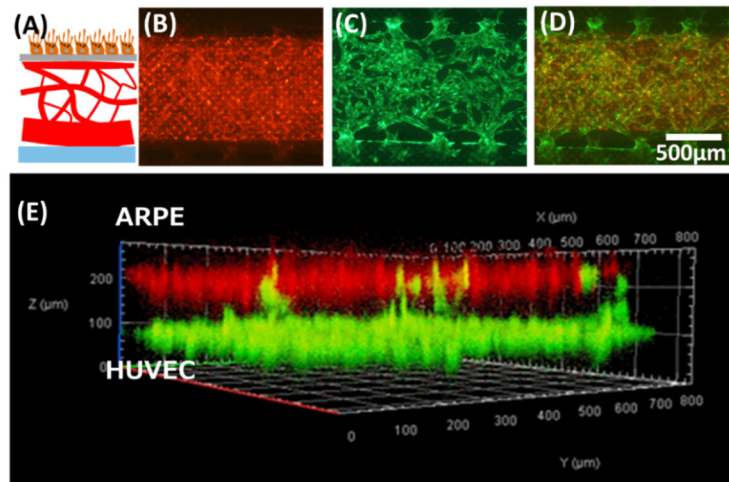
Fig. 4.2.3-2 Formation of the oBRB model prototype built using the two-layer multichannel microfluidic device. (A) Schematic showing the anatomical structure of oBRB (retinal pigment epithelial cells – Bruch membrane – choroids). (B-E) tri-culture of ARPE –HUVEC-NHLF. (B) ARPE cells stained in red were cultured in the upper channel. (C) GFP-HUVEC microvessels were cultured in the lower channel. (D) Overlay of (B) and (C). (E) Confocal microscopic view of the cross section of the co-culture model.

4.2.3.1 oBRB disease model

After the development of the oBRB model, we attempted to use it as a disease model and model interactions of ARPE- and the choroids (Fig. 4.2.3-3 schematics). Pro-inflammatory microenvironments was induced by imposing hypoxia on ARPE. As characterized in Chapter 3, ARPE under hypoxia secrete a higher amount of VEGF, and it was hypothesized that the elevated VEGF would stimulate growth of the HUVEC microvessels. However, morphological structure of HUVEC microvessels under hypoxia did not support the hypothesis (Fig. 4.2.3-3). There are multiple factors involved, one of which, is the problem with alignment of upper and lower microchannels and PDMS-PDMS bonding that we had. We speculated that such problems resulted in the leakage of $CoCl_2$ into the lower channel, impeding growth of HUVEC microvessels. Further experiments are needed to test the models.
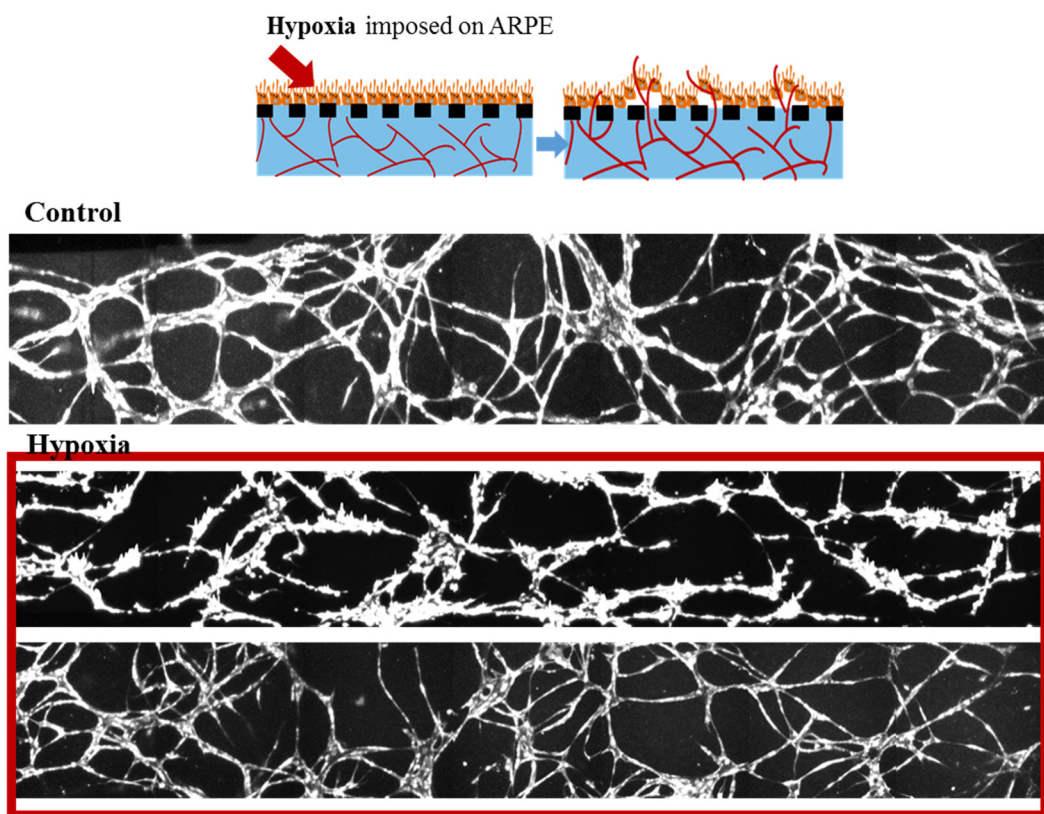
Fig. 4.2.3-3 oBRB disease model.

4.2.4 Two-layer multichannel microfluidic device for TEER measurement

Design of the two-layer multichannel microfluidic device

The feasibility of the proposed device as a platform for top-down multi-culture of cell-vessel was demonstrated by building a model of the human outer blood-retina barrier (oBRB). In addition, the versatility of the device was shown by modifying the device, allowing TEER evaluation of a cell monolayer. Although we only demonstrated the prototype of oBRB here, the device can be modified for specific organ-on-a-chip applications and studying physiological responses after taking allometric scaling and fluidic shear stress into account. Cell-vascular models are widely applicable to the human organ system, ranging from the blood brain barrier (BBB) and glial interactions to interactions of trophoblasts and the blood vessels in placenta. We have been developing integrated TEER measurement of the microfluidic system to evaluate the state of monolayer cells in real-time (unpublished); such system is applicable to evaluating the response of a monolayer to its environment, such as the BBB, the airway epithelium under shear stress, and mechanisms regulating intestinal epithelium. The model we proposed here is customizable and adaptable to different organs of origin, with potential extensibility for quantification of physical parameters such as barrier resistance and shear stress. We foresee that our proposed device has a potential in disease modelling and drug testing.
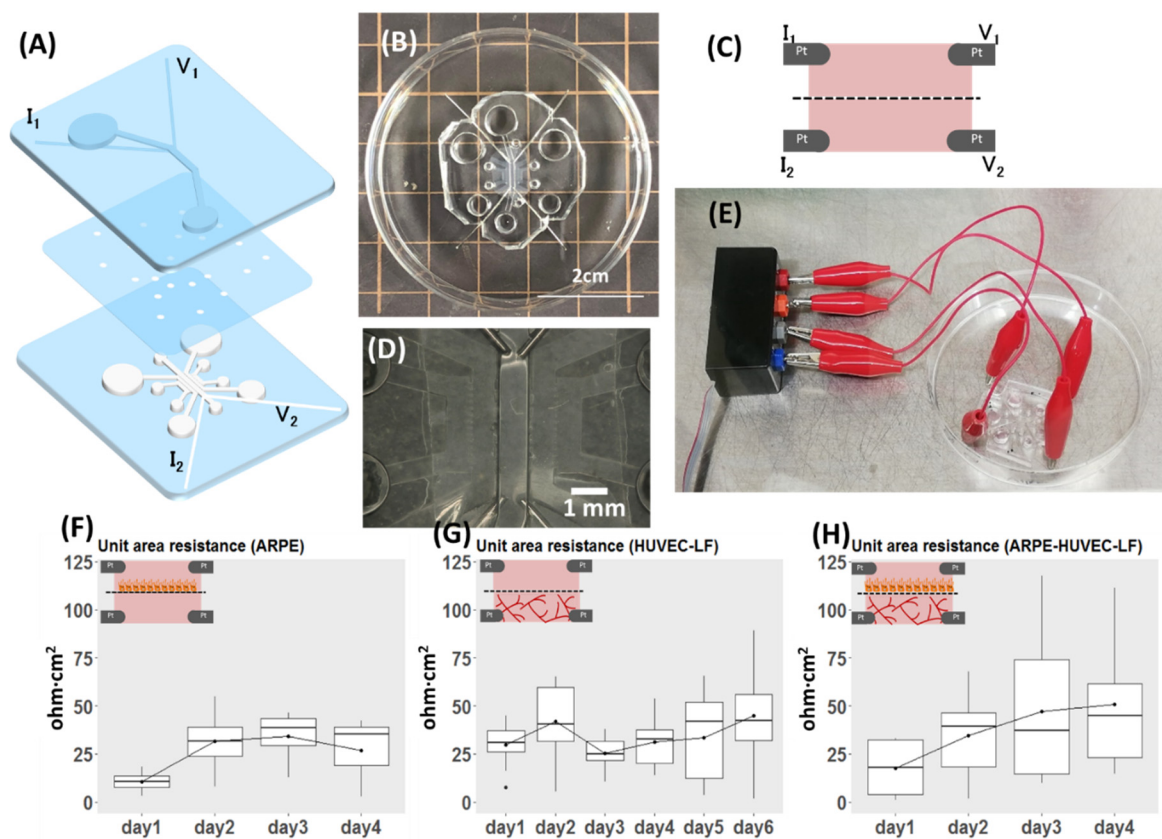
Fig. 4.2.4-1 Demonstration of the versatility of the proposed design, with modification for measuring TEER.
(A) Exploded view of the device. (B) Top view of the assembled device. (C) Schematic view of the cross-section showing position of voltage and current electrodes. (D) Magnified view of (B) focusing on position of electrodes inside the device. (E) Part of the system set-up showing connection of the device to the electrode adapter, which is connected to the EVOM instrument for TEER measurement. (F-H) Results of TEER measurement, reported as unit area resistance. The inset for each plot shows what was measured of. (F) TEER of ARPE monolayer (n=4). (G) TEER of co-culture of HUVEC and NHLF (n=10). (H) TEER of the oBRB model (n=11).

Versatility of the proposed device

To demonstrate the versatility of our proposed microfluidic device, we modified it to allow for direct TEER measurement. TEER provides a quick, non-invasive, label-free and real-time indication of the state of cells as an alternative to perfusion of fluorescent-labeled molecules such as FITC-dextran in evaluation of the barrier property. Both evaluation methods have their pros and cons: TEER offers instant, real-time assessment of the state of cells while permeability assay is a simple yet elegant way that is typically used as an end-point assessment of the barrier integrity of a cell monolayer. In the designed device, two Pt wire in the upper channel corresponded for voltage and current measurements, the same configuration for the lower central channel (Fig. 4.2.4-1). Four-electrode measurement system was adopted here to be compatible with the EVOM instrument. The advantage of the four-electrode system is the negligible effect of double layer capacitance, as the current supply and voltage measuring electrodes are separated (8). As an alternative, two-electrode measurement system can also be used here if we wish to take the impedance spectroscopy using a potentiostat. The two-layered microfluidic TEER device and the connection to the EVOM instrument are shown in Fig. 4.2.4-1 E

and Fig. 4.1.4-1.

Many microfluidic TEER models had been proposed; a square culturing chamber was adopted by Helm et. al, (9), while some measured the TEER of cells cultured in long microchannels (10,11). Here, we further modified our device for TEER evaluation of a top-down cell-vessel model. We first measured the TEER of ARPE-19 monolayers and HUVEC-NHLF separately before conducting experiments on the oBRB models. TEER readings of ARPE monolayers (Fig. 4.2.4-1 F) increased by days after seeding, corresponding to proliferation of cells inside the device. There was no obvious trend from the co-culture of HUVEC-NHLF (Fig. 4.2.4-1 G), due to the nature of the fenestrated vessels. We also evaluated ARPE-19 of the oBRB model by measuring the TEER (Fig. 4.2.4-1 H), where the readings indicated the proliferation of ARPE-19. TEER values for HUVEC-NHLF culture and the oBRB model were higher than ARPE monolayer culture, perhaps due to the presence of fibrin gel and influence of microvessels. The readings, however, were subjected to fluctuations arising from changes in temperature, and movement of electrodes during clipping. According to the datasheet of EVOM from World Precision Instruments, there is a 10% variability in TEER reading using the commercial STX2 chopstick electrodes on the transwell TEER measurement due to non-uniform current density flowing across the membrane, arising from variations in the electrode position. Such variation is expected to be even higher in the microfluidic system (12). In our system, one of possible causes to variations in reading between devices could be due to variations in length of protrusion of electrodes inside the microchannel, although we attempted to keep it the same (1mm) as much as possible. Also, as the distance between measuring electrodes is 5 mm, we did not anticipate non-uniformity in the current density but suspected the fluctuations in readings as the result of differences in temperature when reading was taken, as observed in our real-time TEER measurement system (unpublished).

4.2.5 Single microvessel as the angiogenesis model

Results from the microfluidic device showed cells were found to possess certain in vivo characteristics to some extent and the heterotypic interactions of co-culture. However, the culturing surface was still not realistic enough for growth of microvessels. PDMS membranes coated with fibronectin was enough for cell attachment and proliferation, but the innate self-organizing ability of the endothelial cells into a tubular network is suppressed (Fig. 4.2.5-1 A). Therefore, the current microfluidic device was not good enough for the growth of more realistic microvessels. Although the device made of hydrogel is mechanically weak in terms of controlling and handling, hydrogel definitely provides a more native growth environment. In order to incorporate hydrogel into the device, it underwent an evolution of designs. The most prevalent designs used are the subtractive method and the hybrid method utilizing soft lithography as explained in respective part in Chapter 2. Here the preliminary results were presented, along with reasons why the design was abandoned.
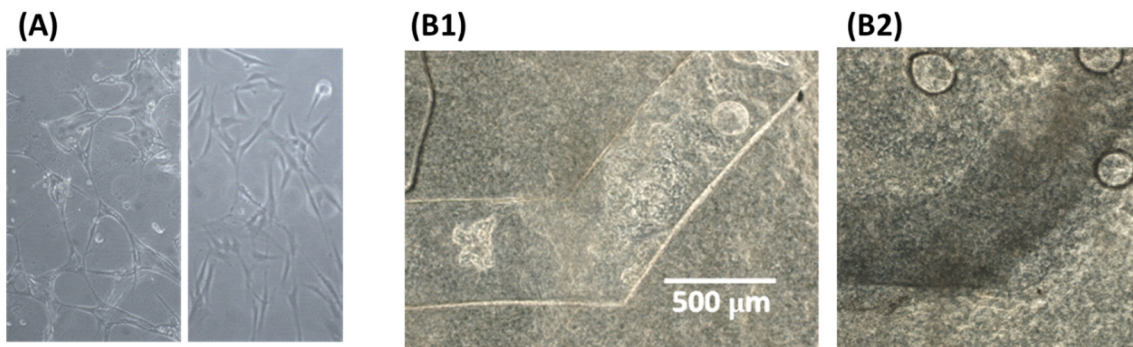
Fig. 4.2.5-1 Tissue engineered blood vessel: hydrogel-embedded single-microvessel model.
(A) HUVEC embedded in hydrogel and on a tissue culture treated dish viewed at 200X. Note the difference in morphology. (B1) Gelatin channel embedded in collagen, (B2) dissolved by heating the device on a water bath.

4.2.5.1 Hydrogel-embedded model

Carbohydrate and gelatin were both used as sacrificial elements in this method. Carbohydrate sugars template could be made rapidly but vessel diameter was very hard to control. The carbohydrate solution solidified inside a syringe before the template could be made. Also the vessels could not be made with homogenous diameters. For gelatin template (Fig 4.2.5-1, B), the procedure was tedious and the template did not separate from the glass or PDMS slab easily. Often it broke apart resulting in incomplete channel.

4.2.5.2 Subtractive method

Handling was relatively easier – if the needle could be pulled out smoothly (Fig. 4.2.5-2), the success rate was high. The platform also provides ideal co-culture environment as the chamber is open. The only problem associate with this design is that medium reservoir is not big enough for cells to survive past 24 h. Attaching a lid to set up a perfusion system is possible, but with a low success rate so far.
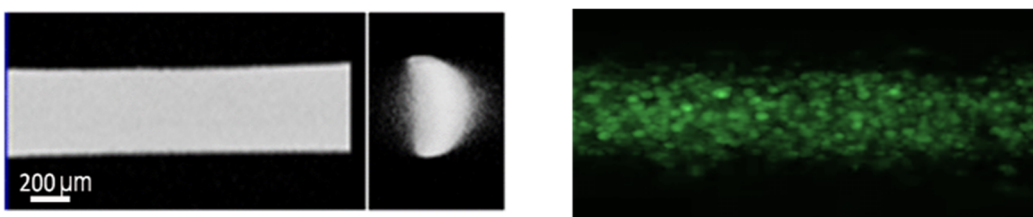

Fig. 4.2.5-2 Tissue engineerd blood vessel: subtractive method.
Left: Microvessel viewed under a confocal microscope. Right: flowing with fluorescent microbeads.

The concentration of the hydrogel used will affect the cell growth and therefore experimental results. Concentration of the fibrin precursor or collagen monomers corresponds to the stiffness of the resulting surface that supports endothelial cells. A surface that is "too hard" will inhibit invasion of endothelial cells into the matrix whereas if the matrix is too soft, the cells will invade and distort the vessel structure. In addition, vessel diameter should also be regulated due to difficulties in distributing and achieving sufficient EC densities versus nutrients supply and waste removal within small diameter templated channels.

4.2.5.3 Hybrid model of hydrogel and the microfluidic device

The hybrid model incorporated hydrogel inside closed chambers of a microfluidic device. This approach further simplifies the cell seeding and handling – it combines advantages from the aforementioned designs. Several groups have had this approach in investigating the effect of pericytes to endothelial cells (13). Preliminary results are promising (Fig. 4.2.5-3) and we are inclined to follow this approach to build the next angiogenesis model focusing on eye diseases. The next challenge is to search for possible co-culture method in order to co-culture ARPE-19 and HUVEC at the same time for disease modeling.
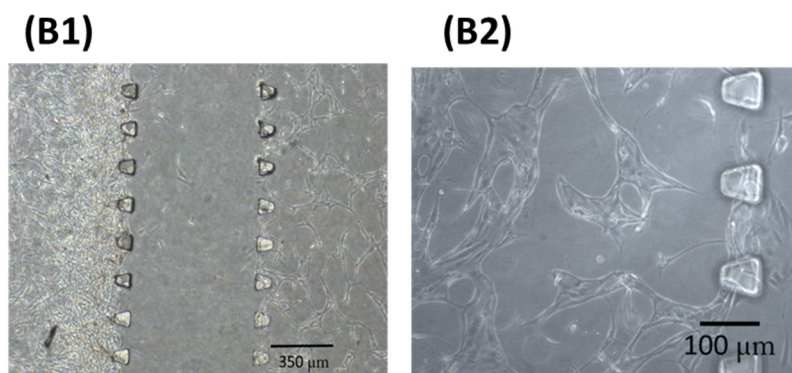

Fig. 4.2.5-3 Tissue engineerd blood vessels: hybrid method.

Microchannels separated by micropillars with HUVECs and human dermal fibroblasts embedded in fibrin gels, seeded in separate channels (left, viewed at 40X). Figure on the right is a magnification on HUVEC (200X). Notice that HUVEC were forming tubular structures.

4.3   Summary of the oBRB cell-vascular model

Focusing on microvessels and vasculature development, microfluidic models of microvessels and barrier properties have been extensively studied. Some of the models particularly focus on recapitulating the functionalities, i.e. the restrictive barrier properties or the responsiveness of the in vitro microvessels to the exogenous stimulations. Wang et. al. performed a tri-culture of pericytes, astrocytes and endothelial cells inside microfluidic devices with embedded Ag/AgCl wire in order to characterize the restrictive barrier of blood-brain barrier (BBB) (8). To study neuroinflammation of BBB, Herland et. al. performed a tri-culture of astrocytes, pericytes and endothelial cells in a single microchannel and subjected the model under tumor necrosis factor-alpha (a pro-inflammatory cytokine) (7). Functional responses of the microvessel under stimulation (endothelial permeability and cytokine release) was analyzed. Using a similar approach, Price et. al tested the effect of mechanical factors on the restrictiveness of the EC barriers using a single microvessel. On the other hand, multi-channel microfluidic devices that allowed examinations on vascular formation and tracking morphology of microvessels over the course of experiments and under different stimulations have been developed and used in various applications.

Based on the pre-established design of a multi-channel microfluidic device, we modified the device based on

Jeon research group (15) and Kamm research group (16) into top-down, direct cell-cell or cell-vascular co-culturing. Using the device, we built a model of outer blood-retina barrier (oBRB), mimicking the in vivo retinal pigment epithelial cells-Bruch membrane-fenestrated choroids using human retinal pigmental epithelial cells (ARPE-19) and human umbilical vein endothelial cells (HUVEC). To demonstrate the versatility of the device, we slightly modified the design by embedding four Platinum electrodes (diameter 300 µm) for trans-epithelial electrical resistance (TEER) measurement (Fig. 4.2.4.1 A, B). Using the modified device, we quantified the TEER of ARPE monolayers, and the oBRB model. The device proposed in this study can be used as a multi-culturing cells and/or vessels model for various applications, with the potential of connecting individual fluidic devices in a fluidic network, mimicking human physiology as demonstrated in the work of Edington et. al.

We proposed a microfluidic device consisting of a single upper microchannel and multi-lower microchannels for direct cell-vessel co-culture. The co-culture model was demonstrated by making the outer blood-retina barrier, made up of retinal pigment epithelial cells, endothelial cells and the supporting cells. The versatility of the device was demonstrated by modifying the device for insertion of Pt electrodes for TEER measurement. We measured the TEER of ARPE monolayer, and that of the oBRB model (ARPE-HUVEC-NHLF culture). Although only one aspect of the versatility design was demonstrated in this work, it is however, unlimited but extensible for investigation of the effect of shear stress on the multi-culture model by additionally gluing PDMS ports to the in/outlets of the device, or connect modular devices in an integrated fluidic network for studying physiological responses.
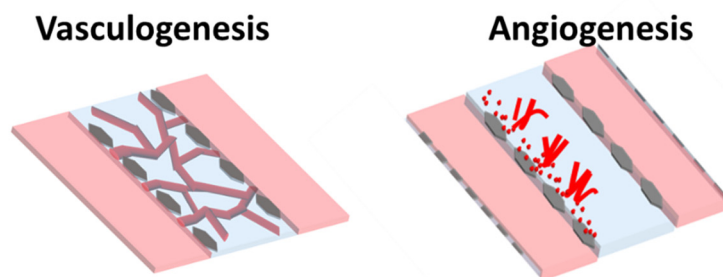
References

1. Jeon JS, Bersini S, Whisler JA, Chen MB, Dubini G, Charest JL, et al. Generation of 3D functional microvascular networks with human mesenchymal stem cells in microfluidic systems. Integr Biol (Camb). 2014 May;6(5):555–63.

2. Kim S, Lee H, Chung M, Li Jeon N. Engineering of functional, perfusable 3D microvascular networks on a chip. Lab on a Chip. 2013;13(8):1489–500.

3. Nathan Hotaling. DiameterJ [Internet]. ImageJ. [cited 2020 Jan 13]. Available from: https://imagej.net/DiameterJ

4. Y Z, Y S. A fast parallel algorithm for thinning digital patterns. Communications of the ACM [Internet]. 1984 Mar 1 [cited 2020 Jan 13]; Available from: https://dl.acm.org/doi/abs/10.1145/357994.358023

5. Aran K, Sasso LA, Kamdar N, Zahn JD. Irreversible, direct bonding of nanoporous polymer membranes to PDMS or glass microdevices. Lab Chip. 2010 Mar 7;10(5):548–52.

6. Miller JS, Stevens KR, Yang MT, Baker BM, Nguyen D-HT, Cohen DM, et al. Rapid casting of patterned vascular networks for perfusable engineered three-dimensional tissues. Nature Materials. 2012 Jul 1;11(9):768–74.

7. Chen L-J, Ito S, Kai H, Nagamine K, Nagai N, Nishizawa M, et al. Microfluidic co-cultures of retinal pigment epithelial cells and vascular endothelial cells to investigate choroidal angiogenesis. Scientific Reports. 2017 Jun 14;7(1):3538.

8. Theile M, Wiora L, Russ D, Reuter J, Ishikawa H, Schwerk C, et al. A Simple Approach to Perform TEER Measurements Using a Self-Made Volt-Amperemeter with Programmable Output Frequency. JoVE (Journal of Visualized Experiments). 2019 Oct 5;(152):e60087.

9. van der Helm, Marinke W., Odijk, Mathieu, Frimat, Jean-Philippe, van der Meer, Andries D., Eijkel, Jan C.T., van den Berg, Albert, et al. Direct quantification of transendothelial electrical resistance in organs-on-chips. Biosensors and Bioelectronics. 2016 Nov 15;85:924–9.

10. Henry OYF, Villenave R, Cronce MJ, Leineweber WD, Benz MA, Ingber DE. Organs-on-chips with integrated electrodes for trans-epithelial electrical resistance (TEER) measurements of human epithelial barrier function. Lab Chip. 2017 Jun 27;17(13):2264–71.

11. Odijk M, Meer AD van der, Levner D, Kim HJ, Helm MW van der, Segerink LI, et al. Measuring direct current trans-epithelial electrical resistance in organ-on-a-chip microsystems. Lab Chip. 2015 Jan 22;15(3):745–52.

12. Douville NJ, Tung Y-C, Li R, Wang JD, El-Sayed MEH, Takayama S. Fabrication of Two-Layered Channel System with Embedded Electrodes to Measure Resistance Across Epithelial and Endothelial

Barriers. Anal Chem. 2010 Mar 15;82(6):2505–11.

13. Stratman AN, Malotte KM, Mahan RD, Davis MJ, Davis GE. Pericyte recruitment during vasculogenic tube assembly stimulates endothelial basement membrane matrix formation. Blood. 2009 Dec 3;114(24):5091–101.

5 Angiogenesis sprouting model of the inner blood-retina barrier

In analysis of microvessels, this chapter reoriented the focus from vascular network to local sprouting of microvessels. As opposed to the choroids in the oBRB which form based on vasculogenesis, sprouting models of retinal microvessel based on angiogenesis are developed. The barrier integrity of human retinal microvascular endothelial cells (HRMEC) under inflammatory conditions were characterized. In order to understand the mechanisms of angiogenic sprouting under inflammatory conditions, matrix metalloproteinase (MMPs) activity of HRMEC was evaluated. As hepatocyte growth factor (HGF) is one of the factors regulating proliferation of HRMEC, the barrier tightness co-culturing HRMEC and normal human lung fibroblasts (NHLF) under inflammatory conditions was also investigated. Finally, angiogenesis sprouting models of the iBRB formation from different configurations of HRMEC monoculture, HRMEC-human retinal pericytes (HRP) co-culture, and HRMEC-HRP-NHLF tri-culture were investigated to obtain the optimal angiogenesis sprouting model of the iBRB.

Graphical abstract of this chapter, comparing the models based on vasculogenesis in the previous chapter to angiogenesis, the focus of this chapter.

5.1 Materials and Methods

5.1.1 Cells and experimental conditions

Human retinal microvascular endothelial cells, human retinal pericytes and normal human lung fibroblasts are used in building the iBRB sprouting model. Specific culturing conditions are described in Chapter 2.2.1.2.

Culturing condition

Following supplements were added into the culturing medium to sustain the growth of HRMECs.

- Vascular Endothelial Growth Factor (VEGF, Wako) at 100 ng/ml
- Tumor Necrosis Factor α (TNFα, Wako) at 5 ng/ml
- Basic fibroblast growth factor (bFGF,) at 25 ng/ml

GFP-HRMEC was used to track daily growth of sprouts. In other cases, PECAM-1 antibody was used to stain HRMEC, desmin was to stain HRP. Immunostaining protocol is given in chapter 2.

5.1.2 Plate experiment

As a primary screening to characterize HRMEC, monolayers of HRMEC were seeded onto inserts of the transwell plate (Fig 5.1.2-1 A) and subjected to different experimental conditions. Separate samples were collected to quantify secretion of cytokines, and total proteins. In addition, permeability of the HRMEC monolayer to FITC-dextran 40 kDa was investigated. For all experiments, HRMEC was seeded into inserts with a pore diameter of 3 um of the 12-well plate format. Cells were seeded as 4000 cells/ cm^2 and cultured for 5 days until they were confluent before experiments. Medium was changed every 48 h. Culturing of cells were described in Chapter 2. Where HRMEC were co-cultured with NHLF, NHLF were seeded separately in the well and let them proliferate for 3 days before placing the HRMEC monolayers in inserts (Fig 5.1.2-1 B).
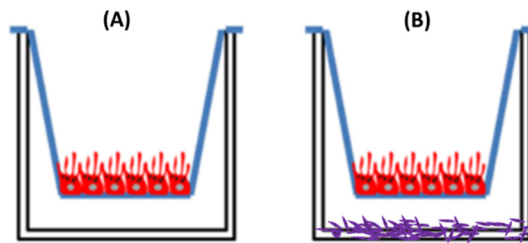

Fig. 5.1.2-1 Cell-seeding layout for the plate experiment.

(A) HRMEC in the insert. (B) HRMEC in the insert, NHLF in the well.

Stimulations on HRMEC monolayers:
- High glucose (HG): additional D+glucose of 20 mM was added to the serum-free culture medium.
- Hypoxia (HYP): CoCl2 of 100 uM was added to the serum-free culture medium. Formulation was described in Chapter 2.2.1.2.
- TNF-alpha: a final concentration of 10 ng/ml was added to the serum-free culture medium.

HRMEC were conditioned in serum-free medium for 24 h and stimulated for 24 h before samples were collected for quantification and being to FITC- permeability evaluation. Quantification of cytokines using FACS were described in Chapter 2.4, bioassays.

5.1.3 The one-layer multichannel microfluidic device as the angiogenesis sprouting model
5.1.3.1 Device specification

The model used in this model is based on the one-layer multichannel microfluidic device (Fig 5.1.3-1). Fabrication is based on the methods explained in Chapter 2. The single-layer PDMS slab was bonded to a 24

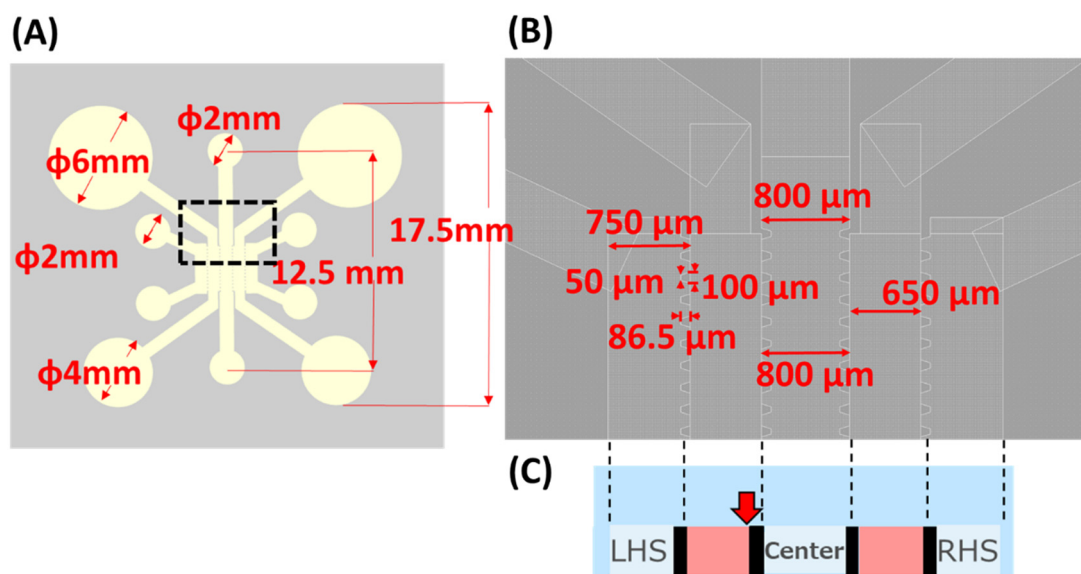mm x 24 mm, 0.2 mm thick glass slide to make the one-layer multichannel device.

Fig. 5.1.3-1 Device dimensions used in building the microfluidic iBRB model.
(A) Top view and (B) magnified view of the dashed black box in (A). (C) Cross-section of the device, with dashed lines corresponding the top view to the side view. Red arrow shows where HRMEC were seeded and let attach to initiate sprouting. Center, RHS (right-hand side), LHS (left-hand side) refer to conventional labeling used in this chapter for ease of referencing seeding configuration later on.

5.1.3.2 Formation of the iBRB sprouting model

Angiogenesis within fibrin gels in vitro is regarded as an accurate model for wound healing and tumor angiogenesis, as tumor cell-derived VEGF/vascular permeability factor promotes leakage of fibrinogen from the tumor vasculature and formation of a fibrin-rich proangiogenic provisional matrix (1,2). The same as the vasculogenesis model in Chapter 4, fibrin hydrogel is used in forming the angiogenesis sprouting model.

The general procedure of formation of angiogenic sprouts from HRMEC monoculture is summarized in Fig 5.1.3-2. Acellular fibrin gel at 2.5 mg/ml is loaded into the central channel. After the gel has polymerized, warm culturing medium was loaded from the *right* medium reservoirs (i.e., left side of the microchannel is kept unwetted). The medium loaded device is kept in an incubator for an hour at 37 degrees. Thereafter, HRMEC (3ul at 10^7 cells/ml) were seeded from the left medium reservoir. The device was tilted immediately and placed in an incubator for 30 minutes for the cells to attach. Thereafter, 100 ul of warm medium was introduced from the left medium reservoir to wash out unattached cells. Fill all medium reservoirs with culturing medium and let cells proliferate overnight. Change medium after 24 h (the next day) supplemented with angiogenic growth factors (VEGF 100 ng/ml, bFGF 25ng/ml, TNF-alpha 5 ng/ml).
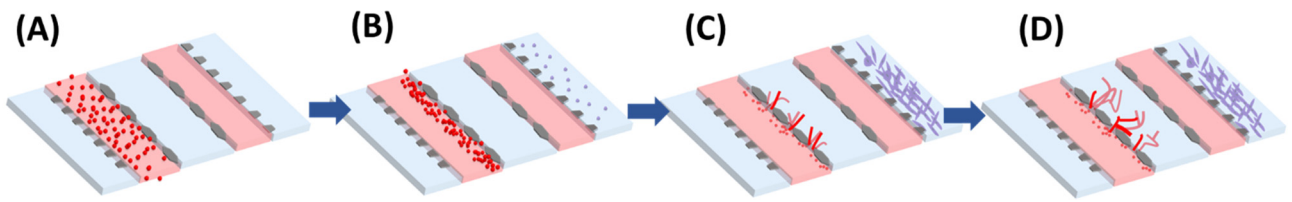
Fig. 5.1.3-2 Formation of iBRB model: graphical protocol.

For cases where co- or tri-culture with NHLF and/or HRP, NHLF and/or HRP are seeded first before HRMEC. Different cell seeding configurations are shown in Fig 5.1.3-3, forming different angiogenesis sprouting models of the iBRB. NHLF is seeded at 10^7 cells/ml while HRP is seeded at 1/5 of HRMEC (in cell number).
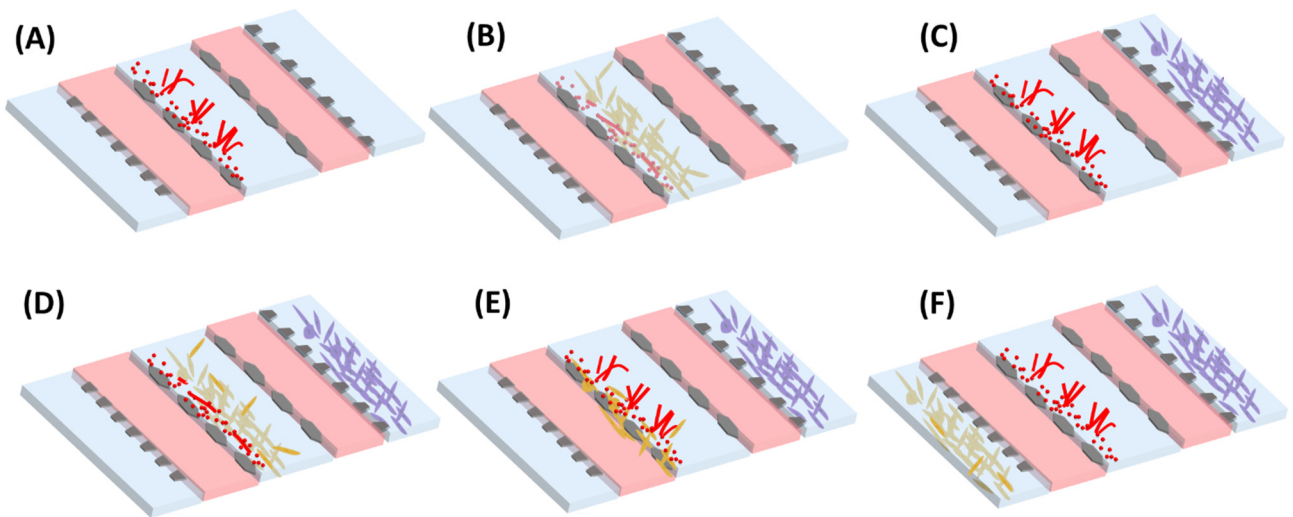
Fig. 5.1.3-3 Different cell seeding configuraions toward development of iBRB models.
Configurations of different cell chambers in developing the angiogenesis model. Cells in red: HRMEC; yellow: HRP; purple: NHLF. (A) HRMEC only. (B) HRMEC + HRP (center). (C) HRMEC + NHLF (RHS). (D) HRMEC + HRP (center) + NHLF (RHS). (E) HRMEC + HRP (mixed seeding) + NHLF. (F) HRMEC + HRP (LHS) + NHLF (RHS). RHS indicated the right hand side of the side channel when viewed from the top. Similarly, LHS (left hand side) indicated the side channel on the left.

5.1.4 Evaluation of MMP activity using the gelatinase kit

Fluorometric gelatinase degradation assay kit (ab234057, Abcam) was used as a crude measurement of the non-specific MMPs activity in a small number of biological samples. MMP-2 (gelatinase A) and MMP-9 (gelatinase B) belong to the gelatinase subgroup; both digest gelatins and cleave types IV and V collagen. Additionally, MMP-2 but not MMP-9 digests fibronectin and laminin, among other ECM (3). MMPs are synthesized as inactive zymogens, and must be enzymatically activated by hydrolytic cleavage of a propeptide domain (4) .

Experiments here were limited to detection of extracellular MMPs, so conditioned medium was collected as samples. MMPs (gelatinase) in the sample digest the quenched gelatin, subsequently cleaved a fluorophore molecule which can be quantified using a microplate reader, schematically shown in Fig. 5.1.4-1.

The reagent preparation, standard and sample preparation and the assay procedure were all followed the protocol provided (4).
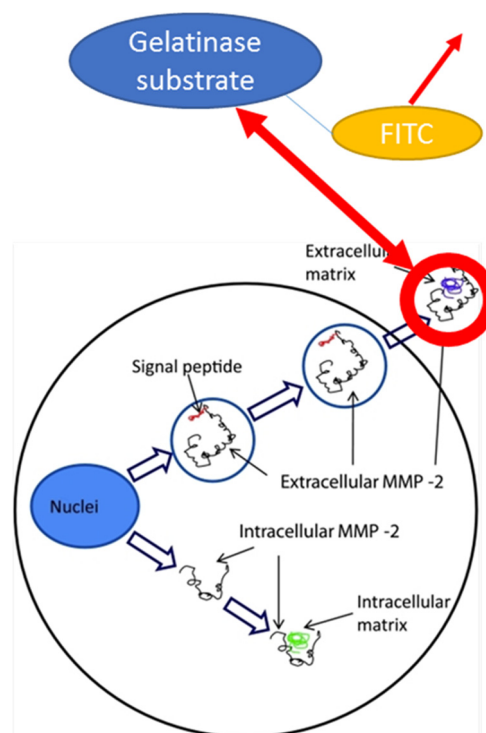

Fig. 5.1.4-1 Mechanism of the fluorometric gelatinase degradation assay kit.

5.1.5 Total protein quantification

Amount of total protein of each sample was quantified and used as the base to which gelatinase content and cytokines are normalized to compare observations across independent assays. Pierce BCA protein Assay Kit (Thermo 23227) was used following the Microplate Procedure. All standards and samples were diluted 2 times in all experiments. Microplates were read using Thermo Scientific Multiskan, and JXAscent software.

5.1.6 Evaluation of iBRB barrier tightness

For both plate experiments and microfluidic models, iBRB barrier was evaluated by perfusing FITC-dextran 40 kDa (0.5 mg/ml) from the luminal (apical) side; i.e., from the insert of the transwell plate or from the left medium reservoir of the microfluidic model.

Initial conditions:
- Plate experiment: Insert: 250 ul (FITC-dextran 0.5 mg/ml), well 1 ml medium.
- Microfluidic device: 150 ul medium in all medium reservoirs. Add extra 50 ul medium (including 0.5 mg/ml FITC-dextran) to the top left medium reservoir to initiate the experiment (i.e., t0).

Experimental conditions:
- Plate experiment: collect samples (100 ul from the well) every 10 min, over 30 minutes. Add 80 ul of

warm medium back to the well after each measurement.

- Microfluidic device: collect samples (25 ul from the bottom right medium reservoir) every 5 minute over 30 minutes. Add 10 ul of warm medium back to the sample collection port.

Fluorescence intensity was read using Gemini XPS, Molecular Devices.

5.1.7 Quantification of sprouting length

Tip cells of sprouts are manually picked out in ImageJ in the following steps:

Calibration (set scale)

- Draw a line onto a known distance (scale bar)
- Analyze > set scale   > enter the known distance and the corresponding pix
- Check the global box to apply the same parameters to all images (same magnification)

Open the images to be quantified,

- Draw a line from trapezoid-shaped supporting posts and leading tip cells to define a region of interest (ROI).
- Ctrl-M to get the measurement. Save the output into a csv file.

Tip cells were defined as the right most single point(s) of the input image, which are the maximum intensity projection of stacks as shown in an example in Fig 5.1.7-1.
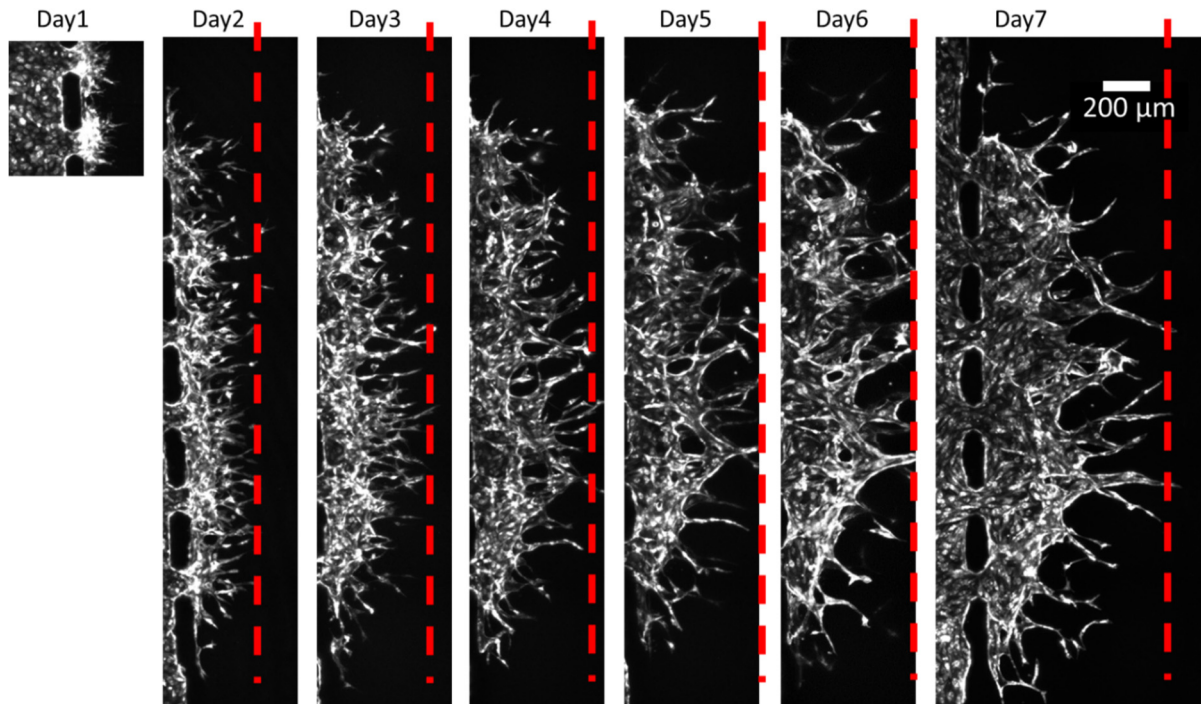

Fig.   5.1.7-1 Quantification of sprout length: example of procedure.

Example of quantification of sprout length based on position of tip cells. *HUVEC* microvessels per day were captured and red lines indicated from where measurement points were taken to obtain the sprout length.

5.2 Results and Discussion

Results from plate experiments and microfluidic models were discussed, within each, HRMEC cells/sprouts under pathological microenvironment were studied by characterizing the barrier properties, and response of cells/sprouts by looking at morphology, and secretion of cytokines.

5.2.1 Characterization of hRMEC (plate experiment)

In order to develop the prototype of the angiogenesis sprouting model of iBRB, the polarity and the response of hRMEC to pro-inflammatory cytokine (TNF-alpha), oxidative stress (High glucose) and hypoxia ($CoCl_2$) were characterized in the transwell culture plate. The presence of NHLF and the resultant integrity of barrier and cytokine secreted were quantified.
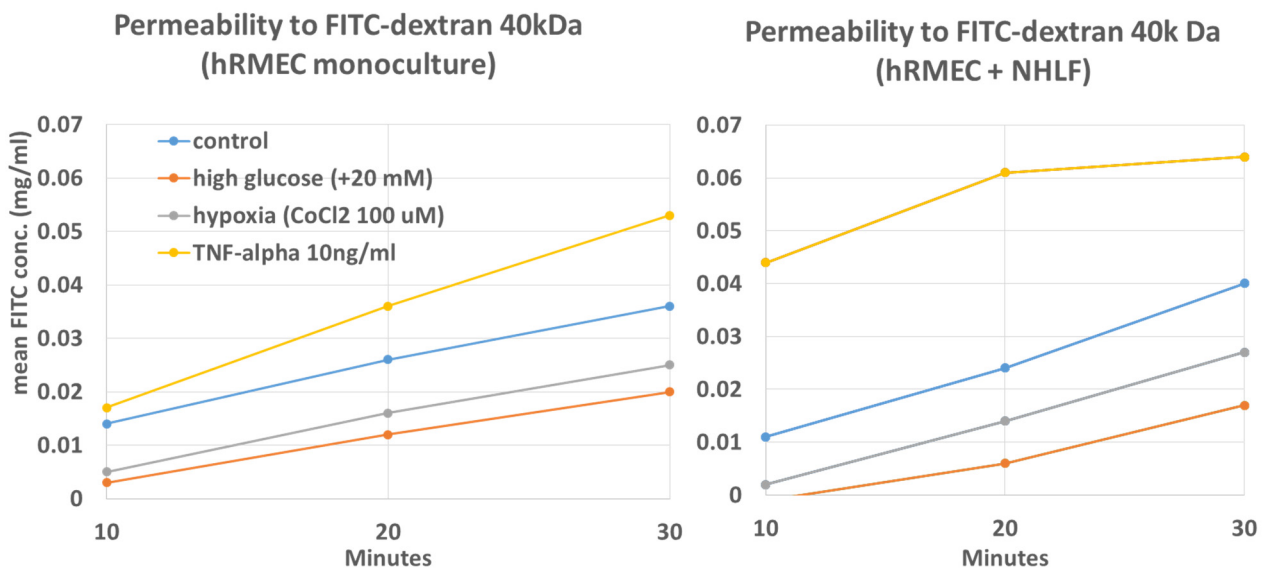

Fig. 5.2.1-1 HRMEC under pathological microenvironment: plate experiments (permeability)

Experiments were conducted 2 or 3 samples and repeated for 2 independent experiments. The patterns follow the one as shown in Fig. 5.2.1-1, where stimulated under TNF-alpha resulted in a leakier barrier for both HRMEC monoculture and HRMEC-NHLF co-culture. Strangely, however, comparing across HRMEC monoculture and HRMEC-NHLF co-culture response under stimulation, barriers of the HRMEC monoculture were leakier than HRMEC-NHLF in one set of experiment but the trend was exactly opposite in another set of experiment (data not shown). More experiments are needed to reach a firm conclusion, on whether NHLF plays a role in guarding the HRMEC monolayer under stimulation as it is known that microvessels interact with the underlying smooth muscle cells and pericytes which collectively are regulated by local glucose levels {Cai, 2002 #633}.
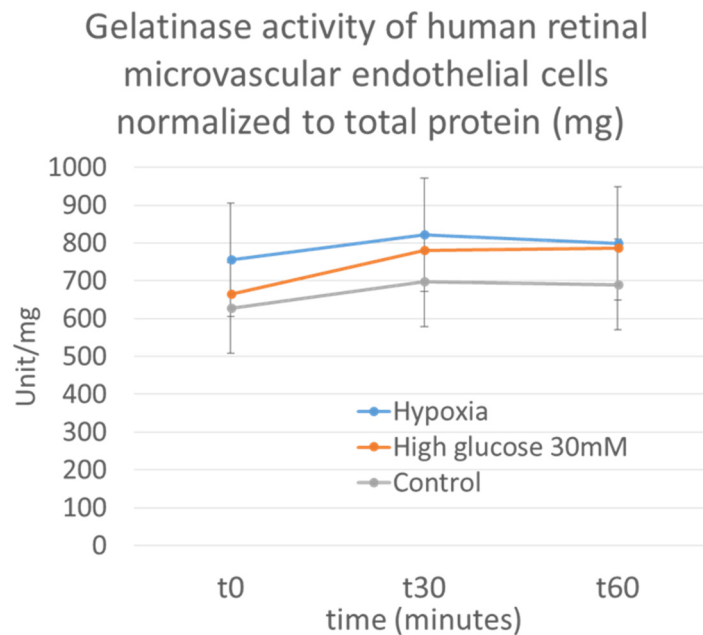
Fig. 5.2.1-2 HRMEC under pathological microenvironment: plate experiment (gelatinase activity)

Understanding roles of ECM in neovascularization is as important as understanding angiogenic sprouting events itself. Extravascular fibrin also has multiple inflammatory roles, including the stimulation of cytokine and chemokine production (5), indicating angiogenesis is also affected by numerous extracellular stimuli. Changes affecting ECM composition or enhanced ECM degradation by MMPs, as observed in AMD, stroke, DR, or chronic inflammation, may affect endothelial integrin activity and thereby contribute to endothelial barrier bareakdown/ alterations in integrin activity can affect the sealing of endothelial cell-cell contacts.

Mechanisms of retinal ischaemia in diabetes have been proposed, including thickened basement membranes, platelet aggregation, leukocyte activation/adherence or a combination {Cai, 2002 #633}. Early hyperglycemia is sufficient to increase the synthesis of BM components in the retina which in turn may contribute to the closure of the capillaries. mRNAs for fibronectin and collagen type I, III, IV and V are found to be upregulated in the retinal basement membrane of diabetic retinopathy. Furthermore, in the retina of diabetic patients increased immunostaining is observed compared to normals for vitronectin in the arterioles, collagen types I, II, III, IV in the venules and laminin and fibronectin in both arterioles and venules. Animal models also show that retinal expression of collagen type IV and fibronectin increases in hyperglycaemic rats. Diabetic basement membrane thickening appears to involve qualitative alterations of specific basement membrane markers at an advanced disease stage, with the appearance of diabetic retinopathy {Cai, 2002 #633}.

Hypoxia in a growing tumor mass results in the production of HIF, which stimulates the production and release of growth factor and proteolytic enzymes. Angiogenesis GF bind to specific receptors located on the EC and stimulate their proliferation and migration. Protease such as MMPs degrade the BM and ECM, allowing migration of cells (toward the tumor mass/ angiogenic stimuli) and growth with the help of integrins (adhesion molecules). Formation of BV/lumens by depositing ECM and remodeling with the aid of mural cells.

Gelatinase activity is a non-specific indicator of matelloprotease MMPs. Different families of MMPs exist, with MMP2, MMp9, MMP14 the common ones involved in angiogenesis process. Based on gelatinase activity of HRMEC (Fig 5.2.1-2), a higher activity was detected under hypoxia and high glucose, showing that HRMEC responded to hypoxia and oxidative stress. It has been characterized that under hypoxia, HIF-alpha gene expression is upregulated, leading to upregulation of VEGF expression. This leads to breakdown of tight junctions, resulting in leakier barriers. Align with this findings, a higher gelatinase activity is an evidence that HRMEC degrades the surrounding ECM, and possible sprouting takes place, which was tested on the microfluidic models in Chapter 5.2.2. The gelatinase activity of HRMEC monoculture was normalized to the respective total protein concentration in order to compare across samples. An abnormally higher total protein concentration between samples could be the result of differential initial conditions (significantly more cell numbers, etc.), misleading interpretations.

Interestingly, HRMEC seemed to have a polarity response such that a higher gelatinase activity was detected from the well samples (basolateral side) than the insert samples (luminal side), in all conditions (data not shown). To further test the polar response of HRMEC, cells cultured in transwell were subjected to high glucose, and hypoxia from either the well or the insert of the transwell plate. There was not much difference in total protein concentration observed under luminal and abluminal stimulations, although barrier of HRMEC monolayer is leakier when the conditions was imposed on the luminal side (insert).

The current study lacks investigation on tissue-repair angiogenesis, which is also involved with matrix deposition. Tissue repair-associated angiogenesis usually involves cell invasion in to a fibrin structure and the presence of inflammatory cells. Tissue-type plasminogen activator is stored in endothelial cells and can be released acutely into the vessel lumen upon stimulation of the endothelium to activate fibrinolysis and to prevent fibrin deposition. At the basolateral side of the cell, urokinase-type plasminogen activator (uPA) bound to a specific cellular receptor is involved in the proteolytic modulation of matrix proteins and cell-matrix interaction.

5.2.2   Development of the microfluidic iBRB angiogenesis sprouting model

In contrast to analyzing vascular networks, sprouting of vessels mimicking in vivo iBRB was the focus in this chapter. Therefore, instead of relying on the self-organization of the microvascular network, sprouting of HRMEC were formed by let cells attach on one side of the fibrin and subsequently stimulated the growth by adding angiogenic growth factors. In contrast to the HUVEC microvessels (leaky, similar to the in vivo fenestrated choroids underneath the Bruch's membrane), in vivo retinal microvessels form an extremely tight barrier that could guard low molecular weight molecules from entering into the neural retina. Hence, in addition to morphological analysis of sprouting, permeability of FITC-dextran was used to characterize the functionality of the barrier. The extracellular environment, specifically the secretion of cytokines and proteases, was analyzed in conjunction as part of the analysis of sprouting events.

Sprouting under different conditions were investigated; namely, the presence of angiogenic factors, the role(s) of mural cells, HRP. As NHLF secretes various growth factors, among those, VEGF, bFGF, and HGF, which are angiogenic factors that stimulate proliferation of HRMEC. Different configurations of cells were therefore investigated to obtain the optimal angiogenesis sprout model. It is believed that the cytokines secreted by NHLF and the interactions between HRMEC and HRP affect the growth of sprouts.

5.2.2.1 Importance of angiogenic factors in sustaining sprouting of HRMEC

Sprouts formed from HRMEC required exogenous angiogenic growth factors. While sprouting microvessels formed using HUVEC have been attempted (Fig. 5.1.7-1), sprouting was sustained with the culturing medium and the NHLF culture. Microvessels of HRMEC, however, did not sprout into fibrin under normal culturing medium (Fig. 5.2.2-1). Even if cells sprouted into the fibrin, it did not sustain over 2 day of culturing. Similarly, when HRMEC was co-cultured with HRP, sprouting of HRMEC was not initiated, while HRP proliferated inside the fibrin.
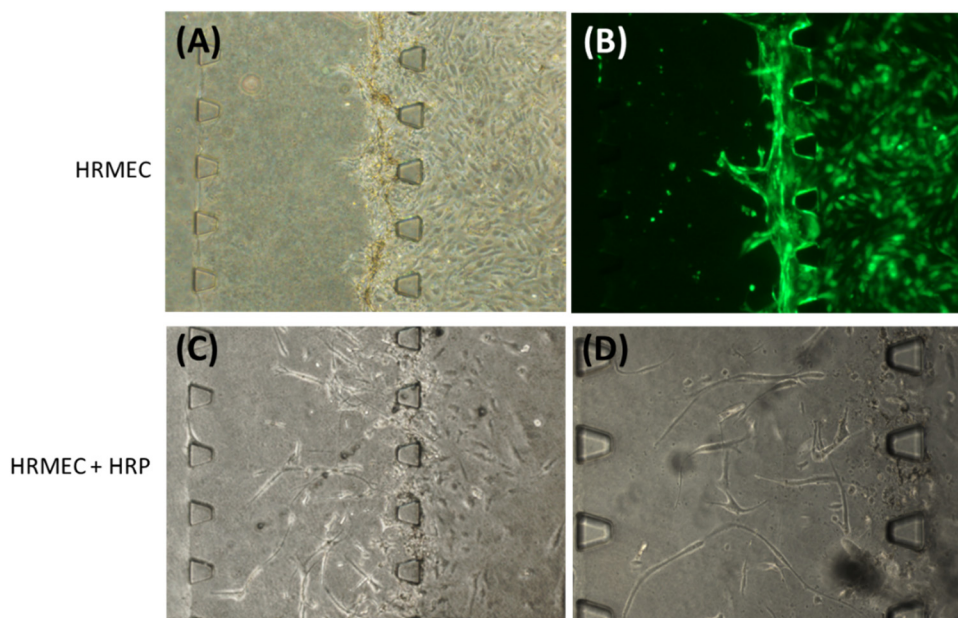

Fig. 5.2.2-1 Sprouting model with no angiogenic growth factors.
Sprouting under no exogenous angiogenic factors (day 2 after seeding). (A-B) HRMEC-only seeding; (C-D) HRP seeded in the central channel. (D) is a magnified view of (C). Note that HRMEC were seeded from the LHS channel in the above cases.

Endothelial tubulogenesis within fibrin gels was found to be dependent on the presence of either angiogenic factors or tumour cells since HUVECs and HDMECs grown within fibrin gels in standard serum-containing EC growth medium with no exogenous added growth factors produced very few tubular structures (1).

It is known that HRMEC are proliferative under angiogenic growth factors such as bFGF, and VEGF. Therefore, the following cocktail were applied globally to the subsequent models to induce sprouting. The results herein were from models supplemented with the angiogenic cocktail based on the published report (6,7):

- VEGF 100 ng/ml
- bFGF 25 ng/ml
- TNF-alpha 5ng/ml

The cytokine tumor necrosis factor-alpha (TNF-alpha) cooperates with the angiogenic factors basic fibroblast growth factor (bFGF) and vascular endothelial growth factor (VEGF) in inducing human microvascular endothelial cells in vitro to invade a three dimensional fibrin matrix and to form capillary-like tubular structures (8). As higher levels of serum can prevent sprouting have been reported (9), addition of exogenous angiogenic factors should be added with caution.
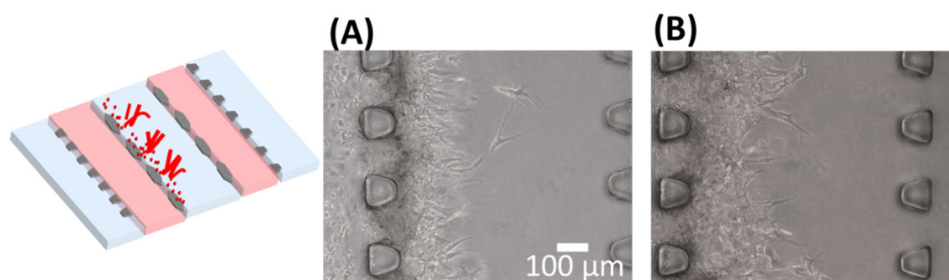
Angiogenesis sprouting of HRMEC.

Fig. 5.2.2-2 HRMEC sprouting model under globally applied angiogenic growth factors.

(A) 2 days and (B) 3 days after seeding. Sprouting was observed.
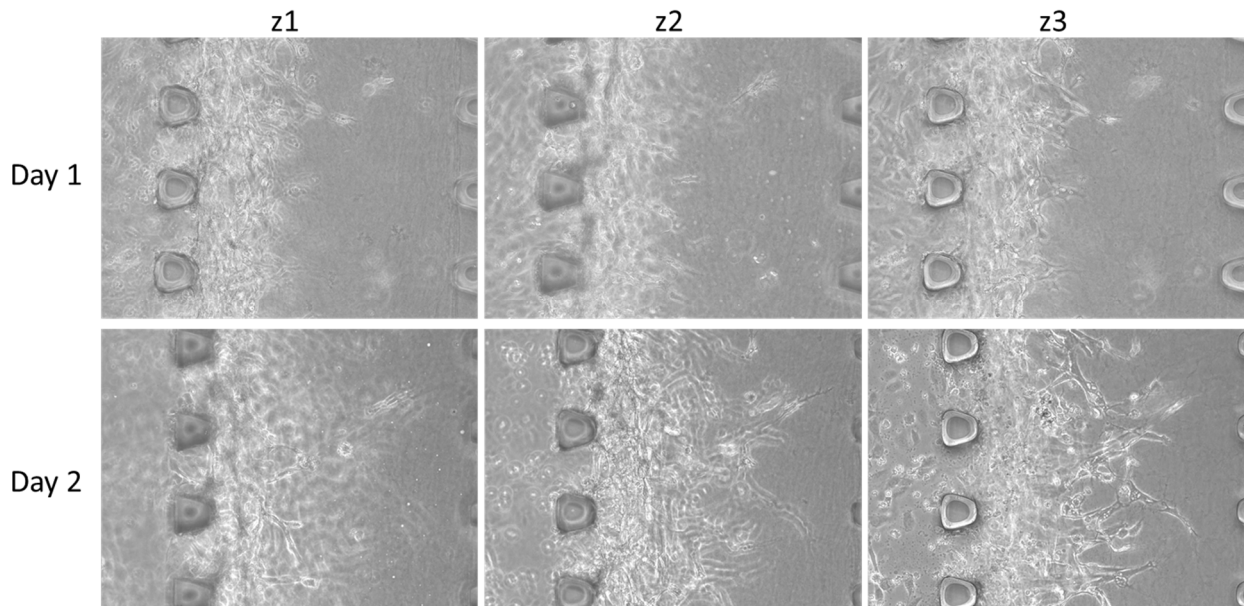
Fig. 5.2.2-3 Montage of snapshots with microscope focus on three non-specific depth into the gel along the z-direction, z1 – z3.

As can be seen from Fig. 5.2.2-2 and Fig. 5.2.2-3, elongation of HRMEC sprout continued, and matrix degradation were observed. Although the exogenous angiogenic factors used were not optimized but based on previous reports (6,10), the findings confirmed the necessity of growth factors in initiating and sustaining the

angiogenic sprouts of HRMEC.

Tube formation is a multi-step process involving cell adhesion, migration, differentiation and growth. The formation of intercellular connections and lumina within EC networks in fibrin gels is dependent upon the actions of VE-cadherin, avb3, a5b1 intergins, the cdc42, Rac1 GTPases, and membrane-type MMPs (2). Angiogenic sprouts are led by a single tip cell, with the trailing trunk cells generate lumens and from which sprouts emerge (9,11). In an in vitro HUVEC-PC co-culture angiogenesis model, sprouting and branching (observed on day4), EC branching and intercellular lumen formation (observed on day6), single vessels (observed on day 10) (11), in comparison to our model which was only cultured up to 5 days.

5.2.2.2 Roles of HRP and NHLF in the iBRB model

After confirming the sprouting of HRMEC monoculture, the role of HRP, the mural cell that wrapped tightly around in vivo retinal microvessels, were co-cultured with HRMEC in an attempt to investigate the relationship between microvessels and the mural cell. NHLF is known to secret many GF, among those, bFGF, HGF, HB-EGF, TGF-beta, VEGF (12), and that VEGF, FGF, HGF are known to stimulate proliferation of HRMEC and vascular angiogenesis, therefore NHLF was incorporated into the iBRB model (13), similar to the experiments conducted in the transwell plate in the previous section (Chapter 5.2.1). Different configurations (seeding chambers) were attempted, to investigate if the presence of angiogenic gradient has any role in the formation of sprouts and the subsequent growth.

The naming convention for the following initial seeding configurations of morphology of sprouting events was summarized below. In all cases, HRMEC were seeded such that they attached on the left side of the central channel.

- *HRMEC + HRP (center):* HRP were seeded with the fibrin gel in the central channel; HRMEC were let attach onto the gel after fibrin has polymerized.
- *HRMEC + NHLF (RHS):* acellular fibrin was loaded into the central channel; NHLF embedded in fibrin was loaded into the right side of the side channel (RHS).
- *HRMEC + HRP (center) + NHLF (RHS)*: HRP embedded in the fibrin gel was loaded into the central channel and NHLF embedded in fibrin was loaded into the right side of the side channel (RHS); HRMEC were let attach onto the gel after fibrin has polymerized.
- *HRMEC + HRP (mixed seeding) + NHLF (RHS):* acellular fibrin was loaded into the central channel; NHLF embedded in fibrin was loaded into the right side of the side channel (RHS). HRMEC and HRP suspensions were mixed at a ratio of 5:1 (HRMEC: HRP cell number), and let attach as HRMEC monoculture seeding.
- *HRMEC + HRP (LHS) + NHLF (RHS)*: HRP embedded in fibrin gel was seeded into the left side of the side channel, NHLF embedded in fibrin gel was seeded into the right side of the channel. Thereafter, HRMEC was seeded following the standard seeding procedure.
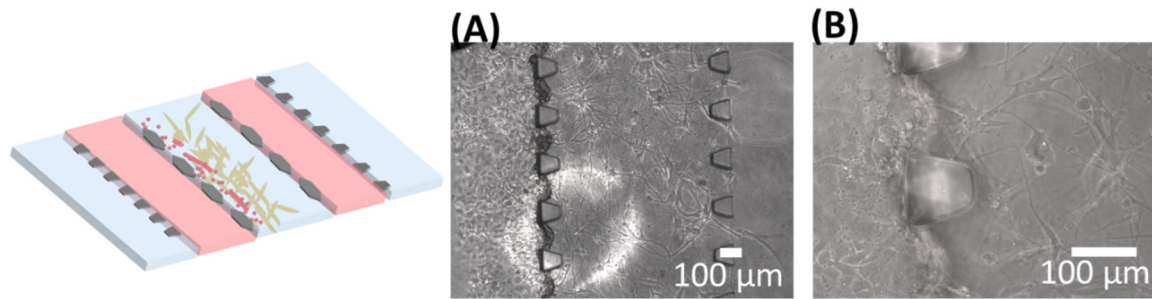
HRMEC + HRP (center).

Fig.   5.2.2-4 iBRB model: HRMEC-HRP co-culture.
HRP (yellow cells in the schematic) were first seeded into the central channel. And HRMEC was seeded under the standard protocol. (A) Day 1 and (B) day2 after seeding. No sprouting was observed.

Interestingly, when HRP was seeded into the central gel channel, HRMEC did not sprout into the fibrin gel, similar to the observations in Fig 5.2.2-1 C,D, even though exogenous angiogenic factors were applied. The finding resonated with a previous report, claiming pericytes inhibited growth of HRMEC (14).

HRMEC + NHLF (RHS).
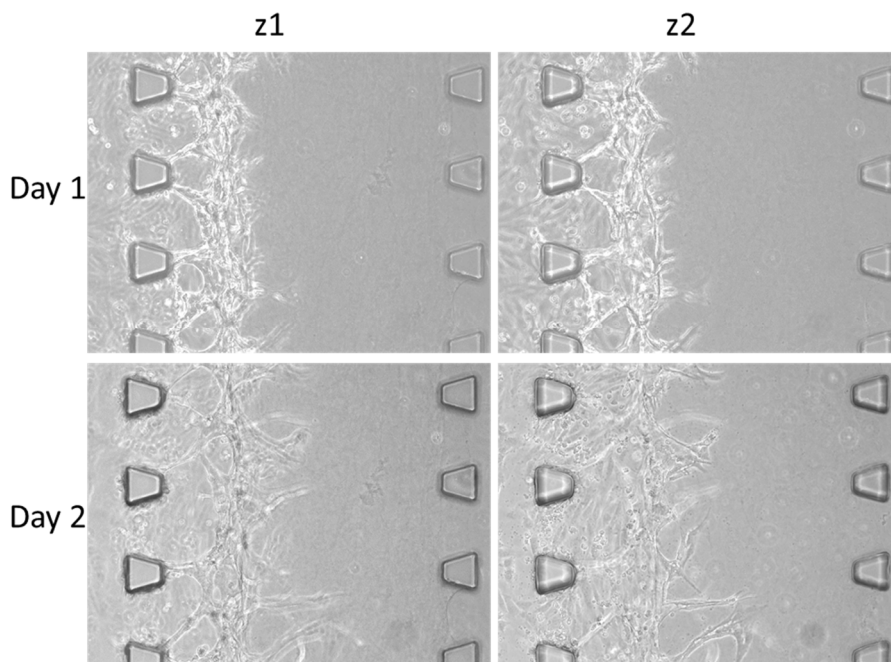
Fig.   5.2.2-5 iBRB model: HRMEC-NHLF co-culture.
Montage of snapshots with microscope focus on two non-specific depth into the gel along the z-direction, z1 – z2.

When HRMEC was co-cultured with NHLF seeded on the right side of the side channel, elongation of sprouts into the gel were observed. In particular, fibrin degradation was considerably more obvious compared to HRMEC-only sprouting events. NHLF seeded on the left side of the side channel (the seeding side of HRMEC) was not tested.

HRMEC + HRP (center) + NHLF (RHS).

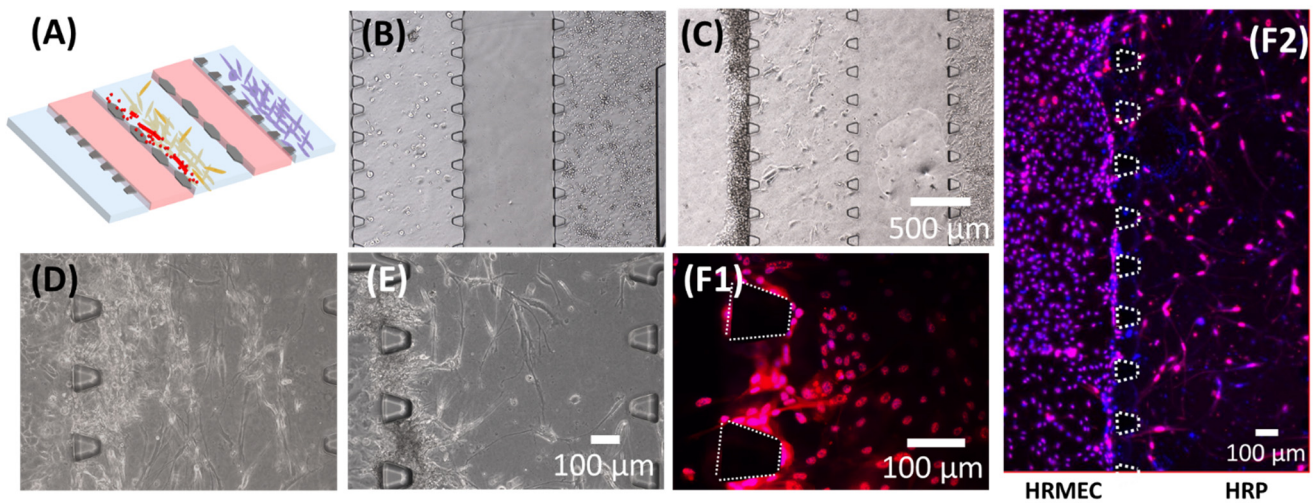**Fig. 5.2.2-6 iBRB model: HRMEC-HRP-NHLF tri-culture (HRP embedded in fibrin gel).**
(A) schematic of the position of HRMEC (red), HRP (yellow), NHLF (purple). (B) Part of the microchannel showing HRP and NHLF after seeding. (C) 30 minutes after seeding HRMEC into the side channel. (D-F) Day 1, Day 2, and Day 3 after seeding. (F1) Overlay images of IF images showing desmin (red) and DAPI (blue). (F2) Maximum intensity projected image of stacks on Day 3 culturing, showing no observable sprouting of HRMEC in to the fibrin.

Despite the fact that sprouting was observed in HRMEC-NHLF co-culture, minimum sprouting event was observed when HRP was cultured in the central gel channel (HRMEC-HRP and HRMEC-HRP-NHLF), leading to the hypothetical guess that HRP might took up the necessary nutrients which impeded proliferation and sprouting of HRMEC. Therefore, following trials were attempted: seeding HRP together with HRMEC and seeding HRP in the LHS side channel, separated from HRMEC.
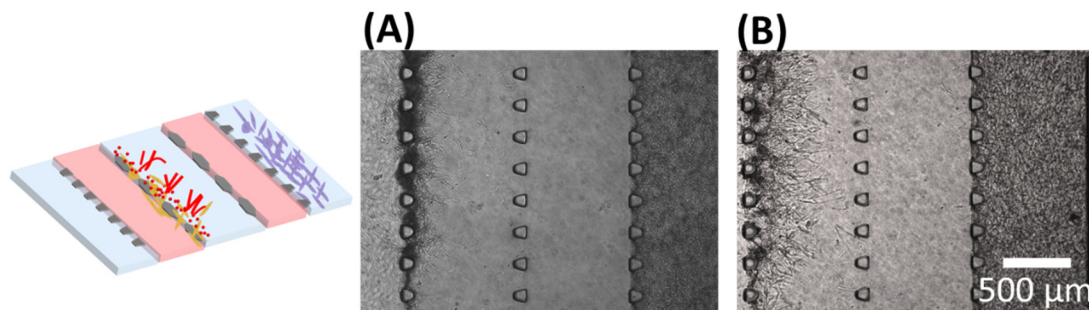
HRMEC + HRP (mixed seeding) + NHLF (RHS)

Fig. 5.2.2-7 iBRB model: HRMEC-HRP-NHLF tri-culture (HRP seeded from side).
(A) Day 1 and (B) day2 after seeding. Sprouting events were observed in all samples.
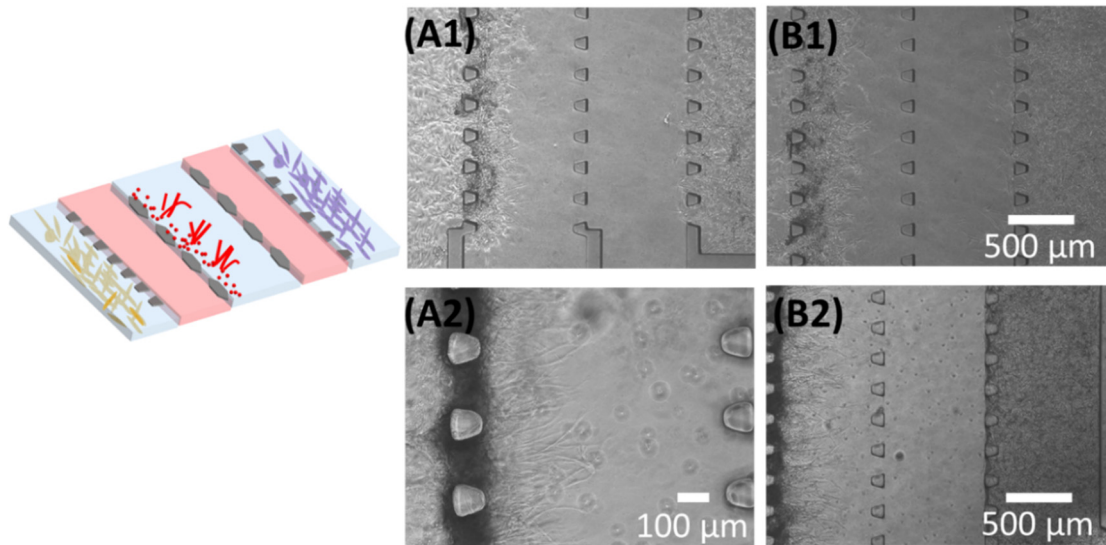
HRMEC + HRP (LHS) + NHLF (RHS)

Fig. 5.2.2-8 iBRB model: HRMEC-HRP-NHLF tri-culture (HRP embedded in fibrin in the side channel). (A~) Day 1 after seeding (showing n=2 samples); (B~) day 2 after seeding.

Similar to the Fig 5.2.2-7, intensive sprouting of HRMEC was observed in this configuration in all samples when HRP was seeded from the RHS of the side channel. It is speculated that perhaps HRMEC was not deprived of the necessary growth factors under this configuration of co-culture. The presence of NHLF did not seem to affect the sprouting of HRMEC.

In order to further test the hypothesis, selective configurations were repeated and more experiments were conducted. The morphology of sprouting was captured using a confocal microscope (LSM700, Carl Zeiss MicroImaging Co., Ltd) at every 2 um interval, spanning the entire height of the culturing chamber. The stacks of each image were processed and the following images are the maximum intensity projection of each stack. Maximum intensity projection images were created by obtaining z-stacks of areas of interest and flattening them to produce a single projection. As appropriate, image brightness was balanced between image stacks to better represent the morphological structure.

Fig 5.2.2-9 labeling A-D refers to the following sprouting models:
Fig. (A) HRMEC + HRP (LHS) + NHLF (RHS)
Fig. (B) HRMEC + HRP (mixed) seeding + NHLF (LHS)
Fig. (C) HRMEC + NHLF (LHS)
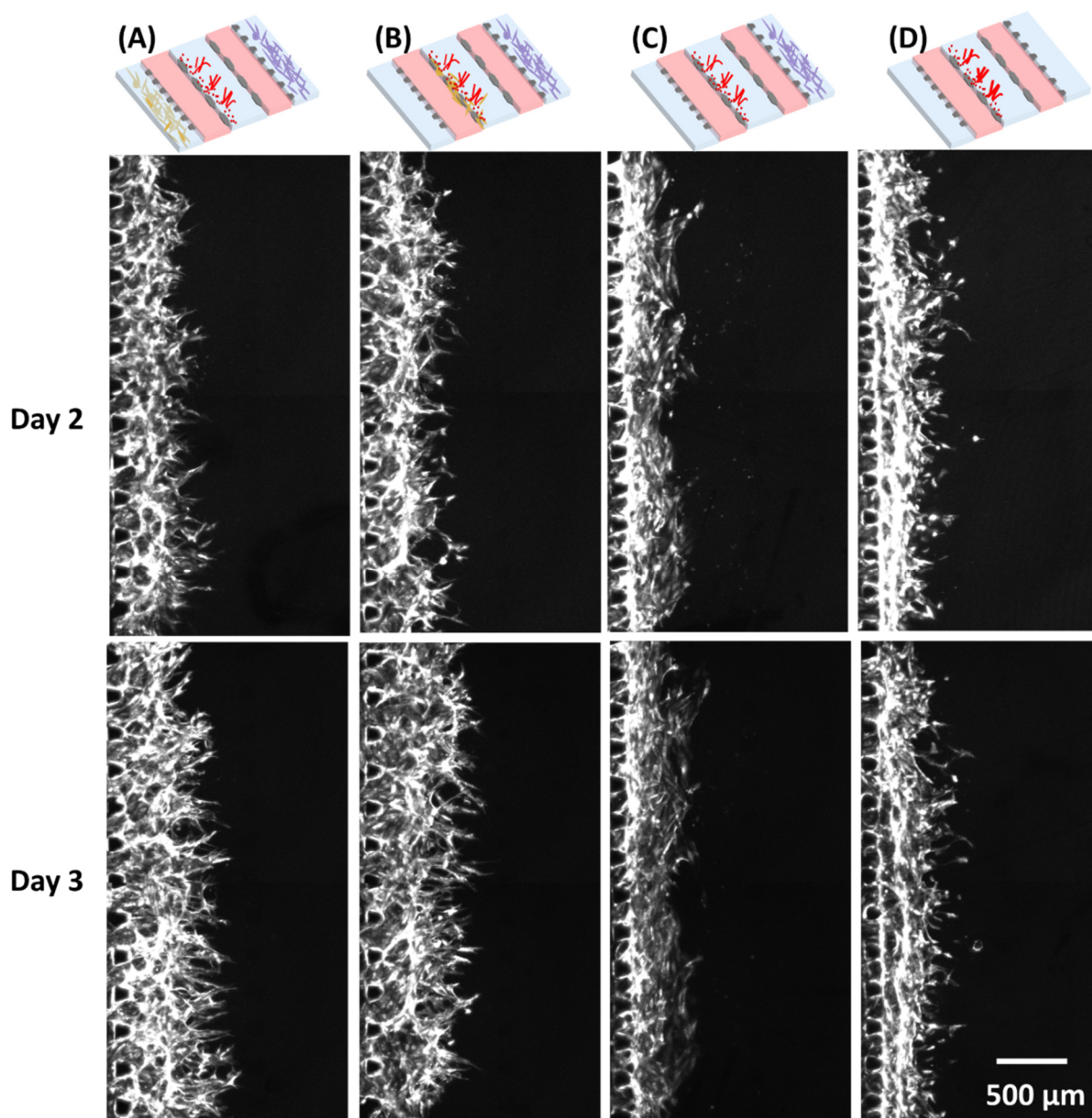Fig. (D) HRMEC monoculture

Fig. 5.2.2-9 Proposed iBRB sprouting models.

Qualitatively assessing the sprouting events across the samples, sprouting occurred in all cases (with exogenous growth factors globally supplied). However, sprouting formed from solely HRMEC monoculture was considerably weaker (qualitative, exploratory assessment). More single cells, as opposed to elongation of collective cells, were observed. In contrast, when HRP co-cultured with HRMEC either in the LHS side channel or mixed seeding (Fig 5.2.2-9 A, B), the sprouting appeared to be robust and elongation of sprouts into the gel was faster compared to HRMEC-NHLF co-culture or HRMEC monoculture (Fig 5.2.2-9 C,D) under the same culturing condition. Sprouting evens of HRMEC-NHLF co-culture seemed to be governed by a different angiogenesis mechanisms, where excessive gel degradation and collective migration of cells took place. As angiogenesis is a dynamic progress that is also involving coordination of multiple cells within a sprout, disturbance to cytoskeletal regulators such as Rho GTPase proteins (RhoA, Rac and Cdc42) would evidently affect the migration speed, and collective migration and also the filopodia formation (15).

121

5.2.2.3 Effect of stimulations on the sprouts

As the final part of the assessment of the sprouts, the proposed four models were subjected to hypoxia and inflammatory microenvironments by exogenous addition of TNF-alpha. The model were stimulated for six hours and the morphology before and after the experiments were observed (Fig. 5.2.2-10). In conjunction, permeability to FITC-dextran 40 kDa was analyzed together.

Hypoxia and TNF-alpha were imposed on the model. Under hypoxia, HIF regulates the expression of hypoxia-inducible genes that promote neovascularization ¥cite{Rodrigues3863}. Therapies targeting the HIF-regulated gene product VEGF for the treatment of diabetic macular edema have been shown to be successful, highlighting the importance of HIF (hypoxia inducible factors) in diabetic eye disease.

While a low TNF-alpha concentration was supplemented to the culturing medium to aid growth of sprouts, an overly elevated TNF-alpha concentration imposed an inflammatory microenvironment to the microvessels, similar to the in vivo inflammatory conditions. TNF-alpha induced NF-kB, a transcription regulator. Activation of the NFkB pathway triggers cytokines, chemokines, and adhesion molecules involved in inflammatory responses (16): IL-6 triggers angiogenesis; IL-8 (proteins encoded by CXCL8) upregulates VEGF and VEGFR2 expression in ECs, thus triggering autocrine angiogenic activation. CXCL8 is known to promote activation and recruitment of macrophages and monocytes – a prerequisite for the switch from acute to chronic inflammation. **Chronic inflammation can be detrimental to the nascent vessels, either directly via cytokine or chemokine signaling or indirectly through inflammatory cell activation**. Augmented levels of inflammatory cytokines, such as IL-1beta, IL-6, TNF-alpha are found in the vitreous of patients with ischemic retinopathies and corresponding animal models. Unlimited to TNF-alpha, many cytokines such as MCP-1 also mimicked inflammation by elevating inflammatory marker of HRMEC although the present investigation is only limited to TNF-alpha. A cohort of inflammatory cytokines, as well as, oxidative stress such as elevated glucose levels, could perhaps activate different pathways therefore generate a different response to the stimulation.
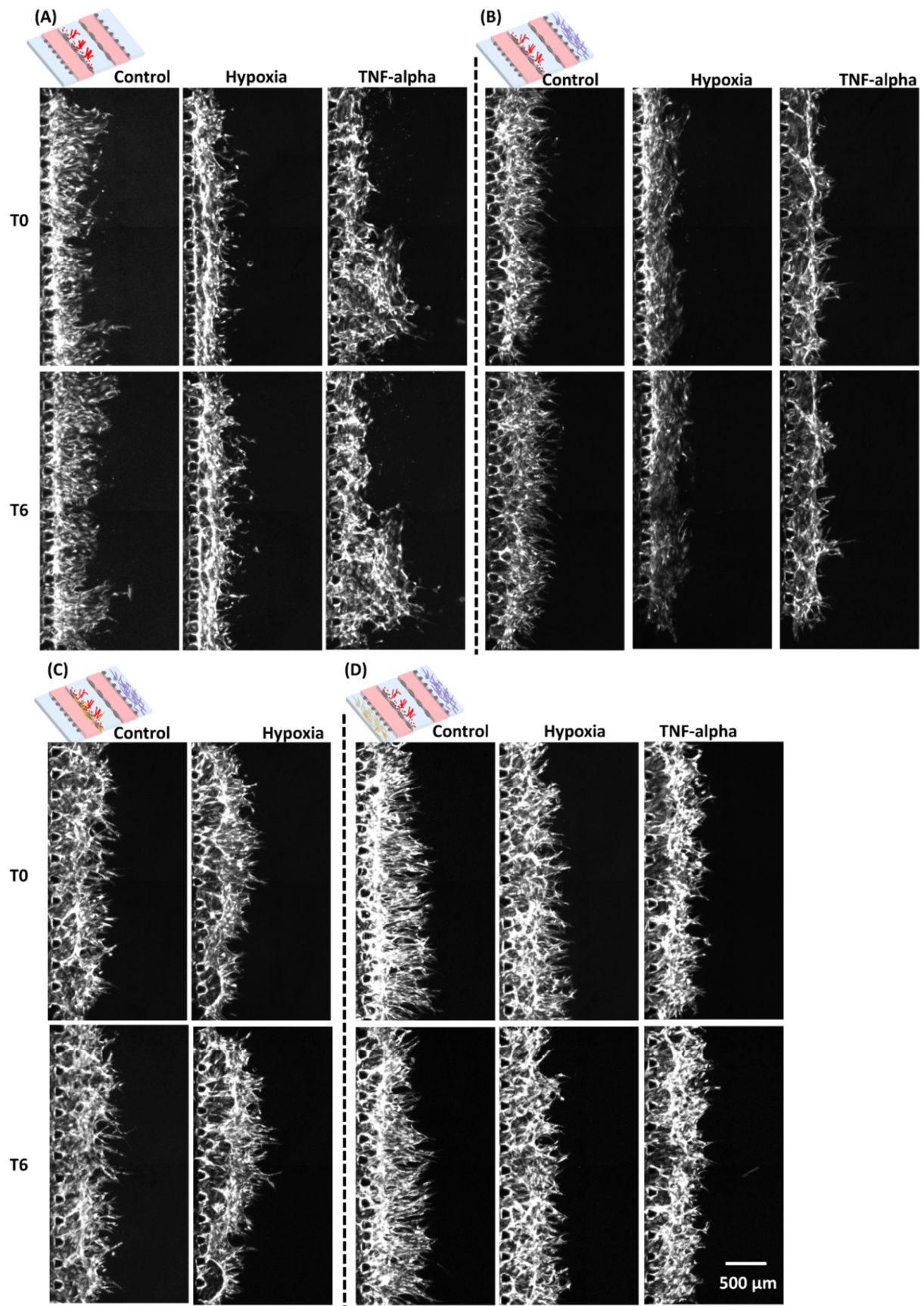
Fig. 5.2.2-10 Proposed iBRB models under pathological microenvironments.

T0, T6 refer to the time 0 and 6 h after the stimulations.

5.3   Summary of the angiogenesis sprouting model of the iBRB

HRMEC under inflammatory conditions, and the roles of human retinal pericytes (HRP) and hepatocyte growth factor (HGF) in angiogenesis sprouting are investigated, adding to understanding of different factors involved in controlling angiogenic sprouting. Limitations include the absence of mural cells in the models, unlike the in vivo iBRB. Although relations between ECM and non-specific MMPs were evaluated, other families of proteases (serine protease, etc.) were neglected. In addition, among the cytokine networks and multiple interconnected downstream pathways, the cytokines analyzed were non-exhaustive. A comprehensive understanding by combining findings from proteomic and gene profiles /mRNA and single protein level with regard to angiogenic and/or inflammatory activation.

Building a biomimetic on-chip model is challenging. Combining knowledge on specific biomarkers, development in novel immunoassay capture strategies could accelerate progress in point-of-care testing. Thus, by identifying markers that can separate physiological and pathological angiogenesis, we can selectively deliver antiangiogenic or vascular disrupting agents to the diseased tissues. More importantly, having an understanding on the inconsistency in the results obtained between animal and on-chip models is required in order to translate the results for clinical uses. The missing anatomical structures in the in vitro settings mean the whole organ responses cannot be recapitulated and often lead to inconsistent conclusions. Contrasting observations on in vivo and in vitro shear stress studies arise from the fact that glycocalyx, a structure that is required for shear stress-induced release of nitric oxide (NO) is missing in the in vitro model. NO is released when endothelium is subjected to acute change in shear stress in vivo, leading to a weaker barrier function. In contrast, in vitro model has shown that shear activates the small GTPase Rac, which leads to active reorganization of actin filament. In vivo shear stress is regulated by multiple mechanisms and as a result of the structural difference, inconsistent conclusions on barrier-promoting effects of shear stress in different models were obtained. It is therefore necessary to evaluate the in vitro data against in vivo observation to gain a deeper insight into the pathogenesis of the diseases.

References

1. Endothelial tubulogenesis within fibrin gels specifically requires the activity of membrane-type-matrix metalloproteinases (MT-MMPs) | Journal of Cell Science [Internet]. [cited 2020 Jan 13]. Available from: https://jcs.biologists.org/content/115/17/3427

2. Fibrin In Vitro Angiogenesis Assay | Sigma-Aldrich [Internet]. [cited 2020 Jan 13]. Available from: https://www.sigmaaldrich.com/catalog/product/mm/ecm630?lang=en&region=US

3. Proteinases and Matrix Degradation. 2017 Jan 1;106–25.

4. Guide to MMP-2 and MMP-9 experiment techniques | Abcam [Internet]. [cited 2020 Jan 13]. Available from: https://www.abcam.com/research-areas/measuring-activity-of-gelatinase-enzymes

5. Szaba FM, Smiley ST. Roles for thrombin and fibrin(ogen) in cytokine/chemokine production and macrophage adhesion in vivo. Blood. 2002 Feb 1;99(3):1053–9.

6. Cooperative effect of TNFalpha, bFGF, and VEGF on the formation of tubular structures of human microvascular endothelial cells in a fibrin matrix. Role of urokinase activity. J Cell Biol. 1996 Mar 2;132(6):1177–88.

7. Kim S, Lee H, Chung M, Li Jeon N. Engineering of functional, perfusable 3D microvascular networks on a chip. Lab on a Chip. 2013;13(8):1489–500.

8. van Hinsbergh VW, Koolwijk P, Hanemaaijer R. Role of fibrin and plasminogen activators in repair-associated angiogenesis: in vitro studies with human endothelial cells. EXS. 1997;79:391–411.

9. Martin N. Nakatsu, Christopher C.W. Hughes. Chapter 4 An Optimized Three‐Dimensional In Vitro Model for the Analysis of Angiogenesis. 2008 Jan 1;443:65–82.

10. Role of vascular permeability factor/vascular endothelial growth factor in eye disease | British Journal of Ophthalmology [Internet]. [cited 2020 Jan 13]. Available from: https://bjo.bmj.com/content/81/6/501

11. Winters L, Thambi N, Andreev J, Kuhnert F. Evaluation of Angiogenesis Inhibitors Using the HUVEC Fibrin Bead Sprouting Assay. BIO-PROTOCOL [Internet]. 2016;6(19). Available from: https://bio-protocol.org/e1947

12. Fibrotic human lung extracellular matrix as a disease-specific substrate for 3D in-vitro models of pulmonary fibrosis | bioRxiv [Internet]. [cited 2020 Jan 13]. Available from: https://www.biorxiv.org/content/10.1101/833913v1

13. Yun Y-R, Won JE, Jeon E, Lee S, Kang W, Jo H, et al. Fibroblast Growth Factors: Biology, Function, and Application for Tissue Regeneration. J Tissue Eng [Internet]. 2010 Nov 7;2010. Available from: https://www.ncbi.nlm.nih.gov/pmc/articles/PMC3042641/

14. Y.L. Wang. Effects of pericytes on hypoxia-induced proliferation in retinal microvascular endothelial cells [Internet]. Chinese Ophthalmic Research 28(12):1144-1149. [cited 2020 Jan 13]. Available from: https://www.researchgate.net/publication/289324578_Effects_of_pericytes_on_hypoxia-induced_proliferation_in_retinal_microvascular_endothelial_cells

15. Nguyen D-HT, Gao L, Wong A, Chen CS. Cdc42 regulates branching in angiogenic sprouting in vitro. Microcirculation [Internet]. 2017 Jul;24(5). Available from: https://www.ncbi.nlm.nih.gov/pmc/articles/PMC5505782/

16. Mohr T, Haudek-Prinz V, Slany A, Grillari J, Micksche M, Gerner C. Proteome profiling in IL-1β and VEGF-activated human umbilical vein endothelial cells delineates the interlink between inflammation and angiogenesis. PLOS ONE. 2017 Jun 15;12(6):e0179065.

6 Conclusions and Future Perspective

Many studies have contributed to our current understanding of angiogenesis at different levels through molecular mechanisms, cellular interactions, the whole-organ responses and a combination of different levels. Three microfluidic cellular models of the oBRB and iBRB were developed and discussed in this dissertation. For all of the models, the functional response to stimulations as well as the barrier properties under normal (culturing) condition and pathological conditions (altering glucose concentration, hypoxia and presence of pro-inflammatory cytokines) were quantified. As the oBRB model, RPE-HUVEC cell-cell interactions, RPE cell - HUVEC vessel interactions were characterized. Formation of new blood vessels is not a single specific event that can be separated out; rather, it involves dynamic interactions between ECs and mural cells such as smooth muscle cells and pericytes and the remodeling of cell-matrix interactions. Therefore, the response of HRMEC to stimulations and the MMPs activity were investigated. Effect of cytokines and the role of mural cell (HRP) were also explored in the microfluidic model. For all the models, the tightness of the barriers were evaluated by TEER and permeability of the fluorescent molecules.   As the inherent properties of ECs differ between origins and species, the BRB models developed here adopted ARPE and HRMEC for investigation of inflammation, while HUVEC was used in studying vascularization. The models proposed in this study can be used as a multi-culturing cells and/or vessels model for various applications, with the potential of connecting individual fluidic devices in a fluidic network, studying the systemic effect on the retina.

Current models, however, cannot fully cope with the multifactorial nature of angiogenic processes. The simultaneous consideration of spatiotemporal relationships and multiple pro-/anti-angiogenic factors and cytokines involved in degenerative and regenerative processes will make the models more realistic than single-molecule-specific approaches. Such improvements should be coupled with imaging techniques, in order to verify that the delivery system primarily goes to the targeted tissues. Imaging analyses will also demonstrate the quality of a neovascular network and how well the new network functions compared with native tissues. Novel engineering techniques that can be used for new clinical treatments will undoubtedly require multidisciplinary in vitro and in vivo approaches. The goal of disease modeling is not only to gain a deeper understanding of a specific disease pathophysiology but also to predict the onset and progression of the disease. Coupling disease modeling to regenerative medicine may allow us to accelerate tissue regeneration. Furthermore, with improvements in understanding angiogenesis and improvements in technological solutions, we are one step closer to developing patient-specific diagnostics and personalized anti-angiogenic therapies.

The goal of disease modeling is not only to gain a deeper understanding of a specific disease pathophysiology but also to predict the onset and progression of the disease. Coupling disease modeling to regenerative medicine may allow us to accelerate tissue regeneration. Furthermore, with improvements in understanding angiogenesis and improvements in technological solutions, we are one step closer to developing patient-specific diagnostics and personalized anti-angiogenic therapies.

Acknowledgement

There are so many people that I am thankful of and I cannot possibly list every single person who lent me your time, gave me your smile, had your ear for listen and spared your hands to help but I am glad to have had you from the bottom of the heart. Below I would like to acknowledge the following people who add colours to my palette during my six years in Sendai, Japan.

Family and friends:

To my beloved parents, brother and relatives for the love, patience and support all the way until the end of the PhD marathon and for always believing in me, especially at times when I do not believe in myself. Your verbal, emotional and all the little deeds power me to move forward. To Mr. Hiroshi Takahashi and Mrs. Yuko Takahashi (Sendai), Mr. Toshiyuki Kawaii (Hiroshima), the Yamane family (Komatsu) and Mr. Kudo (Hirosaki), my dearest Japanese family, who enrich my life so much: it is through your warm hospitality that I got to taste the Japanese drums (taiko), the summar festival, traditional style of Japanese hot bath, the Japanese New Year, the concerts and set my foot in many places in Miyagi, Aomori, Ishikawa, Hiroshima and Shikoku islands. Also to my friends, the MEXT 2014 family Guestini Fouzia, Fahad Iqbal, Isrrar, Viliame Savou, Abed Motshiwa, and Jamil Sharif with whom I embarked the fascinating journey and stumbled to master a foreign language in order to live in Japan. Although there is no forever gathering and most of you are scattered in different corners of the world, memories left and friendship remains for years to come.

Academic supervisors:

First and foremost, I am sincerely grateful to Professor Hirokazu Kaji for accepting me to the lab, opening the door to wonderful opportunities and helping me to grow both academically and personally. I enjoyed the freedom you gave me in conducting the research, yet pulled me back to track when I started to go astray. I am sure all your students acknowledge your full support, either research-related matters or personal life, just like you giving me daily rides helping me commuting up and down the mountain to the lab due to my personal health issue. It is perhaps not the cell models, but the moments of us embracing the breeze while cycling in Montreal, Canada and bathing in warm sunshine at the Philadelphia Art museum, USA while attending conferences that would remain in a corner of my heart. Equally, I am thankful of Professor Matsuhiko Nishizawa for creating an open and stimulating research environment that is also foreigner-friendly. I am also amazed at how you are always the person updating worldwide news to everyone. To Professor Torimitsu for constant care of my well-being and I will always remember your wise words and encouragement. To Prof. Nashimoto and Prof. Torisawa from Kyoto University who started me off on the microfluidic vascular model.

Collaborative research lab mentors and members at the Graduate School of Medicine, Tohoku University:

I would like to express my gratitude to Prof. Abe and Prof. Arima for giving me the opportunity and resource to learn in your lab. To Prof. Nobuhiro Nagai, Prof Yao Wen Chang and Mrs Daigaku: you showed me the fun, on top of the frustration in running biological experiments during my days running ELISA in the Abe laboratory. Although daily experiments became dull at times, especially when lengthy assays output to null, I felt the vibe

through your humour and optimism. I was also privileged to be able to learn culturing trophoblast stem cells under Prof. Okae and Prof. Kobayashi; under your training and guidance, I am confident that I can culture any type of cells from now on. I want to extend the most sincere gratitude to Mrs Akane Kitamura: your nudge and care put me back to myself in time, helped me to stand back up and gave me the strength to move forward again.

The members of the Nishizawa laboratory:
I cannot be more grateful enough to have Bibek Raut, who entertained me both in the lab and outside the lab. We had many crazy outdoor adventure as well as times when we worked through midnights and many weekends. I do hope though, that scribbles such as "9 PM - cell seeding, 12 AM – TEER measurement…" would only be the evidence of our naughty selves in the past that remain in the 2019 Lab Notebook. To Bibek Raut, Shun Ito and Taisei Amanokura: you taught me and challenged me to be a better mentor; without you the work will not be complete to its present form. To Kazuya Yamashita and Shinya Kusama: thank you for caring of my wellbeing and reminding me to look out for the light in the dark. May you continue to be the North Star, forever shining and guiding others around you. Last but the least, I am grateful to be accompanied by Yuina Abe, together we finished the seemingly never-ending PhD marathon.